
GAZİ ÜNİVERSİTESİ
Gazi
1926

MAGNETIC NANOFLUIDS IN THERMAL APPLICATIONS

A THESIS SUBMITTED TO
THE GRADUATE SCHOOL OF NATURAL AND APPLIED SCIENCES
OF
GAZİ UNIVERSITY

BY

Rand Ahmed Adeeb BABAT

IN PARTIAL FULFILLMENT OF THE REQUIREMENTS
FOR
THE DEGREE OF DOCTOR OF SCIENCE
IN
ENERGY SYSTEMS ENGINEERING

SEPTEMBER 2023

ETHICAL STATEMENT

I hereby declare that in this thesis study I prepared in accordance with thesis writing rules of Gazi University Graduate School of Natural and Applied Sciences;

- All data, information and documents presented in this thesis have been obtained within the scope of academic rules and ethical conduct,
- All information, documents, assessments and results have been presented in accordance with scientific ethical conduct and moral rules,
- All material used in this thesis that are not original to this work have been fully cited and referenced,
- No change has been made in the data used,
- The work presented in this thesis is original,

or else, I admit all loss of rights to be incurred against me.

Rand Ahmed Adeeb BABAT

08/09/2023

MAGNETIC NANOFLUIDS IN THERMAL APPLICATIONS

(Ph. D. Thesis)

Rand Ahmed Adeeb BABAT

GAZİ UNIVERSITY

GRADUATE SCHOOL OF NATURAL AND APPLIED SCIENCES

September 2023

ABSTRACT

The performance of three thermal application systems (air-to-air heat pipe heat exchanger system, concentric tube heat exchanger system, and natural convection heat pipe system) have been studied experimentally and numerically by using MATLAB/Simulink® under utilizing different working fluids instead of the commercial ones such as iron-oxide (Fe_3O_4/PW), Ferric oxide (Fe_2O_3/PW), Nickel ferrite ($NiFe_2O_4$/PW) mono-magnetic nanofluids as well as (Fe_3O_4@Fe_2O_3/PW) hybrid magnetic nanofluids. All the magnetic nanofluids were prepared by scattering the magnetic nanoparticles in distilled water with two different concentration ratios of (0.5 wt. % and 1 wt. %). The experimental and the numerical analysis were performed under various operating conditions. Wall temperature fluctuations, index factor (efficiency), Nusselt number, and heat resistant magnitudes, were obtained for distilled water, iron oxide, ferric oxide, nickel ferrite mono-magnetic nanofluids as well as iron oxide-ferric oxide hybrid magnetic nanofluid, in each experiment. The experimental and theoretical results showed that adding magnetic nanoparticles to pure water lowered its boiling pinpoint significantly, and likewise improves the heat transfer in the condenser area. The thermal resistance was decreased while the thermal performance was enhanced by using magnetic nanofluid in the three thermal system.

Science Code	:	92808
Key Words	:	Magnetic Nanofluids, Heat Exchangers, Hybrid Magnetic Nanofluids, Ferric Oxide, Iron Oxide, Nickel Ferrite, Thermal performance enhancement
Page Number	:	116
Supervisor	:	Prof. Dr. Adnan SÖZEN

ISIL UYGULAMALARINDA MANYETİK NANO AKIŞKANLARI

(Doktora Tezi)

Rand Ahmed Adeeb BABAT

GAZİ ÜNİVERSİTESİ

FEN BİLİMLERİ ENSTİTÜSÜ

Eylül 2023

ÖZET

Üç termal uygulama sisteminin (havadan havaya ısı borulu ısı eşanjör sistemi, eşmerkezli borulu ısı eşanjör sistemi ve doğal konveksiyonlu ısı boru sistemi) performansı, farklı çalışma sıvıları yerine MATLAB/Simulink® kullanılarak deneysel ve sayısal olarak incelenmiştir. Demir oksit (Fe_3O_4/PW), Ferrik oksit (Fe_2O_3/PW), Nikel ferrit ($NiFe_2O_4$/PW) mono-manyetik nanoakışkanlar ve ayrıca (Fe_3O_4@Fe_2O_3/PW) hibrit manyetik nanoakışkanlar gibi ticari olanlar. Tüm manyetik nanoakışkanlar manyetik nanoparçacıkların distile su içerisinde iki farklı konsantrasyon oranıyla (wt. % 0,5 ve wt. % 1) saçılmasıyla hazırlandı.Deneysel ve sayısal analiz, çeşitli çalışma koşulları altında yapıldı.Duvar sıcaklığı dalgalanmaları, indeks faktörü (verimlilik) , Nusselt sayısı ve ısıya dayanıklılık büyüklükleri, her deneyde damıtılmış su, demir oksit, ferrik oksit, nikel ferrit mono-manyetik nanoakışkanlar ve ayrıca demir oksit-ferrik oksit hibrit manyetik nanoakışkan için elde edildi. Deneysel ve teorik sonuçlar, saf suya manyetik nanoparçacıkların eklenmesinin kaynama noktasını önemli ölçüde düşürdüğünü ve aynı şekilde kondansatör alanındaki ısı transferini iyileştirdiğini gösterdi. Üçlü termal sistemde manyetik nanoakışkan kullanılarak termal performans iyileştirilirken termal direnç azaltılmıştır.

Science Code	:	92808
Key Words	:	Magnetic Nanofluids, Heat Exchangers, Hybrid Magnetic Nanofluids, Ferric Oxide, Iron Oxide, Nickel Ferrite, Thermal performance enhancement
Page Number	:	116
Supervisor	:	Prof. Dr. Adnan SÖZEN

ACKNOWLEDGEMENTS

First and foremost, I thank God, the Almighty, for having made everything possible by giving me strength and courage to do this work. Secondly, I would like to thank my supervisor Prof. Dr. Adnan SÖZEN for his guidance, encouragement and the patience he demonstrated throughout the work.

Great thanks and respect to Gazi University, and head and staff of the Department of Energy Systems Engineering for their assistance and kindness.

My special thanks go to My Thesis Monitoring Committee (TİK) members, Kurtulus BORAN (Gazi University, Department of Energy Systems Engineering), and Assoc. Dr. İhsan TOKTAŞ (Hecetepe University Department of Mechanical Engineering).

Finally, my deep and sincere gratitude to my father and my mother, for their continuous and unparalleled love, help and support throughout my life and studies. My brother (Adeeb) and my sisters (Hind and Zainab), for their help and assistance

LIST OF CONTENTS

Page

ABSTRACT iv

ÖZET v

ACKNOWLEDGEMENTS vi

LIST OF CONTENTS vii

LIST OF TABLES x

LIST OF FIGURES xi

NOMENCLATURE xv

1. INTRODUCTION 1

2. LITERATURE REVIEW 5

2.1. Air-to-Air Heat Exchanger System 5

2.2. Concentric Tube Heat Exchanger System (Parallel and Counter Flow Regimes) 7

2.3. Thermosyphon Natural Convection Heat Pipe Heat Exchanger System 14

3. MAGNETIC NANOFLUIDS AND THERMOPHYSICAL PROPERTIES 27

3.1. Mono Magnetic Nanofluids 28

3.1.1. Thermal conductivity 28

3.1.2. Specific thermal capacity 28

3.1.3. Viscosity 29

3.1.4. Density 29

3.2. Hybrid Magnetic Nanofluids 30

3.2.1. Thermal conductivity 30

3.2.2. Specific thermal capacity 30

3.2.3. Viscosity 31

3.2.4. Density 31

Page

3.3. Preparation of the Magnetic Nanofluids 32

4. EXPERIMENTAL PROCEDURE 35

4.1. Air-to-Air Heat Pipe Heat Exchanger System 35

4.2. Concentric-Tube Heat Exchanger Apparatus (Parallel and Counter Flow Regimes) 37

4.3. Heat Pipe Thermosyphon System 39

5. THEORETICAL ANALYSIS 43

5.1. Mono Magnetic Nanofluids In (Air-to-Air) Heat Pipe Heat Exchanger System 43

5.2. Mono and Hybrid Magnetic Nanofluids in Concentric Tube Heat Exchanger System (Counter and Parallel-Flow Regimes). 44

5.3. Mono and Hybrid Magnetic Nanofluids in Thermosyphon Natural Convection Heat Pipe 47

5.4. Modeling Thermosyphon Natural Convection Heat Pipe System Utilizing MATLAB/Simulink® Software 51

5.4.1. Thermal-network modelling 51

5.4.2. Correlations of heat transfer coefficients 55

5.4.3. Numerical simulation approach 57

5.4.4. PID control system 58

6. RESULTS AND DISCUSSIONS 61

6.1. Results From (Air-to-Air) Heat Pipe Heat Exchanger System 61

6.2. Results From Concentric Tube Heat Exchanger System (Parallel And Counter Flow Regimes) 66

6.2.1. Wall temperature distribution (°C) 66

6.2.2. Overall heat transfer coefficient (U) 68

6.2.3. Heat transfer coefficient in the hot stream (h_{hot}) 70

6.2.4. Heat transfer coefficient in the cold stream (h_{cold}) 72

6.2.5. Heat transfer coefficient ratio and improvements 74

Page

6.2.6. Performance index (Efficiency %) 77

6.2.7. Nusselt number 79

6.3. Mono and Hybrid Magnetic Nanofluids in Thermosyphon Natural Convection Heat Pipe 81

6.3.1. Wall temperature distributions 81

6.3.2. Thermal efficiency 84

6.3.3. Thermal resistance 85

6.3.4. Nusselt number 87

6.4. Modeling Thermosyphon Natural Convection Heat Pipe System Utilizing MATLAB/Simulink® Software 90

6.4.1. Evaporator and condenser surface temperature 91

6.4.2. Thermal resistance 98

6.4.3. Nusselt number 99

6.4.4. Efficiency 101

7. CONCLUSIONS 103

REFERENCES 105

CURRICULUM VITAE 115

LIST OF TABLES

Table **Page**

Table 2.1. A brief description for research's previous works. 18

Table 3.1. Products specifications. 27

Table 3.2. The constants' values in Eq. 3.3 for Fe_3O_4, Fe_2O_3, and $NiFe_2O_4$ nanoparticles 29

Table 3.3. Chemical composition of $NiFe_2O_4$, Fe_2O_3 as well as Fe_3O_4. 32

Table 5.1. Controller parameters. 59

LIST OF FIGURES

Figure **Page**

Figure 3.1. TEM image of a) Fe_3O_4, b) $NiFe_2O_4$, c) Fe_2O_3 mono-magnetite nanoparticles. 28

Figure 3.2. Experimental and Theortical density diviation..... 32

Figure 3.3. The preparation process of the nanofluid suspensions..... 33

Figure 4.1. The schematic drawing for air-to-air heat pipe heat exchanger experimental Device 36

Figure 4.2. Experimental Rig of the Concentric-Tube Heat Exchanger Sistem..... 38

Figure 4.3. Schematic diagram of the experimental setup..... 39

Figure 4.4. Schematic diagram of the thermocouple's distribution..... 40

Figure 5.1. Schematic Diagram for a) Counter-regime b) Parallel-regime Concentric Tube Device..... 47

Figure 5.2. Schemetic diagrams for thermal resistance-network throgh the (a) condenser part also (b) evaporator part. 52

Figure 5.3. Thermosyphon-system schematic diagram 53

Figure 5.4. Heat pipe system simulation using MATLAB/Simulink®. 58

Figure 5.5. Simulated input power 200W, 300W, and 400W applying PID controller.. 60

Figure 5.6. Evaporator temperature Simulation of 2 independent PID controller regimes. 60

Figure 6.1. Estimated temperature amounts at diverse areas along heat pipe wall under magnetic nanofluid and pure water at (1 wt. %) and 2 KW input heat..... 61

Figure 6.2. Estimated temperature amounts at diverse areas along heat pipe wall under magnetic nanofluid and pure water at (1 wt. %) and 2 KW input heat..... 62

Figure 6.3. Comparison of wall temperature under magnetic nanofluids and pure water at 2KW input heat. 62

Figure 6.4. Comparison of wall temperature under magnetic nanofluids and pure water at 2KW input heat. 63

Figure 6.5. Comparison of improvement rates and efficiency amounts for magnetic nanofluids and pure water under rising Re Number. 65

Figure **Page**

Figure 6.6. Comparison of improvement rates and thermal resistance amounts for magnetic nanofluids and pure water throughout rising Re number. 65

Figure 6.7. Temperature deviation during counter-flow along the system under 14629.6 Re Number of coolant as well as 27161.6 Re Number of hot fluid. 67

Figure 6.8. Temperature deviation during counter-flow along the system under 14629.6 Re Number of coolant as well as 27161.6 Re Number of hot fluid. 68

Figure 6.9. Overall heat transfer coefficient as a function of Re Number at parallel-flow regime under 10 g/s coolant mass flow. 69

Figure 6.10. Overall heat transfer coefficient as a function of Re Number at counter-flow regime under 10 g/s coolant mass flow. 70

Figure 6.11. Heat transfer coefficient in hot stream as a function of Re Number at parallel-flow concentric tube heat exchanger system under 10 g/s coolant mass flow..... 71

Figure 6.12. Heat transfer coefficient in hot stream as a function of Re Number at counter-flow concentric tube heat exchanger system under 10 g/s coolant mass flow..... 72

Figure 6.13. Cold stream heat transfer coefficient as a function of Re Number at parallel-flow concentric pipe heat exchanger system under 10 g/s coolant mass flow..... 73

Figure 6.14. Cold stream heat transfer coefficient as a function of Re Number at counter-flow concentric pipe heat exchanger system under 10 g/s coolant mass flow.....

Figure 6.15. Heat transfer coefficient ratio as a function of Re Numbers at parallel-flow concentric pipe system under 10 g/s (coolant mass flow).... 75

Figure 6.16. Heat transfer coefficient ratio as a function of Re Numbers at counter-flow concentric pipe system under 10 g/s (coolant mass flow).... 76

Figure 6.17. nHeat transfer coefficient enhancement amount in Cold and Hot Streams within parallel systems for both poly and Hybrid magnetic-nanofluid..... 76

Figure 6.18. Thermal efficiency as a function of Re Number through parallel-flow concentric tube system at 10 g/s coolant mass flow..... 78

Figure 6.19. Thermal efficiency as a function of Re Numbers through counter-flow concentric tube system at 10 g/s coolant mass flow rate..... 78

Figure 6.20. The Nu number of poly and poly and hybrid magnetic-nanofluid corresponds to water at counter and parallel-flow concentric tube heat exchanger design. 80

Figure **Page**

Figure 6.21. Nu number of pure water poly and hybrids magnetic-nanofluid at counter and parallel-flow concentric tube heat exchanger design under various Re numbers. 80

Figure 6.22. Comprising among empirical and experimental Nu numbers for Fe_3O_4@Fe_2O_3/PW hybrid nano-fluid. 81

Figure 6.23. Test outcomes of wall temperatures under all operating requirements (a. 200W, b. 300W, and c. 400W) intake heat. 83

Figure 6.24. System efficiency in relation to supplied heat as well as mass flow..... 85

Figure 6.25. Heat pipe thermal resistance reduction percent in both operating fluids within changing operating conditions. 86

Figure 6.26. Average Nu number varies depending on the weight percentage. 88

Figure 6.27. Comparison among theoretical and experimental findings for the Nu number. 89

Figure 6.28. Nanofluid Nu number varies in relation to Rayleigh number and heat supply. 89

Figure 6.29. Base fluid with magnetic-nanofluid proportion versus weight percentage. 90

Figure 6.30. Difference between the predicted and observed magnetic-nanofluid density. 91

Figure 6.31. The Evaporator's temperature as a function of mass flow rate and time and at variance exposed power (a) 200W (b) 300W, & (c) 400W. 94

Figure 6.32. Temperature fluctuation and mass flow rate across the heat pipe wall at various input powers (a) 200W & (b) 400W. 96

Figure 6.33. Comparison between the MATLAB/Simulink model outcomes against experimental findings of evaporator temperature. 97

Figure 6.34. Deviation in the condenser and evaporator's wall temperatures acquired by MATLAB/Simulink model as a function of time. 97

Figure 6.35. Condenser and Evaporator mean wall temperature variance at all operating states. 98

Figure 6.36. Experimentally and empirically estimated thermal resistant as a function of mass flow rates and input powers. 99

Figure 6.37. Ratio of Nu number of magnetic-nanofluids to pure water related to delivered heat and Ra Number. 100

Figure 6.38. Verification of simulated & experimental Nu number. 101

Figure **Page**

Figure 6.39. System’s efficiency as a function of mass flow rate as well as intake heat. 102

NOMENCLATURE

The symbols and abbreviations used in this study are presented below along with their explanations.

Symbols	Explanation
A	Heat transfer area, (m^2)
c_p	Specific heat, (J/kg K)
D	Diameter, (m)
D_h	Hydraulic diameter, (m)
h	Heat transfer coefficient, (W/m^2K)
k	Thermal conductivity, (W/m k)
lpm	Liters per minute, (lpm)
$\dot{m}$	Mass flow rate, (kg/s)
$\dot{Q}$	Heat transfer rate, (W)
Re	Reynolds Number, (unitless)
T	Temperature, (°C)
t	Temperature, (K)
ΔT_{ln}	Log mean temperature difference, (°C)
ΔT	Average temperature difference, (°C)
U	Total heat transfer coefficient, (W/m^2K)
$Nu_{nf(TH)}$	Theoretical Nusselt Number of hybrid and mono-magnetic nanofluid, (unitless)
$Nu_{w(TH)}$	Theoretical Nusselt Number of water, (unitless)
$Nu_{(EXP)}$	Experimental Nusselt Number, (unitless)
$Nu_{f(TH)}$	Theoretical Nusselt number of the working fluid, (unitless)
Pr	Prandtl Number, (unitless)
Pe	Peclet Number, (unitless)
PW	Pure Water
$NiFe_2O_4$	Nickel ferrite

Symbols	Explanation
$\mathbf{V_{avg}}$	Average velocity, (m/s)
L	Length, (m)
$\overline{Nu}_{Exp}$	Average Nusselt number experimental, (unitless)
r	Radius, (m)
R	Thermal resistance, (W/m^2K)
$\bar{h}$	Average heat transfer coefficient, (W/m^2K)
$R_{coolant,conv}$	Coolant convective thermal resistance, (W/m^2K)
$R_{c,w,cond}$	Conduction thermal resistance of the condenser wall, (W/m^2K)
$R_{c,conv}$	Convective thermal resistance in the condenser section, (W/m^2K)
$R_{res,cond}$	Conduction thermal resistance of the electrical resistance wall, (W/m^2K)
$R_{evap,w,cond}$	Conduction thermal resistance of the evaporator wall, (W/m^2K)
$R_{evap,conv}$	Convective thermal resistance in the evaporator section, (W/m^2K)
t	Time, (s)
$T_{evap(avg)}$	Evaporator average temperature, (°C)
$T_{c(avg)}$	Condenser average temperature, (°C)
B	Thermal capacity, (J/°C)
g	Acceleration due to gravity, (m/s^2)
P	Pressure, (pa)
q	Heat transfer flux, (W/m^2)
r	Radius, (m)
ODE	Ordinary differential equation
coolant	coolant
m	Component interface
n	Component interface
I	Integral

Symbols	Explanation
D	Differential

Greek Symbols	Explanation
τ	Time constant, (s)
β	Coefficient of thermal expansion, (1/°C)
η	Efficiency, (%)
φ	Weight percent, (wt. %)
μ	Dynamic viscosity, (Pa.s)
$\emptyset$	Total weight percent, (%)
ρ	Density, (kg/m^3)

Subscripts	Explanation
b	Base fluid
o	outlet
i	inlet
rnf	Regular magnetic nanofluid
rnp	Regular magnetic nanoparticles
nf	Nanofluid
$h(mnf)$	Hybrid magnetic nanofluid
Fe_3O_4	Iron-oxide
Fe_2O_3	Ferric-oxide
T	Total
hot	Hot stream
$cold$	Cold stream
th	Thermal
con	Condenser
evp	Evaporator

Subscripts	Explanation
ex	External
in	Internal
ca	Cold air
d	Heat transfer area (outer), (m^2)
ha	Hot air
u	Useful
w	Cooling fluid
res	resistance
c,a	condenser average
c,w	condenser wall
e,a	evaporator average
l	liquid phase
v	vapor phase
lv	phase change
s	saturated
a	atmosphere
exp.	experimental

1. INTRODUCTION

Energy is one of the most essential inputs for the socioeconomic expansion of countries. Energy resources are very significant in terms of economic and social development. People's demand for energy resources and energy consumption increased with the Industrial Revolution and this increase; population growth has continued with industrialization and urbanization. A large part of this energy needed in the world is obtained from fossil resources. Fossil fuel resources are used intensively in every field in our daily life [1]. The energy demand is growing by about 4-5% from year to year, however, the fossil fuel reserve used to meet the majority of the energy need is rapidly decreasing. In order to solve this problem and to ensure that the existing energy resources can be used more efficiently, the countries of the world, which are more developed in terms of technological innovations and developments, have concentrated on conceiving this problem by looking for new resources.In order to be able to compete with other developed and developing countries in terms of energy, it has gained great importance to use energy more efficiently. It is obvious that the efficient use of energy will contribute significantly to the reduction of energy costs and environmental pollution in the industrial sector, in addition to its numerous benefits to the world. For this reason, studies in the field of efficient use of energy in a global context are of great importance. However, researches on improving heat transfer and increasing the performance in both the technological products we use in our daily life and the heat exchangers, heat pipes, and heat recovery units used in the industry have become widespread and remarkable studies [2].

Heat transfer improvement studies, which are gaining importance today, have a very significant spot in the industrial field and in terms of energy savings. Conventional working fluids (such as water, oil, ethyl alcohol, and air), in industrial, air conditioning, heating, cooling, electronics, etc. play an important role. However, the low heat transfer properties of these conventional working fluids used in heat transfer systems are one of the major obstacles in terms of efficiency enhancement [3]. Various methods have been employed in order to increase the thermal conductivity of the working fluids that are used in thermal systems. One of these methods was by adding Nano-sized solid particles into the base fluid (i.e. the conventional working fluids).These types of fluids have also played an important role in increasing heat transfer efficiency and convection heat transfer coefficient compared to conventional fluids. These working fluids containing magnetic Nano-sized solid particles

are called magnetic nanofluids. Heat pipes are a kind of heat transfer apparatus consisting of three basic parts called the evaporator, adiabatic, and condenser region, in which some fluid is prepared by charging after vacuuming. The evaporator is also called the evaporator zone, where the heat is absorbed by the working fluid from an outside heat source. The region where the heat transfer to the outer environment occurs is called the condenser, and the neutral region in the middle where there is no heat exchange is called the adiabatic part. Various heat exchangers are used for heat recovery, and heat pipe heat recovery units are commonly preferred in recent years.

The aim of This study is to improve the thermal performance and consequently to increase the thermal efficiency of three thermal systems: air-to-air heat pipe heat exchanger system, concentric tube heat exchanger system (parallel and counter regimes) as well as thermosyphon natural convection heat pipe system, with magnetic nanofluids formed by adding different metal oxide particles in Nano size to the conventional working fluid by various methods. Due to these developed working fluids, the particles dispersed in the base fluid increase the surface area and the heat-holding capacity of the working fluid. Thus, the heat transfer capacity of the system is also increased [4].

The aim of this thesis is to study the effects of utilizing different types of magnetic nanofluids (mono and hybrid magnetic nanofluids) on the performance of thermal systems, which was achieved by applying an experimental and numerical study to improve the working fluid by adding magnetic nanoparticles to the base fluid. As a result of the experiments that were carried out with these three systems: the efficiency comparisons of the system under magnetic nanofluids have been done at different input heat powers, cooling fluids flow rates, and various inlet temperatures of the evaporator zone were observed. Moreover, these magnetic nanofluids were prepared with two concentration ratios (1 wt. % and 0.5 wt. %). Experimental data were obtained based on the operating conditions that were applied for each system.

The thermal characteristics of the three thermal systems were evaluated according to the experimental and numerical results. This thesis proposed: Introduction in the first chapter, a literature review in the second chapter, Magnetic nanofluids and their thermophysical properties in the third chapter, detailed information about the experimental procedure and experimental setup, in the fourth chapter, a complete theoretical analysis for each system in

the fifth chapter. Results and discussion in the sixth chapter, conclusions in the seventh chapter.

Looking at the literature review, there is not much research on the use of mono and hybrid magnetic nanofluids for the efficiency improvement of thermal systems. However, today, studies on heat transfer improvement of magnetic nanoparticles continue increasingly. To close this gap in the literature and to contribute to the studies on alternative working fluids, the contribution of this study to the literature is to increase the thermal performance by using iron oxide-ferric oxide (Fe_3O_4@Fe_2O_3/PW) hybrid magnetic nanofluid and iron oxide (Fe_3O_4/PW), ferric oxide (Fe_2O_3/PW), nickel ferrite ($NiFe_2O_4$/PW) mono magnetic nanofluid and pure water in air-to-air heat pipe heat exchanger system, concentric tube heat exchanger system as well as natural convection heat pipe system. According to the experimental and numerical results, the performance of each system has been conducted.

2. LITERATURE REVIEW

Due to their great contribution to thermophysical properties of the traditional base fluids, nanofluids have often been utilized lately for enhancing the thermal performance of heat transfer devices operating with a working fluid. Such nanoparticles which are of magnetic specifications as iron has been using in nanofluid preparation and they are generally called magnetic nanofluid.

2.1. Air-to-Air Heat Exchanger System

As modern technology is rapidly evolving, choosing effective and environmentally friendly tools has become crucial for sustainability. It has been observed that many researchers have a propensity to improve the efficiency of the traditional systems in the context of this objective. Implementations for heat recovery become more significant in this context while the thermal systems that experience significant heat loss have been taken under consideration. Since they are affordable and don't cost a lot to set up and maintain, air-to-air heat pipe heat exchangers are one of the frequently used devices for recovery heat energy through air flowing across a channel [5,6]. The temperature differential between the two air channels has a significant impact on the thermal performance of those passively heat exchangers, as well as the resultant heat recovery rate. Even though the heat recovery for such devices can be simple in situations with greater temperature differences, it will become increasingly difficult as the variation specified narrows. Due to this feature, it is possible to improve the performance of heat pipe that is being used, which enables heat recovery to take place despite lower temperatures. Previous studies have shown that nano-fluids suspensions, whether they use unary or hybrid nanoparticles, can improve the heat transfer properties of heat pipes.

As an example, Parametthanuwat conducted an empirical investigation to ascertain the impacts of nanoparticles of silver upon the thermal enactment of two-phase, thermosyphon operating under various temperature conditions. They looked explored the effects of recharging rate, aspect ratio, and inclined (tilt) angle upon the thermal enactment in a two-phase thermosyphon. Their research revealed that although the charge rate had no impact on thermophysical parameters of the operating fluid within a vertical oriented thermosyphon system, the amount of heat transfer was improved [7].

Using a numerical analytical method, Allouhi and Benzakour Amine looked at how well the heat pipe flat- Plate solar collector performed when used with three distinct nanofluids of TiO_2, Al_2O_3, and CuO nanoparticles. The one-dimensional instantaneous heat transfer theory was taken into consideration in the numerical description they offered. They discovered that the reduced specific heat an amount of the nano-fluids was key to the improvement in thermal stability. They were able to increase the energy and exergy efficiency of CuO/PW water nano-fluid by a highest of 11.1% and 2.7%, accordingly. They claimed that applying of nanofluids may increase the heating efficiency of photovoltaic collectors, as well as the CuO/PW nano-fluid had been the best operating fluid in terms of both energy and exergy performance [8].

Fe-CuO/PW nano-fluid was used as the operating fluid in a basic heat pipe during an empirical study carried out by Martin et al. They created a pure water-based hybrid nano-fluid at an amount of 2%, using FeCuO within a 50:50 mixture. They came to the conclusion that hybrid nano-fluids are able to be used as the operational fluid within heat pipes to achieve larger increases in efficiency and decreases the thermal resistance in comparison to ordinary heat pipes [9] after conducting their tests under different operating circumstances (mass flow rates, heating powers, etc.).

When dealing with several FeO/PW nanofluids suspensions that which formed at three distinct volume concentrations, Huminic and Huminic investigated the thermal behavior of two-phase thermosyphon. They examined the effects of concentrations rates and tilt degree on heat transfer enactment and came to the conclusion that nano-particles had a significant role to play in enhancing the heating capacity of these devices [10].

The heating capacity of an aquatic nanofluid-operated sintering wicking heat pipe was investigated by Sadeghinezhad et al. They put both pure water operating fluid or 0.1 weight percent graphene nanoplatelet nano-fluids into a heating pipe to examine it. The trials used different heating powers that range (20W - 80W) and inclinations of (0^{o} - 60^{o}). They discovered that, in comparison to pure water, the largest decrease in heating resistance being 48.4%. Additionally, for the 60^{o} inclination position, the largest improvements in thermal conductivity occurred at 28.3%, 37.2%, 29.8%, 23.4% under heating amounts of (80, 60, 40, and 20 W) [11].

Titania and silica nano-fluid heat transfer characteristics according to conditions of turbulent flow were studied by Nabil et al. They created experimental nano-fluids utilizing the two-step approach, changing the quantities as (0.5% - 3.0%), and mixed the nano-particles 50:50 before performing a number of forced convective heat transfer studies. The operational temperatures of their device had been 70°C, 50°C, and 30°C, with a continuous heat flux. They employed a water/ethylene glycol (60:40) mixture in base fluid. The results of their experiments showed that the highest augmentation of around 81% at convective heat transfer was accomplished when hybrid nano-fluid was used in place of base fluid. They also came to a conclusion that methods may be developed to increase the pace of heat transmission of any increase in temperature amount, as well as in volumetric concentration [12].

There are more of these research that demonstrate how simple binary and hybrid nano-fluids enhance the efficiency of heat pipes [13-18]. On the contrary, other research have found that using nanofluid suspensions increased AAHX performance. In another investigation, Sözen et al. used an experimental analysis to determine the thermal efficiency of a recuperator, a type of heat recovering unit, which has a number many heat pipes arranged in an asymmetrical arrangement and uses fly ash as unary nanofluids. To combat flocculation and sediment issues, Triton X-100 was added into their 2 vol. % nano-fluid mixtures to serve as surfactants. They determined that nano-fluids are able to be promoted instead of pure water with improving the efficiency using such structures after evaluating the effectiveness of both hot and cold air channels for every nano-fluid and foundation fluid [19].

Aytaç et al. carried out an empirical investigation using spinel oxide-based nanofluids to improve the heat transfer properties of a heat recovery unit that incorporates an air-to-air heat exchanger system. They created water-based nanofluids using spinels like $ZnOAl_2O_3$, $MgOAl_2O_3$, and $FeOAl_2O_3$ and conducted a series of tests. Their research showed that using $FeOAl_2O_3$/PW nanofluids as an operational fluid led to a heat recovered rate of about 92% [20].

2.2. Concentric Tube Heat Exchanger System (Parallel and Counter Flow Regimes)

For thermal systems, heat exchangers are used in a wide range of ways. To increase the performance of such devices, active and passive techniques are frequently used [21]. An external source must be present for the active approach, such as the introduction of an

electrical field, pulsing flow, oscillating heat transfer surfaces, etc. The passive approach, on the contrary, does not require another source. This technique uses swirling equipment, vortex generators, however, stretched surfaces, artificial roughness, and more [22]. However, these methods could result in an increase in drop in pressure and pollution, which would significantly affect the thermal characteristics of heat exchangers. Another passive technique that can improve thermal performance and doesn't result in a significant pressure decrease is the usage of instead of using common fluids, use nanofluid. Numerous studies have used nanofluids in various types of heat exchangers. For example;

Kavitha et al. operated copper oxide nano-fluid within DPHES [23].

Sundar et al. examined the exergy efficiency and thermal entropy through a plate heat exchanger operating diamond/PW nano-fluid [24].

Somasekhar et al. created a CFD-simulating model for a shell and pipe heat exchanger utilizing nano-fluids including Al_2O_3 nano-particles [25].

Huang et al. achieved an analysis for finding out the consequences of hybrid nano-fluids on the enactment of plate heat exchangers [26].

Alklaibi et al. investigated the enactment of a PHE by operating a hybrid nano-fluid including multi-walled carbon nanotubes as well as iron oxide nanoparticles [27].

Sarafraz et al. strived to examine pressure drop and coefficient of heat transfer of a counter-flow doubled tube heat exchanger filled by carbon nano-tube/PW nano-fluid within their study [28].

Babat et al. experimentally investigated the thermal enactment of an air heat pipe system under employing magnetic-nanofluid [29].

The thermal efficiency regarding heat exchangers is improved by using magnetic-nanofluids to be operating fluids. Several of the few investigations that were conducted in this area are explained below;

Vermahmoudi et al. conducted a laboratory study of the effects of replacing pure water with magnetic -nanofluid within an air-finned heat exchange system. Fe_2O_3/PW, with volume percentages up to 0.65%, 0.4%, and 0.15% as well as volumetric flow rates ranging (0.2– 0.5) m^3/h, served as the magnetic-nanofluid used for the present investigation. The cool air flow rates were increased by (740 to1009) m^3/h. The temperatures of the hot fluid inlets were 50 °C, 65 °C, and 80 °C. Convective heat transfer coefficients and total heat transfer coefficients both experienced the largest increases, at 11.5% and13% respectively [30-43].

Fe_2O_3-CNT/water hybrid nano-fluid with volume percentages of 0.2%and 0.1% was used by Aghabozorg et al. to test the effectiveness of a heat exchanger under laminar-transient-turbulent settings. The structure is comprised of a copper tube with interior diameter approximately 11.42 mm & a length about 793 mm. A supply of 150, 120, and 80 volts AC provided the heat flow. Five thermocouples have been fastened to the tube walls in order to measure temperature values. 3 various rates of flow, 3.43, 2.25, and 0.96 lpm, were employed with the system for cooling. According to research, utilizing Fe_2O_3-CNT/water to be the operating fluid increased the convective heat transfer coefficient as much as 27.69% and 13.54% at 0.1% volume percentages under turbulent and laminar circumstances. When the volumetric percentage reached 0.2%, the improvements in rate corresponding to laminar and turbulent circumstances, were and 37.5% and 34.02% respectively. In this case, the AC voltage measurement was 150V [44].

In a doubled tube heat exchanger with a bend Kumar and others conducted an investigation to determine the effects of using magnetic-nanofluid upon total heat transfer coefficients. In this study, a volume proportion of 0.06% and 0.005% containing Fe_3O_4/PW was employed as the operating fluid. Although the volume flow and cool water temp. Were modified up to 8 lpm and 29 °C, accordingly, the magnetic nanofluids intake temperature was set at 60 °C and the volumetric flow rate changed from 8 lpm to 14 lpm by a period of 2 lpm. The findings demonstrated that at a volumetric proportion associated with water of 0.06%, the total coefficient of heat transfer rose to 3.44% [45].

For various amounts with the volumetric percentage of the magnetic-nanofluid made of iron oxides and pure water, Kumar and others empirically examined the convective heat transfer coefficient and friction factor. A double-pipe heat exchange

device was employed in the structure. The pipe had an inside diameter approximately 0.019 meters & an exterior diameter about 0.05 meters. The pipe was 5 meters long. Cold water has been utilized in the exterior tube to provide refrigeration when magnetic-nanofluid made of Fe_3O_4 mixed with water, flows through the internal pipe. Experiments were run for various volume percentage values, including 0.06, 0.03, 0.01, and 0.005%. The outcomes demonstrated that with 0.06% volume percentage and 28970 Re Number, the Nu Number increased approximately up to 14.7%. As Re Number and volume percentage boosted the friction factor improved were 1.079 and 1.092 times, when the Re Numbers was 16,545 and 28,954 respectively, as well [46].

Baba et al. first described the use of magnetic-nanofluids to improve heat transmission in a doubled tube heat exchanger device with internal fins. Fe3O4 nanoparticles were present in the nanofluid utilized in this investigation at volume percentages of 0.4, 0.2, 0.1, 0.08, 0.06, 0.04, and 0.02 %. The investigation is conducted in accordance with predetermined guidelines. Hot fluid flowed at a steady mass flow about 40 lpm while maintaining a temperature about 90 °C. Additionally, the mass flow varied between (2-14) lpm whereas the nanofluid temperature remained fixed at 31 °C. The results showed that magnetic-nanofluid about 0.4% percentage of volume improved their heat transfer rate by approximately 90% to 80%. When utilizing fins, the friction factor is increased by 3–4 times throughout the volume portion equal to 0.4%, and the convective heat transfer coefficient improves with volumetric percentage [47].

The enhancement in heat transmission for three distinct straight channels—circular, square, and triangular—with various cross-sectional areas was theoretically examined by Abdulwahab et al. Fe3O4/PW nano-fluid with volume fractions of 0.6%, 0.4%, and 0.2% were the operating fluid. Each of the tubes had a hydraulic diameter approximately 0.01 meters. To examine the impacts of nano-particles, flow rate, and volumetric fraction, on the convective heat transfer coefficient and friction factor, an initial heat flux equal 5000 W/m2 was applied across the wall. The numerical investigation made employing CFD software, which also includes FLUENT and GAMBIT. The results showed that when Re Number climbed, convective heat transfer coefficient did as well. At 0.6% volume percentage, the curved tube showed the highest amount of the convective heat transfer coefficient. On the contrary, the friction factor fell when the

Re Number elevated in every case, while a circular tubes also showed a decrease in terms of friction factor [48].

In comparison to pure water, Zheng et al. evaluated the effects of utilizing other operating fluids upon the thermal efficiency for plate heat exchanger within a solar system. Working fluids included Al_2O_3, SiC, CuO, and Fe3O4 dispersed in pure water with volume fractions of 1, 0.5, 0.1, and 0.05%. The volumetric flow range (3–9) lpm. These nanoparticles had diameters of 25, 30, and 40 nm, respectively. As Fe_3O_4/PW was employed to be the operating fluid with a percentage of volume equivalent to 1% & 8 lpm volumetric flow, an optimal improvement was achieved. Under such conditions, the amount of pressure drop increased by 10.1% whereas the greatest increase in the convective heat transfer coefficient had been 30.8% [49].

Many varieties have been set aside to improve heat transport as thermal engineering and thermo-science show indications of advancement. Typically, one of them involves the condiments to fluids procedure. Particles with ferromagnetic qualities are dispersed into the base fluids which change the fluids' vehicle features, flow, and heat transfer qualities such that the operating fluid kind can influence the aspect of limiting heat transfer performance [50].

Many varieties have been set aside to improve heat transport as thermal engineering and however, compared to failures with micron- or millimeter-sized nanoparticles, the number of investigations on heat transmission of combined magnetite nano-metal oxides within fluids was constrained due to related technical issues throughout the area of thermal engineering. Similar to large particles, they can cause severe problems with the machinery that is often employed for heat transfer. Particularly, biggish suspended particles are more likely to aggregate than microscopic particles. Therefore, traveling through narrow channels could result in severe congestion and significantly increase the pressure drop. Additionally, these particles' irritating movements cause corrosion in produced components and tubes [51].

Choi was the first to include nanoparticles into conventional fluids and provided a considerable improvement in the fluid's thermophysical characteristics, which included friction factor, thermal conductivity [52], as well as heat transfer implementation for counter-flow double-pipe heat exchanger using NDG/PW has been investigated by

Goodarzi et al. For the estimations of Re Number, that ranged (5000-15,000), and Nano-sheet concentration, that ranged (0-0.06) wt.%, an innovative MATLAB approach was utilized. The capability of the fundamental fluid to transport heat could be improved by an increase in the Re number or concentrations ratio of particles. For instance, adding 0.06 weight percent of particles to the fundamental fluid led into a 15.86% increase in the convective coefficient of heat transfer for pure water. About 16.2% on average, heat transfer coefficient increased. As a result, the implementation of double-pipe heat exchangers is greatly improved when NDG/water is used to be the operating fluid [53].

Sözen et al. observed an enhancement in heat transfer using a cross and parallel-flow centric tube exchanger using a fly-ash nano-fluid & 2 wt. % alumina. When fly-ash nano-fluid was used to be the operating fluid within the system, significant improvements were made to the efficiencies of both the counter and parallel-flow centric heat exchanger tube devices, resulting in 6.9% and 31.2%, respectively. Both heat exchanger's heat efficiency had been enhanced by roughly 2.8%and 5.1%, respectively, while using alumina nano-fluid in the system's operating fluid [54].

The effect of employing Al_2O_3/PW upon the heating capacity of a doubled tube heat exchanger was analytically investigated and assessed by Bahmani et al. using the (finite-volume) technique. The working fluid's percentage, which ranged as a range of (0-10) % within a 2% intervals. The theoretical study's findings showed that increasing the nanoparticle volume percentage significantly improved the convective heat transfer coefficients and Nu number. Moreover, the Re number has increased. Thermal efficiency increase the highest average Nu number have been established to be 32.7% and 30%, respectively. Additionally, increasing the nano-particle proportion resulted in a substantial increase within the operating fluid output temperature and wall temperatures also [55].

Shahsavar et al. The effects of the hybrid nano-fluid upon the thermal efficacy of a counter-flow heat exchanger device were investigated. Throughout the tube's interior, the hybrid nano-fluid operates as a cooler while hot water runs through the annular side. The hybrid nano-fluid was made using tetramethylammonium hydroxide-coated Fe_3O_4 nano-particles and carbon nano-tubes, two different types of nanoparticles. The results demonstrated that the non-Newtonian hybrid nano-fluid consistently displays a higher heat effectiveness, heat transfer coefficient, heat transfer percentage, the Newton's hybrid

nano-fluid; however, the Newtonian hybrid nanofluid was right in terms of pressure drop, circulating power, as well as performance rating standard. The computation of the 9.71%-1.5% pressure drop, 9.71%-1.5% pumped power, as well as 19.60%-18.24% evaluation of performance criteria leads to a large inaccuracy since the Fe_3O_4-carbon nanotube/PW hybrid nano-fluid represents a Newtonian liquid having consistent viscosity and thermal conductivity [56].

The performance of dual-pipe heat exchanger using Al_2O_3-TiO_2 hybrid nano-fluid was mathematically examined by Maddah et al. Praised equations were used to verify the conclusion. The hybrid nano-fluid dual-pipe heat exchanger's energy efficiency was determined using a full factorial functional structure system. Operating parameters included a concentration ratio of among (0.2-1.5), a Re number of among (3000-12000), and a twisted percentage around 2 to 8. To identify the significant important variables related to exergy efficiency, estimation of statistics using the Student's t-test, variance estimation, F-test, as well as lack of fitting was accomplished. The use of nanotechnology and twisted tapes increased the exergy efficiency comparable to pure water as an operational fluid, according to the results. Additionally, raising the nanoparticle volume percentage and Re Number, along with. Higher energy efficiency could be produced by decreasing the bending ratio [57]

The effects of adding a unique curvature turbulator and using two different hybrid nano-fluids upon thermal performance within a helix doubled-pipe heat exchanger were quantitatively explored by Karouei et al. (MWCNT-Fe_3O_4/water) and silver and graphene nanoparticles/PW are both present in the operating hybrid nano-fluids. The present investigation is divided into two sections: initially, the results of using hybrid nano-fluids were equivalent to pure water during 0.3 vol. %. The hybrid nano-fluid created in the initial stage had been defined and used. Results show that using the present inventive turbulator leads to a higher heat transfer rate. Therefore, at lower mass flow rates, the Ag-HEG/water hybrid nanofluid has a more appropriate thermal enactment. Additionally, the examined helical heat exchange’s index factor, at 0.1 vol. %, is the most insufficient. The thermal enactment was at its peak at 0.7 vol. % [58].

2.3. Thermosyphon Natural Convection Heat Pipe Heat Exchanger System

Today, it is more important than ever before to generalize efficient power transformation processes, especially in industrial facilities. Thermic energy is transmitted through two mediums in commerce using a variety of heating techniques such heat pipes and heat exchangers, which are both widely regarded as effective. Due to their improved thermal performance, light weight, and low cost for construction and maintenance, the primary heat pipe system has over time developed multiple appropriate components for heat transmission. Due to their capacity for transporting large amounts of energy, these devices are used in numerous heat transmission procedures.

Due to temperature deviation that develops within a copper tube, a heat pipe was an item of equipment that transfers heating energy across two places in vacuum [59]. It normally has three domains: the evaporator, wherein heat is usually taken in by the working medium, and the condenser, which is the part wherein heat is discharged to the cooler. Additionally, no heat exchange mechanism was visible in the middle, where there was an adiabatic region. The installation of a heat pipe structure is greatly influenced by the type of working fluid used in them. As a result, in recent years [60] and [61], the adoption of an operational medium containing nanoparticles has begun to increase. Additionally, nanoparticles have been added to fuels as a supplement to increase implementation [62] in numerous studies, it was found through numerical and experimental evaluations that the use of nanofluids in particular improved the performance of the entire system.

Gürü et al. designed a heat pipe and conducted experimental study on the thermal behavior of the bentonite/PW working fluid. They prepared three distinct nanofluids, each containing a different concentration of nanoparticles (0.5, 2, and 4%), in order to determine how the thermal properties are affected by the concentration of these particles. They used pure water and three different bentonites with nanofluid combinations as the operating medium to examine the heat pipe's thermal properties, including index factor, thermal conductivity, and heating resistance, and they noted the ideal nanoparticle weight percent for improving the heat pipe's thermal properties [59].

By using a water-based CuO nanofluid, Venkatachalapathy et al. experimentally constructed a work to ascertain the thermic properties of a copper heat tube with a cylindrical form of

wick construction. In other tests, the inclination tilt and intake heating loads were also changed. With 1.5 wt. %, the pipe's resistance could be reduced by up to 23.83%. Additionally, at 1% weight for each nanofluid, a decrease of as much as 10.43% was made. When nano-particles were added to the fundamental fluid, it turned out that the evaporation and condensation heat transfer coefficients enhanced. As a result, it was discovered that CuO was the working medium within the system with the 60° tilting angle that produced the greatest amount of improvement in the heat pipe's thermal properties [63].

Additionally, Tharayil et al. examined the thermal characteristics of a tiny heat pipe that operated by injecting an aqueous nanofluid made of graphene. In this study, a heat pipe was experimentally evaluated by delivering a heat load to the evaporator part that ranged from 20 to 380 W. In this study, aqueous-graphene nanofluid and pure water were used as the operational mediums. Additionally, experiments were done to see how changing the weight percentage of the working fluid and the heat pipe's declination angle affected the thermal performance. According to the results of this experimental study, using nanofluid as an operating medium enhanced the heat pipe's thermal index factor and decreased the temperature in the evaporator region. Additionally, it was discovered that the ideal nanofluid. The biggest advancements in heat transport were revealed by the weight percent of 0.006 wt. % [64].

In an experiment conducted inside a copper natural convection heat pipe, Menlik et al. validated a nanofluid solution containing MgO nano-particles having a weight percent equivalent to 5%. It was discovered that the heat pipe's wall temperature, effectiveness, and heat resistance varied noticeably. The outcomes showed that using MgO nanofluid, which is equivalent to pure water, boosted the system's efficiency by 26% [65]. Sözen et al. investigated the effects of using nanofluids on the thermal characteristics of a two-phase closed thermosiphon. Nanoparticles made from combustion furnace slag were used for preparing the operating fluid for a series of studies under various experimental conditions. The results showed that using this kind of operating fluid in place of commercial ones increased the heat pipe's index factor about 22% [66].

Similar research was conducted by Sözen et al., who used experimental analysis to examine the effects of both the surface-active mechanisms and the insertion of nano-particles to the foundational fluid on the index factor for the natural convection heat pipe category. When

making the operating fluid, Triton X-100, Sodium Dodecyl Benzene Sulfonate, and TiO_2 nano-particles were added as separate surface-active mechanisms to pure water. A theoretical as well as experimental investigation into the nanofluid's surface tension was also conducted. On the contrary, there were no effects on the surfactants on the heat pipe's thermal conductivity, and the thermal system's heat resistance and improvements were greater than those of Triton X-100 [67].

Kiseev and Sazhin looked at the enhancement of heat transmission in a circulated-thermosiphon device powered with a nanofluid. In addition to using the metal nanoparticles to prepare the nanofluid mixture, researchers also examined the effects of nanoparticle diffusion within the fluid, preparation methods, operating fluid thermophysical characteristics, filled ratio, geometry, as well as the weight percentage of particles upon the system's thermal energy characteristics. Utilizing nanofluids that are identical to pure water might considerably increase heat transfer coefficients reaching up to 20% [68].

More severely than ever before [69] and [70] has the idea of efficiency in energy conversion techniques, notably in industrial facilities. It is generally advised in industry to move thermic energy between two mediums using a variety of heating techniques, such as heat pipes and heat exchangers [71-73]. Because of its high thermal performance, light weight, and low cost of development and maintenance, heat pipe systems in particular have developed into very practical devices for heat transport quickly [74]. Due to their capacity for transporting large amounts of energy, these machines are used in several heat transmission operations.

A heat pipe is a piece of machinery used to transfer thermal energy between two areas in vacuum situations as a result of temperature variations in copper pipes [59]. It typically consists of three parts: the evaporator, which supplies energy to the working fluid; the condenser, which transfers heat to the coolant. A diabetic region is also present in the center. There is no energy transmission during the adiabatic portion.

Su et al. used nanofluid in this investigation to look into heat pipe evacuated tube solar collector. The results demonstrated how the heat pipes' thermal efficiency increased when working with nanofluids. According to the analysis's findings, using nanofluids in evacuated tube solar collectors has the following benefits: higher temperatures for operation, increased thermal conductivity, and reduced thermal resistance [75].

The thermophysical properties of Indonesian fly-ash nano-fluid with thermal usage were empirically determined by Kenti et al. The results of the experiment showed that while specific heat was decreased, thermal conductivity, viscosity, and density improved by increasing nanofluid percentages. Fly ash's thermal conductivity was 3.9% more than that of SiO_2 [76]. In a tube containing fly ash-Cu hybrid nano-fluid, Kenti et al. performed empirical and theoretical research on heat transfer, entropy, and pressure reduction during turbulent flow conditions. For hybrids nano-fluid as well as fly-ash nano-fluid, the greatest increase within Nu number has been shown as being 57.1% and 8.95%, respectively, at 2.0 wt. % comparable to pure water. At a 2% concentration, it was discovered that the thermal efficiency factor could be improved to a maximum level up to 1.52 [77].

An artificially intelligent simulation on the thermal characteristics of Al_2O_3-CuO/PW hybrid nanofluids was created by Marulasiddeshi et al. The findings showed that under 1.0 vol. %, 60°C, and 30°C, respectively, Al_2O_3 nanofluid had a rise in thermal conductivity as well as viscosity of 14.6% and 6.5%, respectively. Al_2O_3 and Al_2O_3-CuO improved viscosity with a highest about 14.9% and 21.4%, respectively, when compared to pure water under 30°C and 1 volume percent [78].

The effects of micro-structure roughness on surface on the pool's boiling properties of TiO_2 nanofluid were investigated by Roodbari et al. According to the findings, increasing the nanofluid volume content to 0.005% caused a tendency for boiled heat transfer coefficients to increase, but less than that caused a decrease in heating surface roughness by 1.213 m. TiO_2 nanoparticle as well as water's interfacial thermal conductivity were studied by Roodbari et al. Kapitza conductivity went up 20% whereas the Lennard-Jones (LJ) potential's connection strength increased from 0.5 to 4 [80]. Within table 2.1, the researchers' works are briefly described.

Table 2.1. A brief description for research's previous works.

Authors	Magnetic nanofluids	Volume Fraction range	Dependent variables such as: Temperature, flow rate, heat flux ... etc.	Type of study	Obtained results
Parametthanuwat et al., 2010	silver nanoparticles	-	inclination (tilt) angle, charging rate, aspect ratio	silver nanoparticles in two-phase, closed thermosiphon	thermophysical characteristics of the working fluid provided improvement in heat transfer rate
Allouhi and Benzakour Amine, 2021	three different nanofluids of CuO, Al_2O_3, and TiO_2 nanoparticles	-	one-dimensional transient heat transfer model	performance of a heat pipe flat plate solar collector under three different nanofluids	The thermal efficiency of the solar collectors could be enhanced with the use of nanofluids, and, CuO/PW nanofluid was the most appropriate working fluid
Martin et al., 2020	Fe-CuO/PW	2 wt. %	heating powers, mass flow rates weight percent	nanofluid as the working fluid in a plain heat pipe	hybrid nanofluids can be employed as working fluid in heat pipes for achieving more increments in efficiency and decreasing in thermal resistance of the plain heat pipes
Huminic and Huminic, 2011	FeO/PW	-	influences of inclination (i.e. tilt) angle and	two-phase closed thermosiphon working with various nanofluid	Nanoparticles had a crucial situation for improvement of thermal performance of these instruments.

Table 2.1. (continue) A brief description for research's previous works.

Sadeghinezhad et al., 2016	graphene nano platelets pure water	0.1 wt. %	the tilt angles of 0º and 60º, and heating powers ranging from 20 W to 80 W	sintered wick heat pipe operating with an aqueous nanofluid	The maximum decline in thermal resistance, compared to pure water, was 48.4%. Moreover, for the 60º tilt angle, the maximum improvement in thermal conductivity value was 37.2% at 60 W heating power.
Nabil et al., 2018	titania&silica nanofluids in water/ethylene glycol (60:40 vol.)	0.5 to 3.0, vol. %	operating temperatures of 30°C, 50°C, 70°C, and constant heat flux	heat transfer properties of titania&silica nanofluids under turbulent flow conditions	a maximum enhancement rate of 81% in convection heat transfer was achieved
Sözen et al., 2019	alumina as well as fly ash	2 vol. %	Concentration ratio as well as input power	experimentally analyzed the thermal performance of a recuperator	Nanofluids can be preferred in place of pure water for the performance enhancement of such systems.
Aytaç et al., 2020	$ZnOAl_2O_3$, $MgOAl_2O_3$, and $FeOAl_2O_3$ to prepare water-based	2 vol. %	Various type of spinel oxide-based nanofluids	empirical study via spinel oxide-based nanofluids	Their findings displayed that an approximately 92% heat recovery rate was obtained with the usage of $FeOAl_2O_3$/PW

Table 2.1. (continue) A brief description for research's previous works.

Vermahmoudi et al., 2014	Fe_2O_3/PW	0.15, 0.4, and 0.65 vol. %	Hot and cold volume flow rates, hot fluid inlet temperature,	magnetic nanofluid in an air-finned heat exchanger instead of water experimentally	The highest enhancement in the overall heat transfer coefficient and convection heat transfer coefficient was 13% and 11.5% respectively
Aghabozorg et al., 2016	Fe_2O_3-CNT/PW	0.1&0.2%	80, 120, &150V 0.96, 2.25, and 3.43 lpm	MNFs used in a heat exchanger	Using of MNF enhanced the (CHTC) by 13.54% and 27.69% in laminar and turbulent conditions.
Kumar Ravi et., al 2016	Fe_2O_3/PW	0.005% and 0.06%	8 to 14 lpm	The effect of using MNF on the OHTC in DPHE with curve bend.	The results showed that using MNF could improve OHTC by 3.44% compared to water.
Kumar et al., 2017	Fe_3O_4/PW	0.005, 0.01, 0.03, & 0.06%	60 °C	Using MNF in the DPHE.	The FF increases with both VF and Re Number, the FF increments were 1.079-times & 1.092-times when Re Number 16,545 & 28,954 respectively.
Zheng et al., 2020	Water based nanofluids including Al_2O_3, SiC, CuO, and Fe_3O_4 nano particles	0.05%, 0.1%, 0.5%, and 1%	3-9 lpm and volume flow rate.	The impact of using various magnetic nanofluids in a solar system	The maximum CHTC was 30.8% (working fluid: F_3O_4/water nanofluid with 0.1% VF and 8lpm VFR.)

Table 2.1. (continue) A brief description for research's previous works.

Baba et al., 2018	Fe_3O_4/PW	0.02%, 0.04%, 0.06%, 0.08%, 0.1%, 0.2%, 0.4%	40 lpm	Magnetic nanofluids used in counter-flow DPHE with fins placed inside	Using MNF enhanced the thermal performance by 80% to 90%.
Abdulwahab et al., 2020	Fe_3O_4/PW	0.2, 0.4, & 0.6%	5000 W/m^2	MNF used in three different straight channels with different cross-sectional areas; circular, square, and triangular by GAMBIT & FLUENT software.	The CHTC increases with the increase of Re number. The maximum values of CHTC appeared in the circular tube at 0.6% VF
Goodarzi et al., 2016	NDG/PW	0.00 wt. % to 0.06 wt. %.	Re number range from 5000 to 15,000	studied the friction factor and heat transfer enactment of a counter-flow double-pipe heat exchanger	The average growth in heat transfer coefficient was about 16.2%. while using NDG/PW as a working fluid
Sözen et al.,2016	alumina and fly-ash	2 wt. %	Mass flow rate, input power	Heat transfer improvement of a parallel and cross-flow concentric tube heat exchanger under nanofluids working fluid	the efficiencies of the parallel and the counter-flow concentric tube heat exchanger systems, which were 31.2% and 6.9%, respectively, in the case of utilizing fly-ash nanofluid as a working fluid in the system

Table 2.1. (continue) A brief description for research's previous works.

Bahmani et al., 2017	Al_2O_3/PW	varied from 0 to 10 vol. %	Concentration ratio as well as mass flow rate	impact of operating nanofluids on the thermal performance of a double pipe heat exchanger by utilizing the (finite-volume) approach	The maximum average Nu number and thermal efficiency improvement rate were found as 32.7% and 30%, respectively.
Bahiraei et al., 2017	(CMC/PW)	0.4 wt. %	weight percent and size of the nanoparticle	Optimization of the thermal attributes for a non-Newtonian (CMC) Carboxymethyl Cellulose working fluid flow through a mini-scale concentric-tube heat exchanger system.	The convective heat transfer coefficient was increased inside the internal and external walls of the annulus.
Shahsavar et al., 2019	tetramethylammonium hydroxide-coated Fe_3O_4	-	pressure drop, pumping power	counter-current double-pipe mini-scale heat exchanger was examined to investigate the impacts of the hybrid nanofluid	they guides to a high error in the calculation of 1.5%–9.71% pressure drop, 1.5%–9.71% pumping power, and 18.24%–19.60% performance evaluation criterion.
Maddah et al., 2018	Al_2O_3-TiO_2	0.2 to 1.5 vol. %	Reynolds number was (3000-12000 twisting proportion between 2 to 8	theoretically studied the performance of a double pipe heat exchanger utilizing hybrid nanofluid	Results showed that using nanocomposites and twisting tapes boosts the exergy efficiency corresponding to pure water as a working fluid

Table 2.1. (continue) A brief description for research's previous works.

Karouei et al., 2020	(HEG)/PWMWCNT-Fe_3O_4/PW	0.1-0.7 vol. %.	Mass flow rate and concentration ratio	numerically investigated, the impact of inserting a creative curved turbulator and employing two kinds of hybrid nanofluids on thermal enactment in a helical double-pipe heat exchanger	The Ag-HEG/PW hybrid nanofluid has a more suitable thermal enactment at lower mass flow rates. Also, the index factor of the evaluated helical heat exchanger is most deficient at 0.1 vol. %. While at 0.7 vol. % the thermal enactment was maximum.
Babat et al., 2022	Fe_3O_4/PW & Fe_2O_3/PW	0.5 wt. %.	Mass flow rate and concentration ratio	The effects of using magnetic nanofluids on the convective heat transfer coefficient and the thermal efficiency of a parallel-flow and counter-flow concentric tube heat exchanger system	The thermal conductivity of the (Fe_3O_4/PW) & (Fe_2O_3/PW) magnetic nanofluids was approximately 15% and 10.28% more heightened than pure water which was the base fluid.
Gürü et al., 2019	bentonite/ PW	0.5, 2, and 4 wt. %	Mass flow rate, input heat, weight percent	researched experimentally the thermal functioning of nanofluid were used in the heat pipe	Remarked that the optimal nanoparticle weight percent for boosting the thermal properties of the heat pipes.
Venkatachalapathy et al., 2015	CuO/PW	1 and 1.5 wt. %	inclination tilt also intake heating loads	experimentally assembled a work to determine the thermic characteristics of a copper heat pipe with a cylindrical	Up to 23.83% reduction in heat pipe resistance was performed at 1.5 wt. %

Table 2.1. (continue) A brief description for research's previous works.

Tharayil et al., 2015	aqueous-graphene	0.001 to 0.006 wt. %	Input power, weight percent, and the declination angle	analyzed the thermal attributes of a small-scale heat pipe working by injecting nanofluid	Employing nanofluid as an operating medium improved both the thermal index factor of the heat pipe and reduced the temperature in the evaporator region.
Menlik et al., 2015	MgO/PW	5 wt. %	Mass flow rate, input heat, weight percent	experimented nanofluids inside a copper natural convection heat pipe	The results demonstrated that the efficiency of the system was increased by 26% under utilizing MgO nanofluid corresponding to pure water.
Sözen et al., 2017	Combustion furnace slag nanoparticles	3 wt.%	Mass flow rate, input heat, weight percent	The impacts of employing nanofluids on the thermal aspects of a two-phase closed thermosyphon	The findings demonstrated that the index factor of the heat pipe was improved by 22% by utilizing this type of working fluid instead of commercial ones.
Sözen et al., 2018	TiO_2/PW TiO_2/Triton X-100 TiO_2/ SDBS	0.5 wt. %	Mass flow rate, input heat, various base fluids.	experimentally studied the surface-active mechanism effects, and the impacts of the adding nanoparticles to the base fluid, on the performance of the natural convective heat pipe type	The heat resistant and the enhancements of the thermal system were higher than that of Triton X-100 surfactant, on the other hand, there was no impacts of the surfactant on the thermal conductivity of the heat pipe.

Table 2.1. (continue) A brief description for research's previous works.

Kiseev and Sazhin, 2019	Fe_2O_3/PW	0.5 wt. %	working fluid thermophysical attributes, filling ratio, geometry, and the nanoparticles weight percent	examined the heat transfer improvement in a circulated-thermosyphon worked by nanofluid	Heat transfer coefficients could be improved significantly up to 20% by employing nanofluids corresponding to pure water.
Su et al., 2019	Fe_3O_4/PW	0.5 wt. %	Mass flow rate, heat flux	investigated a heat pipe evacuated tubular solar collector by using nanofluid	The findings indicated that the heat pipes' thermal efficiency improved under nanofluids operating medium.
Kenti et al., 2021a	Indonesian fly-ash//PW SiO_2/PW	1.52 - 2 wt. %	Mass flow rate, input heat and weight percent	experimentally determined the thermophysical characteristics of nano-fluid in thermal applications	The experiment findings demonstrated that thermal conductivity, viscosity, and density improved by increasing nano-fluid concentrations. The thermal conductivity of fly ash was higher than that of the SiO_2 by 3.9%.
Kenti et al., 2021a	fly ash-Cu/PW	1.5 - 2 wt. %	Mass flow rate, input heat and weight percent	experimentally and theoretically conducted the heat transfer, entropy, and pressure drop under turbulent-flow regime in a tube with hybrid nanofluid	The maximum increase in Nu number was found as 57.1% at 2.0 wt. % corresponding to water.

Table 2.1. (continue) A brief description for research's previous works.

Rehman et al., 2022	Nickel paraffin/ PW	0.2-0.6 vol. %	Mass flow rate, input heat and weight percent	Investigated experimentally the performance of the heat pipe under using nanofluids	the heat sink-base temperature was decreased by 18.6% when a paraffin phase change material of 0.6 vol. % was counted into nickel.
Marulasiddeshi et al., 2022	Al_2O_3-CuO/PW	1.0 vol. %,	Temperature 30-60, concentration ratio	developed an artificial intelligence model on the thermal properties of hybrid nanofluids	The results displayed that the maximum improvement in thermal conductivity and viscosity of Al_2O_3-CuO was 14.6% and 6.5% corresponding to Al_2O_3 nanofluid at 1.0 vol. %, 60°C, and 30°C, respectively.
Roodbari et al., 2022a	TiO_2/PW	0.001-0.005 vol. %	Various volume concentrations, input temperatures	studied the impact of microstructure surface roughness on pool boiling characteristics of nanofluid	The results showed that by raising the nanofluid volume concentration boosting the boiling heat transfer coefficient.
Roodbari et al., 2022b	TiO_2/PW	0.005 vol. %	(LJ) potential 0.5 - 4	analyzed the interfacial thermal conductance between nano-particles and water	It has been conducted that Kapitza conductance increased by 20% while boosting the coupling strength of Lennard-Jones (LJ) potential

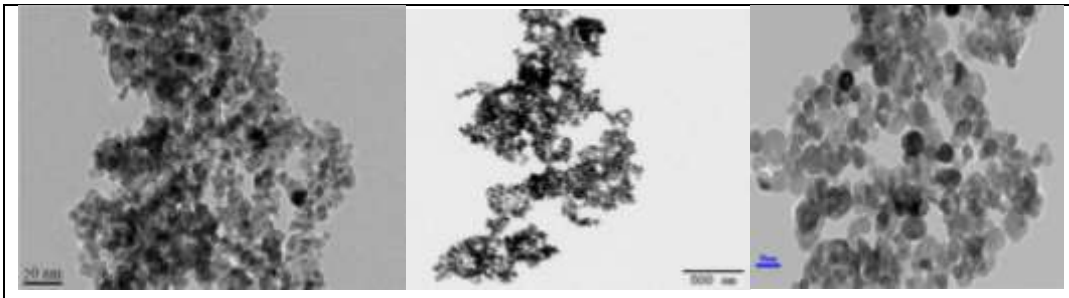
3. MAGNETIC NANOFLUIDS AND THERMOPHYSICAL PROPERTIES

Due to their great contribution to thermophysical properties of the traditional base fluids, nanofluids have often been utilized lately for enhancing the thermal performance of heat transfer devices operating with a working fluid. Such nanoparticles which are of magnetic specifications as iron has been using in nanofluid preparation and they are generally called magnetic nanofluid. The thermal performance of three thermal systems have been investigated experimentally and theoretically by utilizing mono as well as hybrid magnetic nanofluids instead of the traditional ones. The thermophysical properties of each magnetic nanofluid were calculated by applying numerical correlations under different operating conditions. The type of the magnetic nanofluid has been changed based on the type of the system:

In the case of the Air-to-air heat pipe system the magnetic nanofluid that have been applied was iron oxide. While for the Concentric tube heat exchanger system in parallel and counter flow regimes the iron oxide, ferric oxide, mono magnetic nanofluid also iron oxide-ferric oxide hybrid magnetic nanofluid have been for the Heat pipe thermosyphon system Fe_3O_4/PW, Fe_2O_3/PW, and $NiFe_2O_4$/PW mono magnetic-nanofluid as well as Fe_3O_4@Fe_2O_4/PW hybrid magnetic-nanofluid. All of the three systems have been tested under two values of magnetic nanofluid weight percent's which were equal to (0.5 wt. %, 1 wt. %). The significant indicative details of the Fe_3O_4, Fe_2O_3, and $NiFe_2O_4$ magnetic nanoparticles which were utilized in the results of this investigation are provided in table 3.1. TEM images of each magnetic nanoparticles have been shown in Figure 3.1.

Table 3.1. Products specifications.

Product Name	Formula	Appearance (Form)	Appearance (Color)	Formula Weight	shape	Purity (%)
Ferric Oxide	Fe_2O_3	Powder	Red-brown to brown	159.69 g/mol	Spherical	99.55
Iron Oxide	Fe_3O_4		Dark brown to black	231.53 g/mol		98.45
Nickel Ferrite	$NiFe_2O_4$		Brown	236.4 g/mol		98.88



a b c

Figure 3.1. TEM image of a) Fe_3O_4, b) $NiFe_2O_4$, c) Fe_2O_3 mono-magnetite nanoparticles.

3.1. Mono Magnetic Nanofluids

Iron oxide (Fe_3O_4/DW), ferric oxide (Fe_2O_3/ DW), and ($NiFe_2O_4$/ DW) mono magnetic nanofluids have been utilized as an working fluid with three thermal systems under (0.5 wt. %, 1 wt.%) weight percent, the thermal properties of the mono magnetic nanofluid have been calculated applying the correlation bellow:

3.1.1. Thermal conductivity

Eq. 3.1 is used to determine the poly magnetic-nanofluids' thermal conductivity [81].

$$k_{rnf} = k_b \left[\frac{k_{rnp} + 2k_b + 2\varphi\left(k_{rnp} - k_b\right)}{k_{rnp} + 2k_b - \varphi\left(k_{rnp} - k_b\right)}\right] \tag{3.1}$$

where: k_{rnp}, k_b, k_{rnf} thermal conductivity for the magnetic-nanoparticles, foundation fluid, as well as poly magnetic-nanofluid (W/m k) respectively.

3.1.2. Specific thermal capacity

Poly magnetic-nanofluids specific heat capacity was estimated using Eq.3.2 [82].

$$c_{p,rnf} = \frac{\rho_b . c_{p,b}\left(1 - \varphi_{rnp}\right) + \rho_{rnp} . \varphi_{rnp} c_{p,rnp}}{\rho_{rnf}} \tag{3.2}$$

where: $c_{p,rnf}$ the specific heat of mono-magnetic nanofluid (J/kg K). $c_{p,b}$ the specific heat of the base fluid (J/kg K).

The specific heat of the magnetic nanoparticles $c_{p,rnp}$ of the Fe_3O_4, Fe_2O_3, and $NiFe_2O_4$ is calculated by Eq.3.3 [83].

$$c_{p,mnp}{}^{\circ} = a + b.t + c.t^2 + d.t^3 + \frac{e}{t^2} \quad (3.3)$$

where: t represents temperature $\frac{(K)}{1000}$. $c_{p,rnp}{}^{\circ}$ Represents Specific heat ($\frac{J}{\text{mol K}}$).

The value of the constants in Eq.3.3 for Fe_3O_4, Fe_2O_3, and $NiFe_2O_4$ magnetic nanoparticles were provided by table 3.2.

Table 3.2. The constants' values in Eq. 3.3 for Fe_3O_4, Fe_2O_3, and $NiFe_2O_4$ nanoparticles

Magnetic nanofluid	Fe_3O_4	Fe_2O_3	$NiFe_2O_4$
a	104.2096	93.43834	13.69160
b	178.5108	108.3577	82.49509
c	10.61510	-50.86447	27.66900
d	1.132534	25.5868	161.6011
e	-0.994202	-1.61133	-0.092417

3.1.3. Viscosity

The nanofluid practical dynamic-viscosity is delivered using Eq. 3.4 according to the Brinkman criteria.

$$\mu_{rnf} = \frac{\mu_b}{(1-\varphi)^{2.5}} \quad (3.4)$$

where: μ_b, μ_{rnf} were the base fluid dynamic-viscosity as well as poly magnetic-nanofluid, , respectively (Pa.s).

3.1.4. Density

The poly magnetic-nanofluid density were evaluated using Eq.3.5 [84].

$$\rho_{rnf} = \rho_b.\left(1 - \varphi_{rnf}\right) + \rho_{rnp}.\varphi_{rnp} \quad (3.5)$$

where: ρ_b pure water density (kg/m^3), ρ_{rnf} density of poly magnetic-nanofluid (kg/m^3), and φ_{rnp} is the mass percentage of conventional magnetic-nanofluids.

3.2. Hybrid Magnetic Nanofluids

The effect of utilizing Fe_3O_4@Fe_2O_3/PW hybrid magnetic-nanofluid on the thermal performance of concentric tube heat exchanger system under counter and parallel-flow regimes and heat pipe thermosyphon system have been conducted experimentally and theoretically.

3.2.1. Thermal conductivity

The hybrid magnetic-nanofluids thermal conductivity was estimated using Eq.3.6 Maxwell-Model performed at Ghachem et al., study [85].

$$\frac{k_{h(mnf)}}{k_b} = \left[\frac{\left(\varphi_{Fe_3O_4}k_{Fe_3O_4}+\varphi_{Fe_2O_3}k_{Fe_2O_3}\right)}{\emptyset} + 2k_b + 2\left(\varphi_{Fe_3O_4}k_{Fe_3O_4} + \varphi_{Fe_2O_3}k_{Fe_2O_3}\right) - 2\emptyset k_b\right] \times \left[\frac{\left(\varphi_{Fe_3O_4}k_{Fe_3O_4}+\varphi_{Fe_2O_3}k_{Fe_2O_3}\right)}{\emptyset} + 2k_b - \left(\varphi_{Fe_3O_4}k_{Fe_3O_4} + \varphi_{Fe_2O_3}k_{Fe_2O_3}\right) + \emptyset k_b\right]^{-1} \quad (3.6)$$

where: $k_{h(mnf)}$ is the thermal conductivity of the hybrid magnetic nanofluids (W/m k). $k_{Fe_3O_4}$, $k_{Fe_2O_3}$ are the thermal conductivity of the iron-oxide and ferric-oxide mono-magnetic nanofluid (W/m k).

3.2.2. Specific thermal capacity

Specific heat capacity of hybrid magnetic nanofluid is determined by Eq.3.7 [86].

$$C_{p,h(mnf)} = \varphi_{Fe_3O_4}\rho_{Fe_3O_4}C_{p,Fe_3O_4} + \varphi_{Fe_2O_3}\rho_{Fe_2O_3}C_{p,Fe_2O_3} + (1 - \emptyset)\rho_b C_{p,b} \quad (3.7)$$

where: $C_{p,h(mnf)}$ hybrid magnetic-nanofluid specific heat capacity (J/kg K). C_{p,Fe_3O_4}, C_{p,Fe_2O_3} are the specific heat capacity of the Fe_3O_4@Fe_2O_3/PW magnetic-nanofluid (J/kg K).

3.2.3. Viscosity

Eq. 3.8 provides the practical dynamic viscosity associated with the Brinkman-based hybrid magnetic-nanofluid.

$$\mu_{h(mnf)} = \frac{\mu_b}{[1-(\varphi_{Fe_3O_4}+\varphi_{Fe_2O_3})]^{2.5}} \tag{3.8}$$

where: $\mu_{h(mnf)}$, μ_b dynamic viscosity of hybrid magnetic-nanofluid as well as base fluid, respectively (Pa.s).

3.2.4. Density

Hybrid magnetic nanofluids density was calculated by involving Eq.3.9 which was essentially developed using the mixture technique.

$$\rho_{h(mnf)} = \varphi_{Fe_3O_4}\,\rho_{Fe_3O_4} + \varphi_{Fe_2O_3}\,\rho_{Fe_2O_3} + (1-\emptyset)\,\rho_b \tag{3.9}$$

where: $\varphi_{Fe_2O_3}$ and $\varphi_{Fe_3O_4}$ the Fe_2O_3/PW and Fe_3O_4/PW weight percent magnetic-nanofluids. $\rho_{Fe_2O_3}, \rho_{h(mnf)}, \rho_{Fe_3O_4}$ Fe_2O_3/PW, hybrid magnetic-nanofluid, as well as Fe_3O_4/PW density, respectively. $\emptyset$ The combined weight percentage of two different types of nanoparticles is calculated as:

$$\emptyset = \varphi_{Fe_3O_4} + \varphi_{Fe_2O_3}$$

Furthermore, the proportion of fluid mass to volume was used to calculate the densities of poly and hybrid-magnetic nanofluid. Fig.3.2 provided an illustration of the difference between theoretical and experimental densities. This chart shows that the measured and calculated densities have a good percentage of agreement.

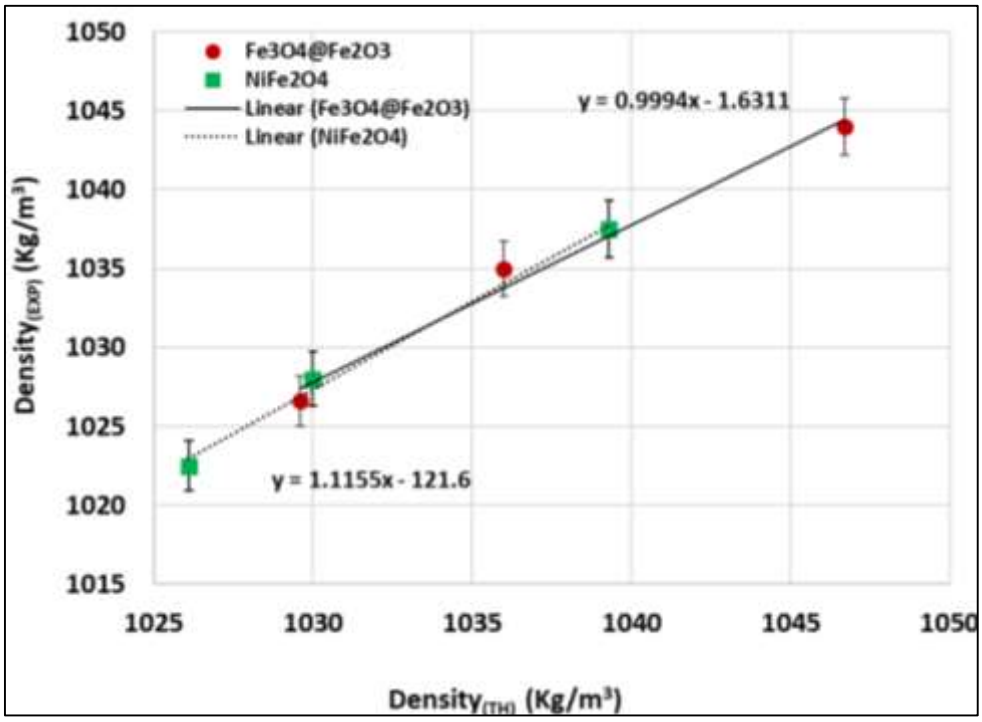


Figure 3.2. Experimental and Theortical density diviation.

3.3. Preparation of the Magnetic Nanofluids

The combination of poly and hybrid magnetic-nanofluids used in our work were made in two steps. First, magnetic-nanoparticles had been produced through smashing the magnetite-like metals $NiFe_2O_4$, Fe_3O_4, and Fe_2O_3. Table 3.3 included the chemical composition of every single magnetic nanoparticle's.

Table 3.3. Chemical composition of $NiFe_2O_4$, Fe_2O_3 as well as Fe_3O_4.

Product Name	Chemical composition									
Ferric Oxide (wt. %)	Ca 0.003	Cr 0.015	Mn 0.14	Al 0.05	SiO_2 0.091					
Iron Oxide (wt. %)	Ca 0.023	Cr 0.0016	K 0.0012	Mn 0.0086	SiO_2 0.14					
Nickel Ferrite (ppm)	Ba 3.5	Ca 2128	Co 92	Cr 14	Cu 25	Mg 298	Mn 828	Na 3062	Sr 16	Zn 46

The iron-oxides (Fe_3O_4), nickel-ferrite ($NiFe_2O_4$), ferric-oxides (Fe_2O_3), all have strong ionization capacities and absorbing structures, which enhance

their absorption and holding properties. The creation of poly and hybrid magnetic-nanofluids was done in two steps. The magnetic nanoparticles were produced using a high-energy roller crusher smashing process (Spex type). In order to create a hybrid magnetic-nanofluid solvent containing Fe_3O_4, Fe_2O_3 merged within a proportion of 50:50 nano-particles, magnetic-nanoparticles were created in the initial stage and dispersed in pure water to be the foundation fluid. In a similar manner, $NiFe_2O_4$ nano-particles were prepared within the base fluid to create a $NiFe_2O_4$ poly magnetic-nanofluid. 0.5 And 1 weight percentages were used to prepare the solutions. After that, a homogeneous solution is produced using an ultrasonic bath for roughly 5 hours. Figure 3.3 showed the steps involved in creating the magnetic nanofluids.



Figure 3.3. The preparation process of the nanofluid suspensions

4. EXPERIMENTAL PROCEDURE

In this section the experimental procedure of each thermal system (air-to-air heat pipe heat exchanger system), (concentric tube heat exchanger system: counter and parallel flow regimes), and (heat pipe thermosyphon system) as well as the process for generating the magnetic-nanofluids have been explained in details.

4.1. Air-to-Air Heat Pipe Heat Exchanger System

The air channels (subsequently directed to the cold-air as well as hot-air streams) were unmixed, which that indicates even waste gas could be employed for heating recovery. The stream's length was 3 m, also the heat pipe was positioned at a 130 cm distance by the entry, which approximated the channel's center zone. Fans were provided to change the air velocity, digital anemometer was used to measure both mass flow rate and velocity. The hot-air stream was developed a little bigger than cold-air stream to be capable to vaporize the largest amount of fluid (magnetic-nanofluids or pure water) circulating in the heat pipes. The air was subjected to an electric heater, where it was heated more thoroughly, through the use of a blower located in hot air channel's entry. The heated air delivered thermal energy into the heat pipe as soon as it reached the center, causing the experimental fluid to circulate through the heat pipe and evaporate. The operating fluid that had evaporated rose towards the heat pipe's condenser region, which is paired by the cold-air stream. The operating fluid condensed and returned into the evaporator portion in its liquid state because heat transfer occurred between them because the cold air temperatures were lower than the heat pipe's condenser surface. As long as there is a variance in temperature across the air passageways, this cycle occurs spontaneously. Additionally, the tests were repeated three times, and the means of outcomes were taken into account in mathematical computations to guarantee both repetition and dependability. Copper heat pipes that were organized in an asymmetrical pattern were used within the heat exchanger. The operating fluids for were magnetic nanofluids as well as pure water generated in two various concentrations.

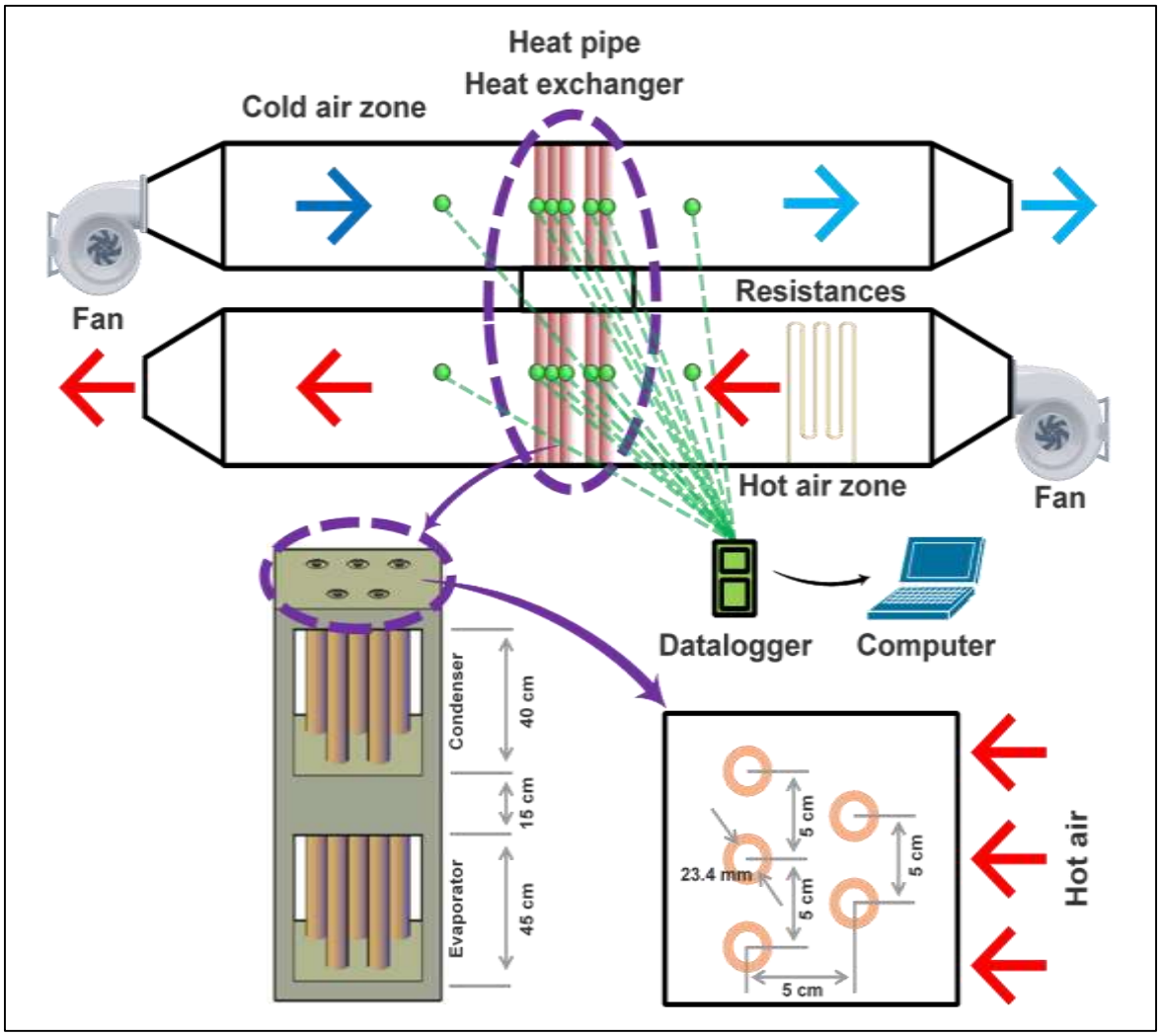


Figure 4.1. The schematic drawing for air-to-air heat pipe heat exchanger experimental Device

Every heat pipe had a length of 1 m, diameter of 23.4 mm, as well as thickness of 1 mm. Every pipe had been vacuumed then loaded with either operating fluids via the valves. As a result, the tests were conducted at sub-atmospheric conditions. The heat pipes' condenser, adiabatic, and evaporator parts had relative heights of 40 cm, 15 cm, as well as 45 cm. Each one was filled independently with 65 ml of operating fluid for each test, which amounts to 1/3 of a typical evaporator portion. Depicted in Figure 4.1. The studies were conducted using heating generates of 2 kW and 1 kW. The hot side's flow rates of air were 50g/s, 70g/s, and 90g/s, whereas the cool side's quantities were 60 g/s and 30g/s. Fe_3O_4/PW having concentrations of (1 wt. % and 0.5 wt. %) also pure water served as the working medium.

4.2. Concentric-Tube Heat Exchanger Apparatus (Parallel and Counter Flow Regimes)

Research can be carried out using both the Counter and Parallel-Flow Concentric Tubes Heat Exchanger types, as illustrated on Figure 4.2. The design of the experiments followed the requirements of the EN 305 European Standards. The results of the experiment was collected in accordance with the aforementioned standard. The testing apparatus was made through PA Hilton Ltd. It consists of two concentric pipes containing three passes, as seen in figure 4.2. Each component is 350 mm long, making the exchanger's overall length 1050 mm. Coolant travels via the gap between each of the outer and inner tubes, hot-fluid travels along the internal pipe, which has an exterior and interior diameter of 9.5 mm and 7.9 mm, respectively. The outer pipe has an interior diameter equal to 11.1 mm as well as an outside diameter equal to 12.7 mm. Figure 4.2 illustrates the hot line's a single direction loop. For the purpose of avoiding rusting, the stainless steel internal tube is attached to a centrifugal pump. Two electric heaters are placed into the stainless steel tank in order to adjust the fluid's temperature. The heaters have a 1.5 kW capacity.

To maintain the tank's walls secure from potential harm brought on by high temperatures, a safety mechanism is installed as a control switch to stop the temperature of the fluid from increasing automatically. In order to maintain pressure regulation within the system, an exterior pressure regulating valve is additionally used. Seeing through the glass in front of the heated water container allows you to monitor the water level. Additionally, flowmeters are used to gauge the flow rates of hot and cold fluids. Ten J-type thermocouples are placed in different places, and they are used to measure the temperatures. The co-current circulation and countercurrent flows represent two of the several operational modes.

Hot-line: The operational fluid that is fed into the internal tube is heated using an electric resistance. It discharges heat while it moves through the heat exchanger and gets cooled by the refrigerant. After that, a flow meter converts it again into a heated water tank. It is heating up once more here. The two drain valves on the bottom right are able to use to remove hot water whenever required. City water is utilized to provide cold water. It goes through an adjustment valve as well as a flowmeter. Control valves have the ability to alter the flow pattern of cold fluid, allowing for the creation of parallel or counter flow forms of motion.

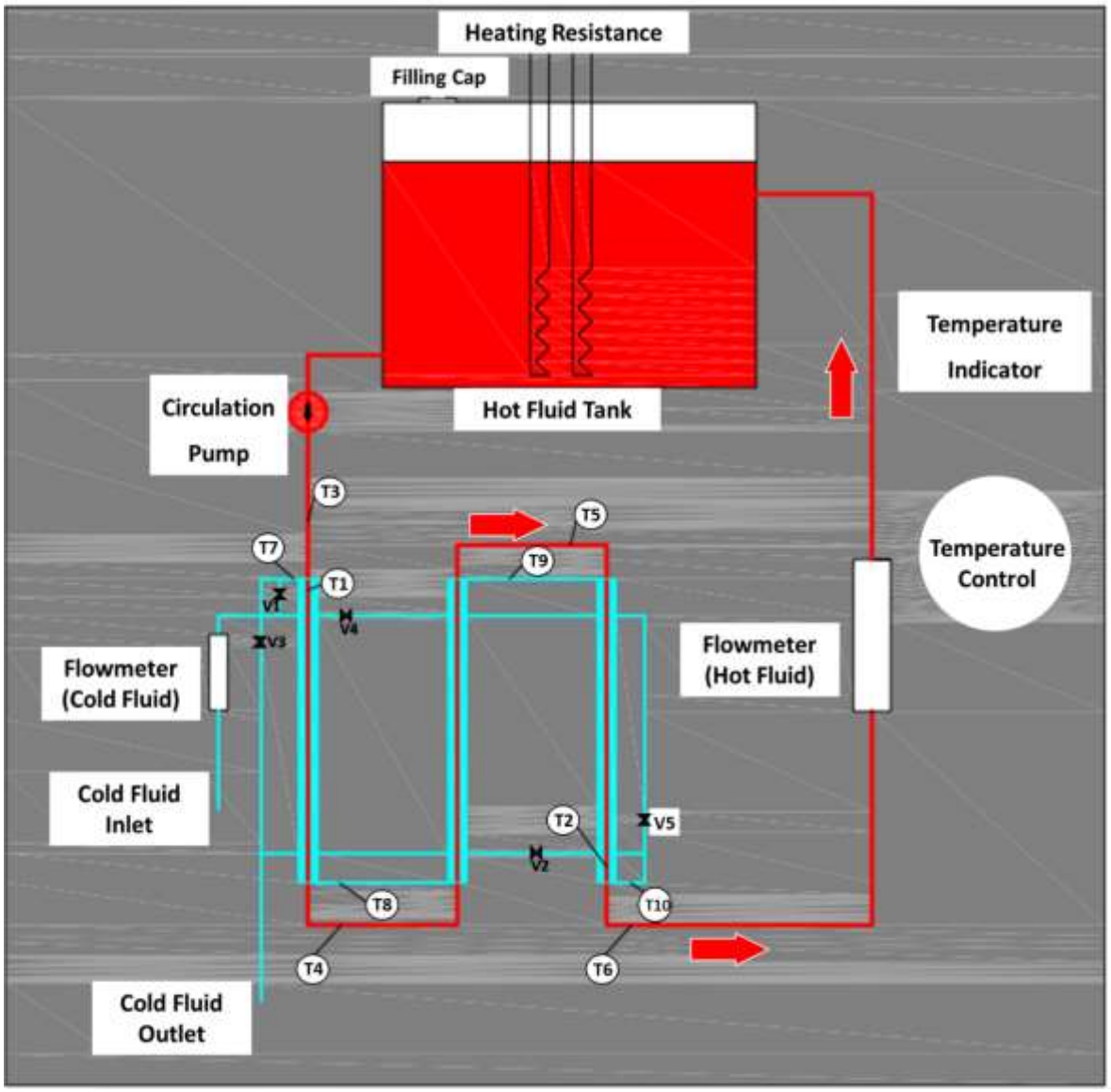


Figure 4.2. Experimental Rig of the Concentric-Tube Heat Exchanger Sistem.

In this framework, two distinct weight percents of 1 wt. % and 0.5 wt. % of (Fe_2O_3/DW) and (Fe_3O_4/DW) poly magnetic-nanofluid and Fe_3O_4@Fe_2O_3/DW hybrid magnetic-nanofluid were utilized. moreover, In this investigation, two flowmeters have been used: The operating fluid flowed throughout the tube's interior at a rate of 3-9 lpm using a 1 lpm intervals on the primary flowmeter. Regarding the cold fluid passing through the annulus-side, the second flowmeter had been set at 10 g/s.

4.3. Heat Pipe Thermosyphon System

The research study was conducted within the thermosyphon heat pipe made of copper, as shown in Figure 4.3, which outer and inner diameters were respectively 22 mm and 18 mm . The evaporator part as well as condenser portion both were 40 cm in length, while the adiabatic zone was 20 cm long, giving the device a total length of 1 m. The heat pipe had been kept vertical during all of the trials, so the circulation within the system was natural convection mode. Every experiment was completed under vacuum conditions. During each experiment, 85 ml of the operating fluid, Third of the heat pipe's total volume was injected into the heat pipe.

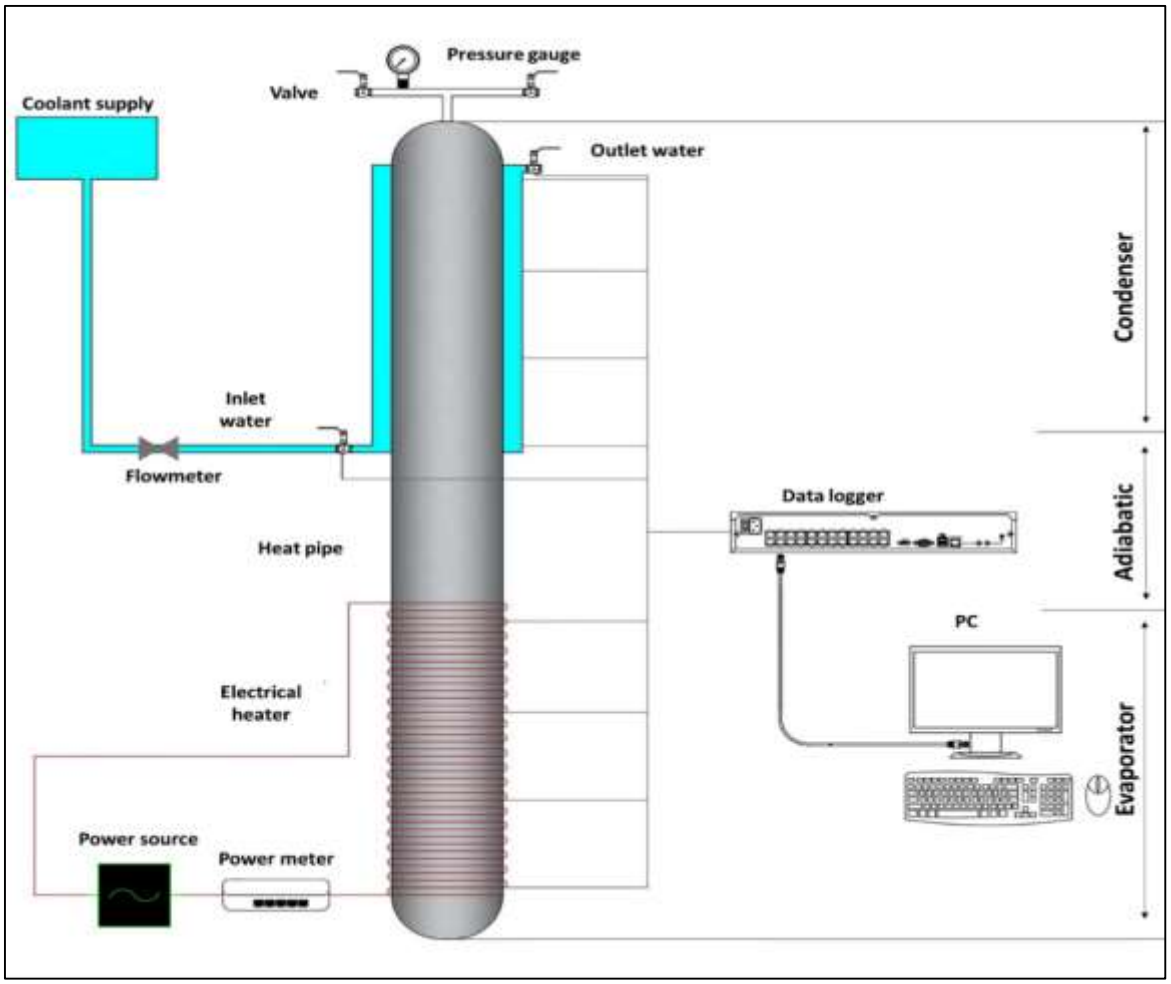


Figure 4.3. Schematic diagram of the experimental setup.

In order to monitor the temperature variation all through the heat pipe elements per test, 10 thermocouples of the K type were fixed onto the heat pipes and attached to the data logger, as illustrated on Figure 4.4. The experimental setup shown in Figure 4.3's schematic

illustration. To reach a stable state, the system had to wait for approximately 35 minutes. The variables were subsequently measured.

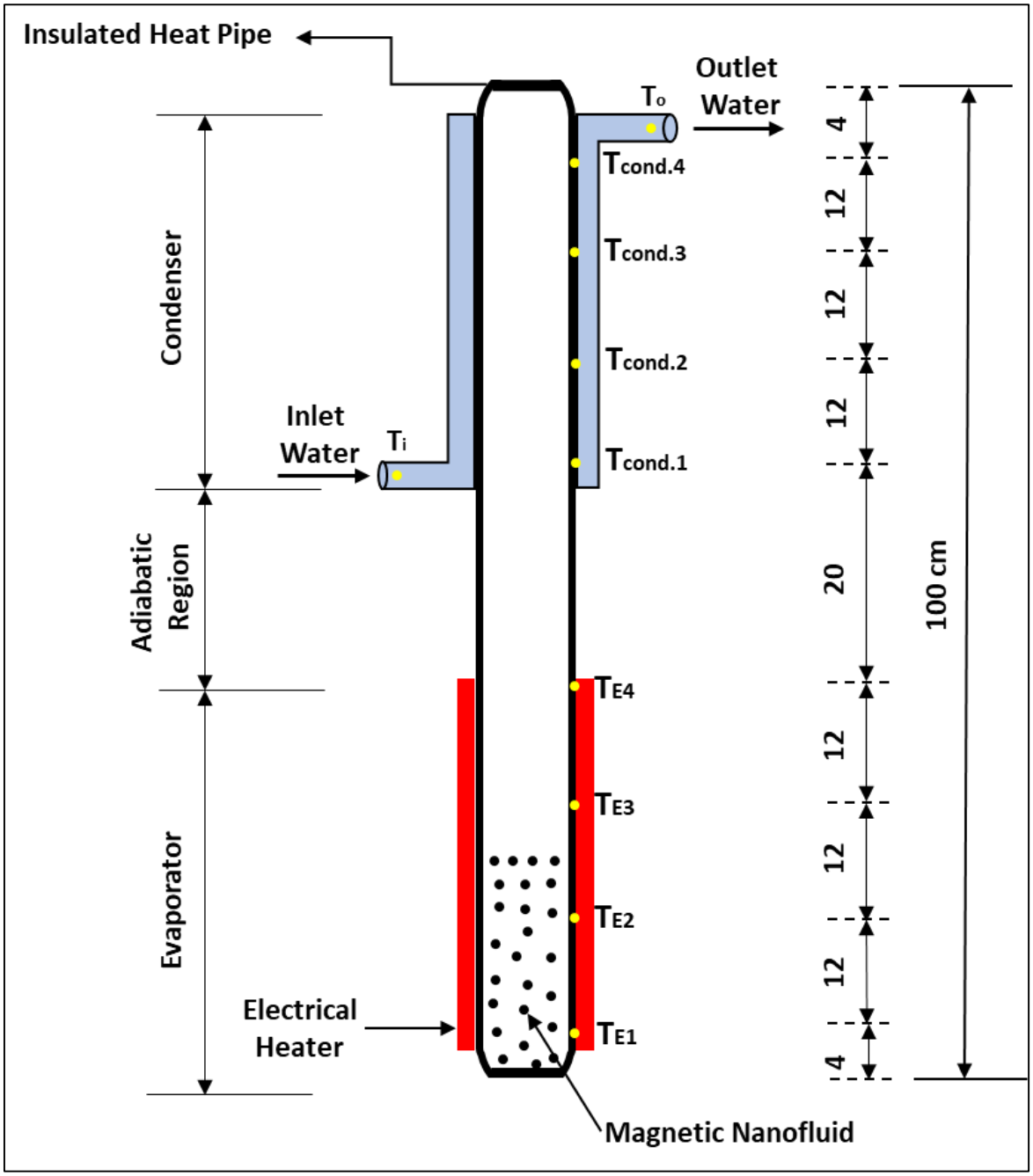


Figure 4.4. Schematic diagram of the thermocouple's distribution.

at the start, the experimentations were performed via employing pure water then consecutivelyFe_3O_4@Fe_2O_3/PW hybrid magnetic-nanofluid (50:50 mixture percentage of Fe_3O_4 and Fe_2O_3 magnetic nanoparticles) and nickel ferrite, iron oxide, ferric oxide mono-magnetic nanofluids. The operating fluid with a concentration of 0.5 wt. % had been injected

to the device. After that, it was removed from the device and refilled with the operational fluid containing 1 weight percent. The evaporator part contained a heating element, and a selector switch was employed to change the amount of supplied heat. 400, 300, and 200 W heating rates were applied to the system to evaporate the working fluid. A circulation pump was installed to supply coolant into the condenser part, which was then under the control of a water flowmeter. The cooling fluid flow rates were 5, 7.5, and 10 g/s.

5. THEORETICAL ANALYSIS

Two main types of magnetic nanofluids were used in this work. Which were mono magnetic nanofluids and hybrid magnetic nanofluids. Also, Three thermal systems have been used in this work, the theoretical analysis have been also discussed for each system regarding conducting the effect of utilizing mono and hybrid magnetic nanofluids on the thermal efficiency, convection heat transfer coefficient, thermal resistance, overall heat transfer coefficient.

5.1. Mono Magnetic Nanofluids In (Air-to-Air) Heat Pipe Heat Exchanger System

For a comparison of the obtained results, resistance and thermal efficiency amounts in an air-to-air heat exchanger have been determined for every fluid. With every operation fluid, the exterior temperature of heat pipes were taken as well and kept record of. The following formula was used to compute thermal efficiency, which is the ratio between heat input to output in the evaporator and condenser sections:

$$\eta = \frac{\dot{Q}_{con}}{\dot{Q}_{evp}} = \frac{\dot{Q}_{ex}}{\dot{Q}_{in}} \tag{5.1}$$

where $\dot{Q}_{con}$ and $\dot{Q}_{evp}$ represents the rate when heat is transferred from cold to hot-air through the condenser and evaporator, accordingly. The two equations shown below were used to determine these rates:

$$\dot{Q}_{con} = \dot{m}_{ca} c_{p,ca} \Delta T_{ca} \tag{5.2}$$

$$\dot{Q}_{evp} = \dot{m}_{ha} c_{p,ha} \Delta T_{ha} \tag{5.3}$$

In these equations, $c_p, \dot{m}$ and ΔT represent specific heat capacity, mass flow, as well as temperature difference, respectively.

The proportion of the energy absorbed via the heat pipes within the evaporator region to the mean temperature disparity across the evaporator and condenser portions was used to compute thermal resistance (Eq. 5.4).

$$R = \frac{\Delta T}{Q_e} \tag{5.4}$$

By using the following proportion, Re numbers (Re) had been individually estimated with the aim to categorize the fluid flow regimes in each channel into either turbulent or laminar.

$$Re = \frac{\rho_a V_{avg} D_h}{\mu} \tag{5.5}$$

To determine how well the air-to-air heat exchanger operated, various experimental setups were used. The experimental findings were displayed using plots that utilized the average Re values for comparison outcomes under similar circumstances. The computations revealed that both channels' turbulence regimes was in charge under all circumstances.

5.2. Mono and Hybrid Magnetic Nanofluids in Concentric Tube Heat Exchanger System (Counter and Parallel-Flow Regimes).

In a heating system, there are received and given heat amounts always. In this study, when the heat received by coolant per unit time was described as $\dot{Q}_{cold}$, given heat by hot fluid per unit time was described as $\dot{Q}_{hot}$. These heat amounts were calculated with Eq.5.6 and Eq.5.7.

$$\dot{Q}_{hot} = \dot{m}_{hot} \cdot c_{p,hot} \cdot (T_3 - T_6) \tag{5.6}$$

$\dot{Q}_{hot}$ heating flow rate throughout the tube side.

$$\dot{Q}_{cold} = \dot{m}_{cold} \cdot c_{p,cold} \cdot (T_7 - T_{10}) \tag{5.7}$$

$\dot{Q}_{cold}$ heating flow rate throughout the annulus side.

The greatest efficiency amount appears while gained and delivered heat quantities were equivalent to individually other (Eq.5.8). Similarly, the conduction heat transfer among the exterior and internal tubes was ignored. Furthermore, the components of types of equipment as well as calibration errors.

$$\dot{Q}_{hot} = \dot{Q}_{cold} \tag{5.8}$$

Eq. 5.9 is used to determine the conductive heat transfer across the liquid and the tube's surface. Heat is transported via the pipe during period of time:

$$\dot{Q} = A.h.\Delta T_{ln} \tag{5.9}$$

Here, h indicates the heat coefficient between the substance and the pipe inner surface. A the internal surface area, and ΔT_{ln} relates to the estimated log mean variation in temperature which is conducted by Eq.5.10.

$$\Delta T_{ln} = \frac{\Delta T_{inlet} - \Delta T_{outlet}}{\ln\left(\frac{\Delta T_{inlet}}{\Delta T_{outlet}}\right)} \tag{5.10}$$

Repositioning Eq.5.6 combining it with the experimental orders and Eq.5.10, we can derive Eq.5.11:

$$\dot{Q}_{hot} = \frac{h_{hot}.A_i.[(T_3 - T_1) - (T_6 - T_2)]}{\ln\left(\frac{T_3 - T_1}{T_6 - T_2}\right)} \tag{5.11}$$

Eq.11 is used to calculate the heat transfer coefficient (h_{hot}) that indicates the total amount of heat given to the hot fluid.

The amount of heat transfer within the pipe's interior surface and the cold fluid is calculated by repositioning Eq.5.7 as:

$$\dot{Q}_{cold} = \frac{h_{cold}.A_d.[(T_1 - T_7) - (T_2 - T_{10})]}{\ln\left(\frac{T_1 - T_7}{T_2 - T_{10}}\right)} \tag{5.12}$$

Heat exchanger's overall heat transfer coefficient was estimated by applying Eq.5.13, which has been found from Eq.6.

$$\dot{Q}_{hot} = A_T.U.\left[\frac{(T_3 - T_7) - (T_6 - T_{10})}{\ln\left(\frac{T_3 - T_7}{T_6 - T_{10}}\right)}\right] \tag{5.13}$$

In order to observe the association of operating fluid Re number within the tube-side as well as Re number in annulus-side with thermal characteristics of the system, Eq.5.5 has been

utilized to determine it at every operating fluid. Thermal efficiency of heat exchanger was calculated by using Eq.5.14.

$$\eta = \frac{\dot{Q}_{cold}}{\dot{Q}_{hot}} \tag{5.14}$$

In the case of calculating theoretical Nu number at turbulent-flow under poly and hybrid magnetic-nanofluids passing throughout the pipe was estimated via Eq.5.15 [87].

$$Nu_{\mathrm{nf(TH)}} = 0.0059\left(1.0 + 7.6286\varphi^{0.6886}Pe_p^{0.001}\right)Re_{nf}^{0.9238}Pr_{nf}^{0.4} \tag{5.15}$$

Eq.5.16 is used for calculating the empirical equation for pure water passing through heat exchanger [88].

$$Nu_{w(TH)} = 0.372Re^{0.687}Pr^{0.3} \tag{5.16}$$

Depending upon the schematic diagram provided by Figure 5.1, equations 5.17 and 5.18 determine the experimental Nu number from poly and hybrid, magnetic-nanofluids, as well as pure water:

$$\bar{h} = \frac{1}{L}\int_0^L h\,.\,|dx|_{r=R_i} \tag{5.17}$$

$$\overline{Nu}_{Exp} = \frac{\bar{h}\,(2R_i)}{k} \tag{5.18}$$

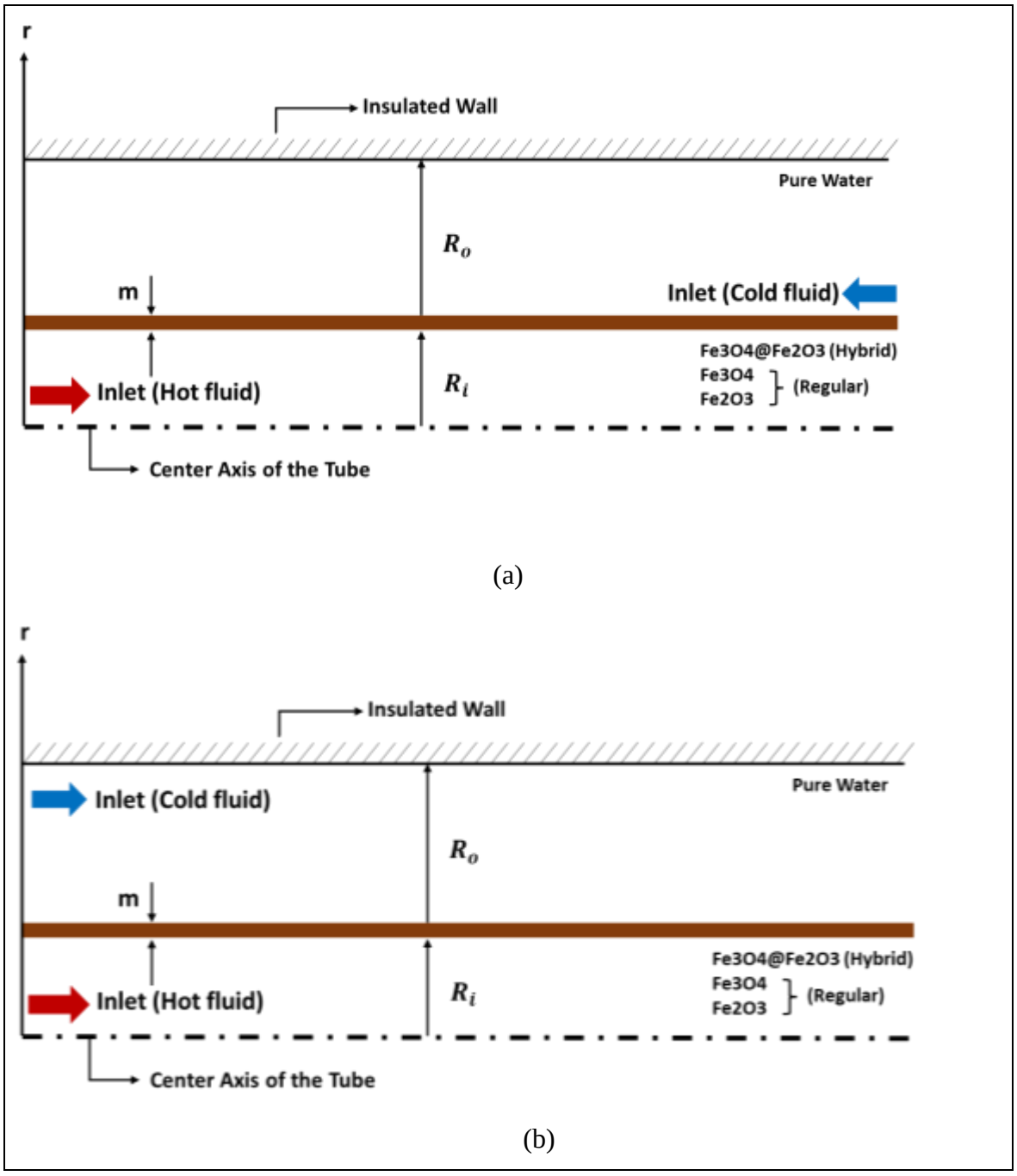


Figure 5.1. Schematic Diagram for a) Counter-regime b) Parallel-regime Concentric Tube Device

5.3. Mono and Hybrid Magnetic Nanofluids in Thermosyphon Natural Convection Heat Pipe

By performing a heat balancing across the heat inputs into the evaporator ($\dot{Q}_{in}$), which could be varied as 200W, 300W, and 400W, as well as output heat leaving the condenser ($\dot{Q}_u$) within time interval, it was possible to explore the heat pipe's capacity to transport heat. In order to investigate the heat transmission through the heat pipe, thermal resistance, Nusselt

number was calculated both empirically and theoretically utilizing imperial correlations, as well as Ra number (Ra).

Newton's law of cooling, which is presented in Eq. 5.19, is used to calculate the amount of beneficial energy which is carried by a coolant through the heat pipe per unit time ($\dot{Q}_u$):

$$\dot{Q}_u = \dot{m}_w C_{p,w} (T_o - T_i) \tag{5.19}$$

Where: $\dot{Q}_u$ the beneficial energy absorbed by the coolant (W), $\dot{m}_w$ mass flow (kg/s) as well as $C_{p,w}$ coolant specific heat (kJ/kg.K). $T_o - T_i$ coolant's outlet and the inlet temperature variances°C.

Heat pipe's thermal resistance and temperature variation among the condenser and evaporator were the two most important factors in determining heat pipe's thermal properties. Eq. 5.20 establishes the heat pipe's thermal resistance. Eq. 5.21 is also used to calculate the system's thermal efficiency.

$$R = \frac{\left[\left(\frac{T_{e1}+T_{e2}+T_{e3}+T_{e4}}{4}\right)-\left(\frac{T_{c1}+T_{c2}+T_{c3}+T_{c4}}{4}\right)\right]}{\dot{Q}_{in}} \tag{5.20}$$

$$\eta_{th} = \dot{Q}_u \Big/ \dot{Q}_{in} \tag{5.21}$$

This analysis emphasizes the natural convective method of heat transfer while using hybrid and poly magnetic-nanofluids with the normal thermophysical suitability previously mentioned. The actions of natural convection and the thermophysical properties are completely changed when nanoparticles are present into the foundation fluid. Ilyas et al. offer a generalized relationship for the Nu number, which is calculated by Eq. 5.22. This correlation depends on the percentage of nanoparticles, the Ra number, also nanofluids thermophysical characteristics [89]. While Kumar and Kalam's empirical correlation Eq. 5.23 was used to obtain the coolant Nu number [90].

$$Nu_{f(TH)} = 4.17\left[\frac{Pr}{Pr-0.343}\right]^{2.51}\left[\frac{Pr}{{k_{wf}}^{3.76}\beta^{3.483}}\right](1-\varphi)^{-0.015}Ra^{0.04} \quad (5.22)$$

where: $Nu_{f(TH)}$ represents the theoretical operating fluid's unitless Nu number, φ weight percentage (%), Pr Prandtl number (unitless), k_{wf} operating fluids thermal conductivity (W/m.K).

$$Nu_{w(TH)} = 0.18\left[\left(\frac{Pr}{0.2+Pr}\right)Ra\right]^{0.29} \quad (5.23)$$

The imperial equation which proposed by Abu Nada and Chamkha was utilized for calculating the poly magnetic-nanofluids Ra number which was given in Eq. 5.24 [91].

$$Ra_{rnf} = \frac{g[\rho_{rnf}(1-\varphi)\beta_{rnf}+\varphi\rho_b\beta_b][T_o-T_i]\rho_{rnf}C_{p,rnf}L^3}{\mu_{rnf}k_{rnf}} \quad (5.24)$$

The Ra number of the hybrid magnetic-nanofluid was given in Eq. 5.25 [92].

$$Ra_{h(mnf)} = \frac{[\varphi_{Fe_3O_4}(\beta)_{Fe_3O_4}+\varphi_{Fe_2O_3}(\beta)_{Fe_2O_3}+(1-\emptyset)(\beta)_b][T_o-T_i]\,\rho^2_{h(mnf)}C_{p,h(mnf)}L^3}{\mu_{h(mnf)}k_{h(mnf)}} \quad (5.25)$$

where: $Ra_{mnf}\ and\ Ra_{h(mnf)}$ the poly as well as hybrid Ra number magnetic-nanofluid, β_{mnf}, β_b , $\beta_{Fe_2O_3}$, $\beta_{Fe_3O_4}$ poly, base fluid, Fe_2O_3 as well as Fe_3O_4 operating fluids thermal expansion.

Uncertainty analysis is a dependable method for defining uncertainties and estimating the results of an experimental study. The uncertainties could result from some parameters such as device calibration, test circumstances, and so on. In the current study, temperatures and mass flow rates were estimated by employing suitable devices. Let finding A is a function that refers to independent variables (x_1, x_2, …, x_n). WF is the uncertainty of the related findings and similarly w_1, w_2, …, w_n are the independent variables' uncertainties. On requirement that all independent variables' uncertainties are presented with identical odds, the outcome's uncertainty that has these odds can be presented utilizing the procedure indicated by [18].

$$W_A = \left[\left(\frac{\partial A}{\partial x_1} w_1\right)^2 + \left(\frac{\partial A}{\partial x_2} w_2\right)^2 + \cdots + \left(\frac{\partial A}{\partial x_n} w_n\right)^2\right]^{1/2}$$

In this analysis, input heat, temperature, and coolant mass flow rate data were measured; thus, the entire uncertainty of these measured data was determined. The total uncertainty of the temperature measurement (W_{A}) could cause by the errors following: thermocouples' accuracy (w_{ta}), thermocouple junctions (w_{tj}) and read-out of the value from apparatus (w_{r}). Consequently, the uncertainty of temperature values (W_{T}) can be computed as follows:

$$W_{\mathrm{T}} = \left[(w_{\boldsymbol{ta}})^{\mathbf{2}} + \left(w_{\mathrm{tj}}\right)^{\mathbf{2}} + \left(w_{\mathrm{tj}}\right)^{\mathbf{2}}\right]^{\mathbf{1/2}}$$

$$= [(0.5)^{\mathbf{2}} + (1)^{\mathbf{2}} + (0.45)^{\mathbf{2}}]^{\mathbf{1/2}} = 1.2052$$

Total uncertainty of the measured coolant mass flow rate (W_{MFR}) could be generated by the flowmeter accuracy (w_{fm}) and the read-out of the data in flowmeter (w_{rfm}). Then, in the mass flow rate measurement, the uncertainty is:

$$W_{\mathrm{MFR}} = \left[\left(w_{fm}\right)^2 + (w_{\mathrm{rfm}})^2\right]^{1/2} = [(0.15)^2 + (0.011)^2]^{1/2} = 0.1504$$

For heater, overall uncertainty of the input power (W_{IH}), likewise, could originate from the two reasons; first, wattmeter's accuracy (w_{wm}) and the second, read-out of the data from apparatus (w_{rwm}). The input heat measurement uncertainty is:

$$W_{\mathrm{MFR}} = [(w_{wm})^2 + (w_{\mathrm{rwm}})^2]^{1/2} = [(0.9)^2 + (0.95)^2]^{1/2} = 1.3086$$

Concerning the total uncertainties of the measured data carried out into account, it was obviously noticed that their amounts were acceptable (acceptable interval is 0−2%). Experimental outcomes' uncertainty was estimated by assuming the divagation in values. As mentioned earlier, the tests were accomplished three times, and mean temperature values at every test were employed for this study. The thermocouples' accuracy and coolant mass flow meter used is ± 0.5 °C and ± 0.15 lpm, respectively; whereas the wattmeter's accuracy is ± 0.9 W. the experiments' uncertainty lies within ± 1.785%.

5.4. Modeling Thermosyphon Natural Convection Heat Pipe System Utilizing MATLAB/Simulink® Software

The proposed and verified simulated model used the thermal-network approach. On the basis of coding the system as a collection of thermal resistance during heat conduction and convection, the mathematical framework was presented. The simulation model provides a condensed path to show the temperatures of the evaporation and condensation. Considering the heat that is transported via Darcy's law from the electrical power source to the evaporator. The relationship between and convection thermal resistance were related to the heat that was transported.

5.4.1. Thermal-network modelling

The device was divided into several sections, each of which was symbolized by a standard thermal resistance. The working fluid that has evaporated traveled upward from the evaporator zone towards the condenser zone via the adiabatic part, where the thermal resistance was supposed to be ignored with from thermal equilibrium. Assumptions also included constant cooling and heating conditions. In order to achieve steady-state, the design requires 35 minutes. The temperatures of the basic working fluids, such as the magnetic nanofluids $NiFe_2O_4$, Fe_3O_4, and Fe_2O_3, as well as the coolant (water), were known variables and were determined using the mean temperature given in experimental findings.

The conduction ($R_{res,cond}$,$R_{evap,w,cond}$ and$R_{c,w,cond}$), and convection ($R_{c,conv}$,$R_{coolant,conv}$ and$R_{evap,w,conv}$) thermal-based network has been presented in Figure 5.2 (a) **and** (b)**.** Despite performing an important role during natural circulation, the falling liquid was not taken into account in the study due to its minimal effects on heat transmission. The following components served as a representation of convective heat transfer: Convection heat transfer occurs in the coolant, condenser operating fluid, as well as evaporator operating fluid. The schematic diagram of the system is shown in Figure 5.3.

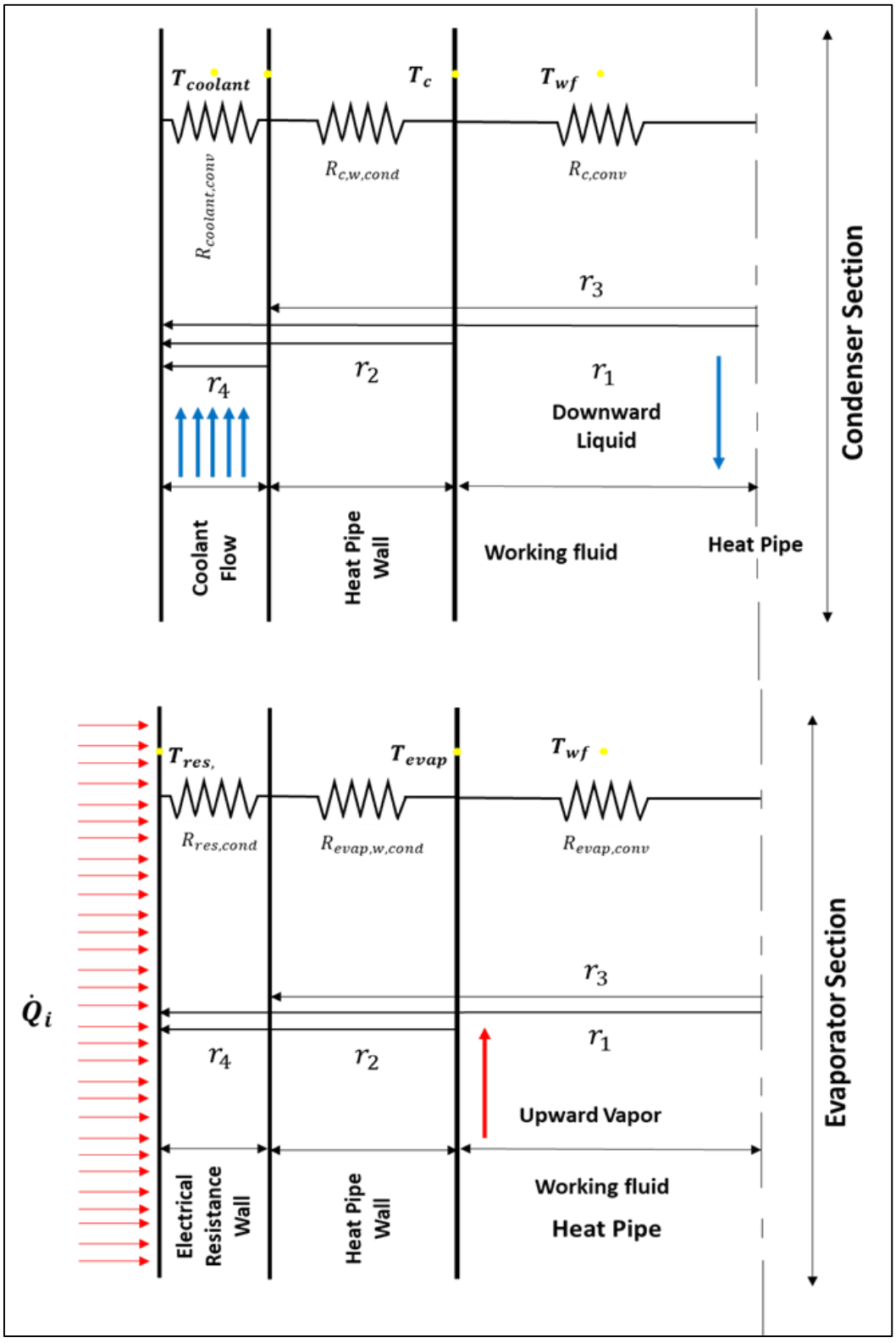


Figure 5.2. Schemetic diagrams for thermal resistance-network throgh the (a) condenser part also (b) evaporator part.

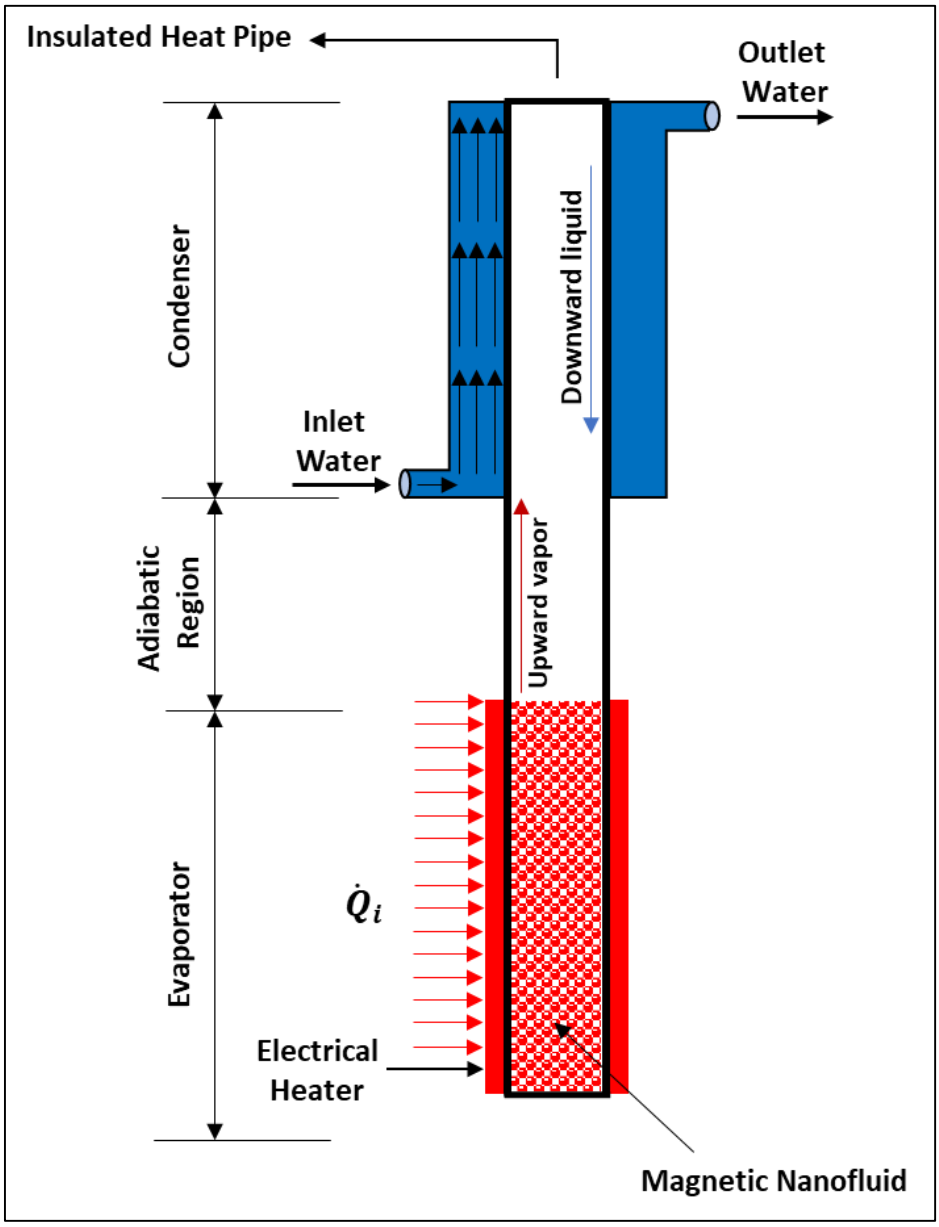


Figure 5.3. Thermosyphon-system schematic diagram

Electrical resistances, along with the evaporator and condenser walls, have shown conduction heat transfer. The electrical resistances power supply provides the heat flux per unit of time ($\dot{Q}_i$). On the basis of energy conservation, a thermal evaluation for the simulated model has been conducted. The control volume energy transmitted throughout each thermal network node was shown in equation 5.26. Based on the presumption that the transient formula could be reduced into a collection of linear differential equations that could be programmed and solved using Simulink [93], a differential model was used to define each node independently.

$$B_m \frac{dT_m}{dt} = \mp \sum \frac{|T_m - T_n|}{R_{mn}} \quad (5.26)$$

Resistance part

A copper pipe with a 40 cm elevation 2.2 cm outside diameter, as well as 0.4 cm in thickness had been utilized to make the evaporator. The evaporator, comprised of a tube made of stainless steel with one centimeter diameter, has been connected with an electrical resistance. Having an overall power of 2KW. Depending upon radial coordinates, Eq. 5.27, which has been derived using Eq. 5.26, presents the balance for the specified control volume:

$$\left(2\rho\pi L r_a (r_1 - r_3) C_p\right)_{res} \frac{dT_{res}}{dt} = \dot{Q}_i - \frac{(T_{res} - T_{evap})}{\frac{ln\left(\frac{r_1}{r_3}\right)}{2\pi k_{res} L_{res}}} \quad (5.27)$$

where: resistance wall temperature was presented by T_{res} and the temperature of the evaporator wall by T_{evap} as well.

Condenser part

Concentric tubes measuring 40 cm in height made up the condenser portion. The coolant circulates within 3.2 cm-diameter exterior tube, whereby the fluid's flow rate has been modified with a flowmeter. The evaporator, which has an interior and exterior diameter equal to (1.8 & 2.2 cm, correspondingly), causes the steam rising to the condenser part. Eq. 5.28 shows the energy balance using the specified control volume. Depends on the radial coordinates and obtained via Eq. 5.26.

$$\left(2\rho\pi L r_{c,a} (r_1 - r_2) C_p\right)_c \frac{dT_c}{dt} = \frac{(T_{wf} - T_c)}{h_c A_c} - \frac{(T_c - T_{coolant})}{h_{coolant} A_c + \frac{ln\left(\frac{r_2}{r_4}\right)}{2\pi k_{cw} L_c}} \quad (5.28)$$

The operating fluid, wall temperature of the condenser, coolant temperature are represented by T_{wf}, T_c , $T_{coolant}$, respectively, which illustrated in Figure 5.3 (a, and b).

Evaporator part

To achieve the energy balance within the evaporator, it was necessary to obtain the evaporator temperatures (T_{evap}), The simulated model's received & discharged energy are taken into consideration as part of the differential equation, which was expressed using Eq. 5.29, that derived using Eq. 5.26 according to radial coordinates.

$$\left(2\rho\pi L r_{e,a}(r_1 - r_2)C_p\right)_{evap} \frac{dT_{evap}}{dt} = \frac{\left(T_{res} - T_{evap}\right)}{\frac{ln\left(\frac{r_1}{r_2}\right)}{2\pi k_{res} L_{res}}} - \frac{\left(T_{evap} - T_{wf}\right)}{\frac{ln\left(\frac{r_2}{r_4}\right)}{2\pi k_{evap} L_{evap}} + h_{evap} A_{evap}} \quad (5.29)$$

5.4.2. Correlations of heat transfer coefficients

Evaporator heat transfer coefficient (h_{evap}) has been evaluated established on Park et al., equation [94], which was specifically developed for a two-phase thermosyphon design, as delivered by Eq. 5.30.

$$h_{evap} = 0.3 \left[\frac{\rho_{l(mnf)}^{0.65} k_{l(mnf)}^{0.3} Cp_{l(mnf)}^{0.7} g^{0.2} q^{0.4}}{\rho_{v(mnf)}^{0.65} h_{lv(mnf)}^{0.4} \mu_{l(mnf)}^{0.1}}\right] \left(\frac{P_s}{P_a}\right)^{0.3} \quad (5.30)$$

Additionally, correlations are used to derive the thermophysical characteristics of the working fluid (5.31, 5.32, 5.33, 5.34, 5.35, and 5.36).

Liquid and vapor-phase densities $\rho_{l(mnf)}$, $\rho_{v(mnf)}$were estimated by Eq.5.31 and Eq.5.32 respectively presented by Pak et al., [84]. Despite the working fluid liquid-phase thermal conductivity $k_{l(mnf)}$ has been determined via Eq.5.33 [89] specific heat capacity of the liquid-phase $c_{pl(mnf)}$ was achieved using Eq.5.34 [82]. As well as, the dynamic viscosity has been determined using Brinkman model Eq.5.35. Also, vaporization latent heat was evaluated using Park et al., Eq.5.36 [94].

$$\rho_{l(mnf)} = \rho_{l(b)}.(1 - \varphi) + \rho_{mnp}.\varphi \quad (5.31)$$

$$\rho_{v(mnf)} = \rho_{v(b)}.(1 - \varphi) + \rho_{mnp}.\varphi \quad (5.32)$$

$$k_{l(mnf)} = 1.4408 - 0.829(lnT) + 0.1588(lnT^2) - 0.0702(1-\varphi) - 0.2151(lnT)(1-\varphi) + \frac{0.5965T}{(1-\varphi)} - \frac{0.39T}{(1-\varphi)^2} \quad (5.33)$$

$$c_{pl(mnf)} = \frac{\rho_{l(b)}.c_{pl(b)}(1-\varphi)+\rho_{l(mnp)}.\varphi.c_{p,mnp}}{\rho_{l(mnf)}} \quad (5.34)$$

$$\mu_{l(mnf)} = \frac{\mu_{l(b)}}{(1-\varphi)^{2.5}} \quad (5.35)$$

$$h_{lv(mnf)} = h_{lv(mnf)} + h_{lv(b)}(1-\varphi) \quad (5.36)$$

where: φ magnetic nanofluids weight percent (%), ρ_{mnp} magnetic nanoparticles density (kg/m^3), $c_{pl,b}$ and $c_{p,mnp}$ specific heat capacity of the liquid-phase base fluid and magnetic nanoparticles specific heat capacity respectively (KJ/kg.K), $\mu_{l(b)}$ base fluid liquid-phase dynamic viscosity, as well as $h_{lv(b)}$ base fluid vaporization latent heat (KJ/kg).

The principal purpose of condensers is to discharge heat to the coolant, which is usually circulated inside the outer tube by employing pumps. Based on Reay et al., condensation [95] heat transfer coefficient h_c may occur fundamentally via condensing the vapor which was created through the evaporator presented by Eq. 5.37 [94]. Which was utilized in this empirical representative. The practical correlation is applied to estimate. The coolant convective heat transfer coefficient ($h_{coolant}$) given by Eq. 5.38 [88]. The operating fluid Nusselt number was obtained by Eq. 5.39 presented by Ilyas et al., [89], which is a function of magnetic nanoparticle weight percent, Rayleigh number, Prandtl Number, and thermal conductivity. Empirical correlation is conducted to calculate the magnetic nanofluids Ra number was presented by Eq. 5.40 [91].

$$h_{con} = 0.943 \times \left[\frac{\rho_{l(mnf)}\, g\, k^3_{l(mnf)}\, (\rho_{l(mnf)}-\rho_{v(mnf)})[h_{lv(mnf)}+0.68Cp_{l(mnf)}(T_v-T_{con})]}{\mu_{l(mnf)}\, L_{con}\, (T_v-T_{con})}\right]^{0.25} \quad (5.37)$$

$$Nu_{coolant} = 0.372Re^{0.687}Pr^{0.3} \quad (5.38)$$

$$Nu_{wf} = 4.17\left[\frac{Pr}{Pr-0.343}\right]^{2.51}\left[\frac{Pr}{k_{wf}{}^{3.76}\beta^{3.483}_{mnf}}\right](1-\varphi)^{-0.015}Ra^{0.04} \quad (5.39)$$

Pr Prandtl number (unitless), k_{wf} working fluid thermal conductivity (W/m.K).

$$Ra_{mnf} = \frac{g[\rho_{mnf}(1-\varphi)\beta_{mnf}+\varphi\rho_b\beta_b][T_{wf}-T_i]\rho_{mnf}C_{p,mnf}L^3}{\mu_{mnf}k_{mnf}} \quad (5.40)$$

5.4.3. Numerical simulation approach

A collection of linear first-order ordinary differential equations were used for describing the numerical simulation. Which were applied to the condenser and evaporator sections' transient operations. The standard solver "ode45" from the Simulink library shown in Figure 5.4 was used for solving those differential equations, whose were coded using MATLAB/Simulink® software version 9.10 (R2021a). With the goal to maximize numerical efficiency, that solver uses the Runge-Kutta 4th-order approach as a function of time step. Which was developed for handling and integrates the subsequent general equation$y' = f(t, y)$. With regards to a set of differential equations from t_0 to t_f within initial conditionsy_0. Every row of the solution array *y* relates to an amount returned within column vector *t*. Every MATLAB/Simulink® ODE solver can work with systems of linear equations with the following form$y' = f(t, y)$, along with problems using a mass matrix, $M(t, y)y' = f(t, y)$. the formats used by the solvers are similar. The initial solvers that ought to be used for the majority of problems is the modular ODE solver ode45s. The temperature differential equation was therefore a function of various factors integrated over a predetermined time period. Which presented as$\frac{dT_{res}}{dt} = f(t, T_{res}, T_{evap})$,$\frac{dT_c}{dt} = f(t, T_c, T_{coolant}, T_{wf}, h_{con}, h_{coolant})$ and$\frac{dT_{evap}}{dt} = f(t, T_{res}, T_{evap}, T_{wf}, h_{evap})$.

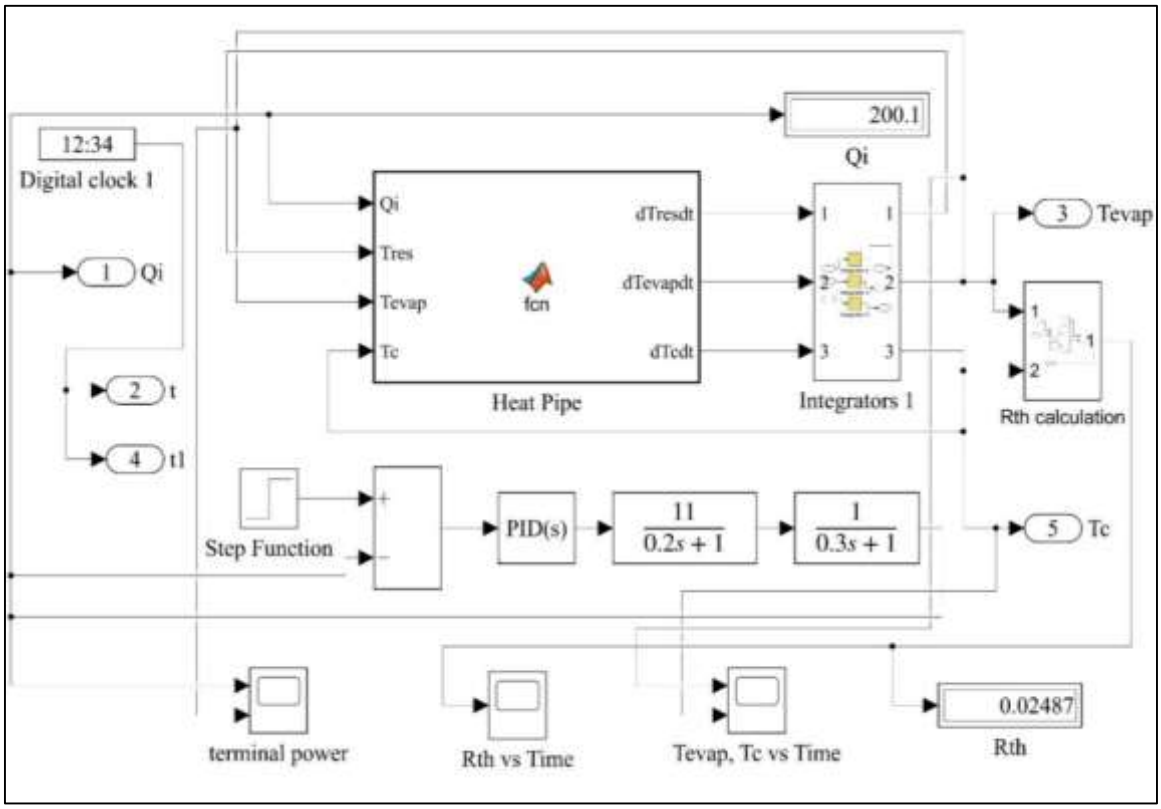


Figure 5.4. Heat pipe system simulation using MATLAB/Simulink®.

5.4.4. PID control system

A major structural instrument of the modern control techniques presented in Fig. 5.4 involves the PID control approach. Numerous commercial applications, including power converter, mechanical, electromechanical, chemical, and control have used this technique. Such a kind of control system's importance has increased for a number of essential causes, including how simple it is to implement. The recommended approach is an achievement finished in discrete time having control signal restrictions appraised, despite the PID controller method being designed and examined within continuous time mode. Employing the correlation given in Wang et al., [96] results in the calculation for the PID controller's signal, u (t).

$$u(t) = K_c e(t) + \frac{K_c}{\tau_I}\int_0^t e(\tau)d\tau - K_c\tau_D\frac{y_f(t)}{dt} \quad (5.41)$$

Here, the response error signal for the transmitted signal is shown as $e(t) = r(t) - y(t)$. $r(t)$ and the output $y(t)$, and $y_f(t)$ denotes the output signal after filtering. It is important to make it clear that all of the signals used in the calculation represent deviations values over

the physical amounts within a steady state procedure rather than the accurate physical quantities expressed in numerical form. To be more exact, the result of the signal $y(t)$ as well as the command signals $u(t)$,, $r(t)$, and t(t) show how the steady state mechanism differs from the initial conditions in terms of the corresponding physical variables. The variance in the controlling quantity u(t) is instantaneously obtained and constructed using the control variation $e(t)$ under the function conditions for the PID controller. Therefore, it is essential for performances when using the PID controller's functional state that information regarding the steady state between the command signal as well as the resultant signal has been established before. Depending on the Ziegler-Nichols tuning approach, which showed the smallest performance errors indicators, the settings used during the PID controller module were stated by table 5.1.

Table 5.1. Controller parameters.

P (proportional)	0.21121
I (integral)	0.18851
D (derivative)	0.05679
N	173.2203

The hit and trail approach is an important process for tuning the PID controller. A PID tuner was provided using MATLAB program. Figure 5.5 shows the PID controller's representation of the input power of the system. This figure illustrates the fluctuation of the signal from the start of the simulation until it reaches steady state in a certain amount of time. While Figure 5.6 depicted the controlled evaporator temperature using two different PID controller modes, it is evident that the PID controller performed better in the PID mode because it autonomously offered the tuned response within a matter of seconds with a zero overshoot.

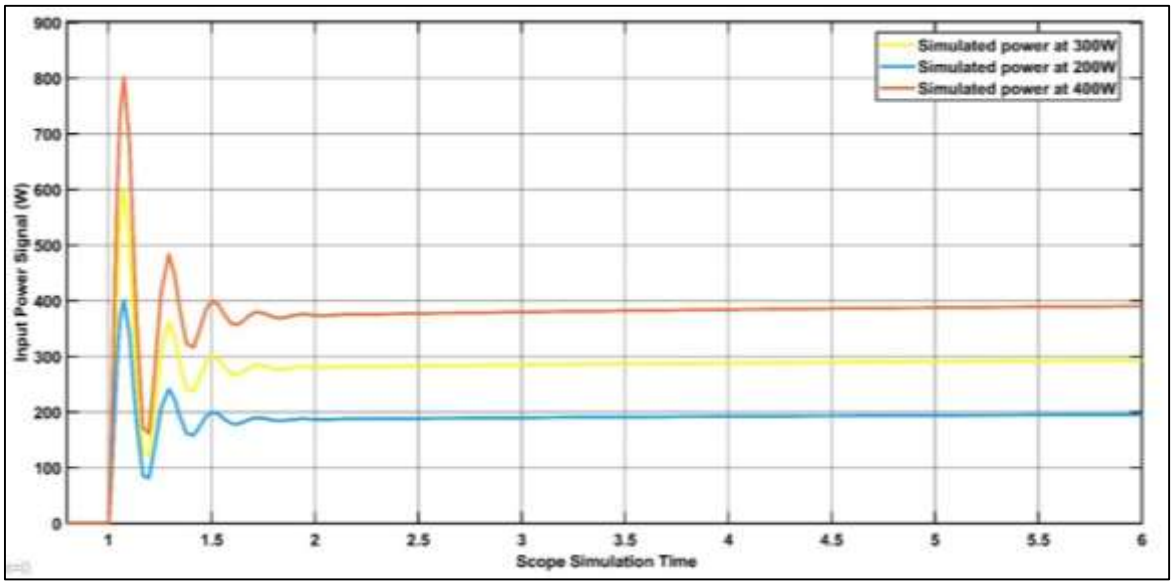


Figure 5.5. Simulated input power 200W, 300W, and 400W applying PID controller.

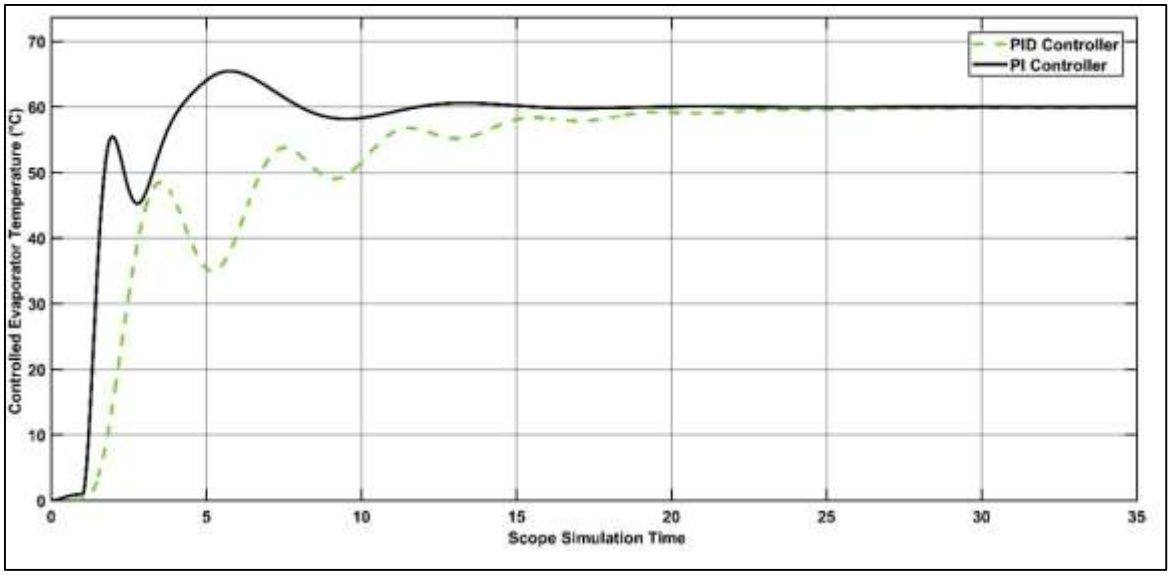


Figure 5.6. Evaporator temperature Simulation of 2 independent PID controller regimes.

6. RESULTS AND DISCUSSIONS

The results that were conducted from the three thermal systems have been presented in this section:

6.1. Results From (Air-to-Air) Heat Pipe Heat Exchanger System

Figure 6.1 and Figure 6.2 discussed the Wall temperature distribution in a heat pipe system operating under magnetic-nanofluids as well as pure water prepared with 1 wt. % concentration ratio and at various Re Number within cold and hot air streams.

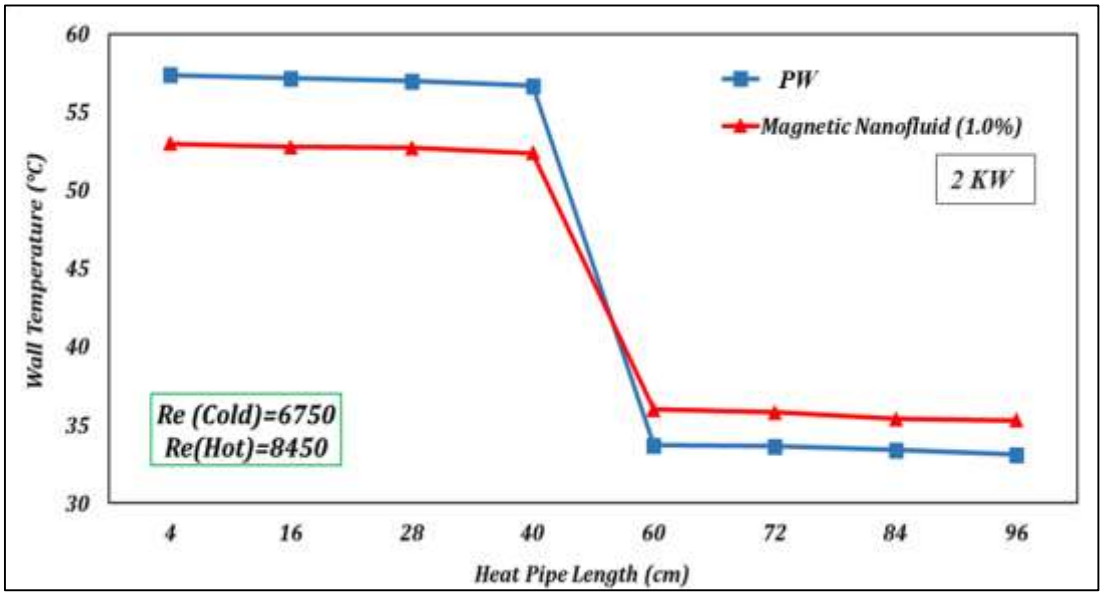


Figure 6.1. Estimated temperature amounts at diverse areas along heat pipe wall under magnetic nanofluid and pure water at (1 wt. %) and 2 KW input heat.

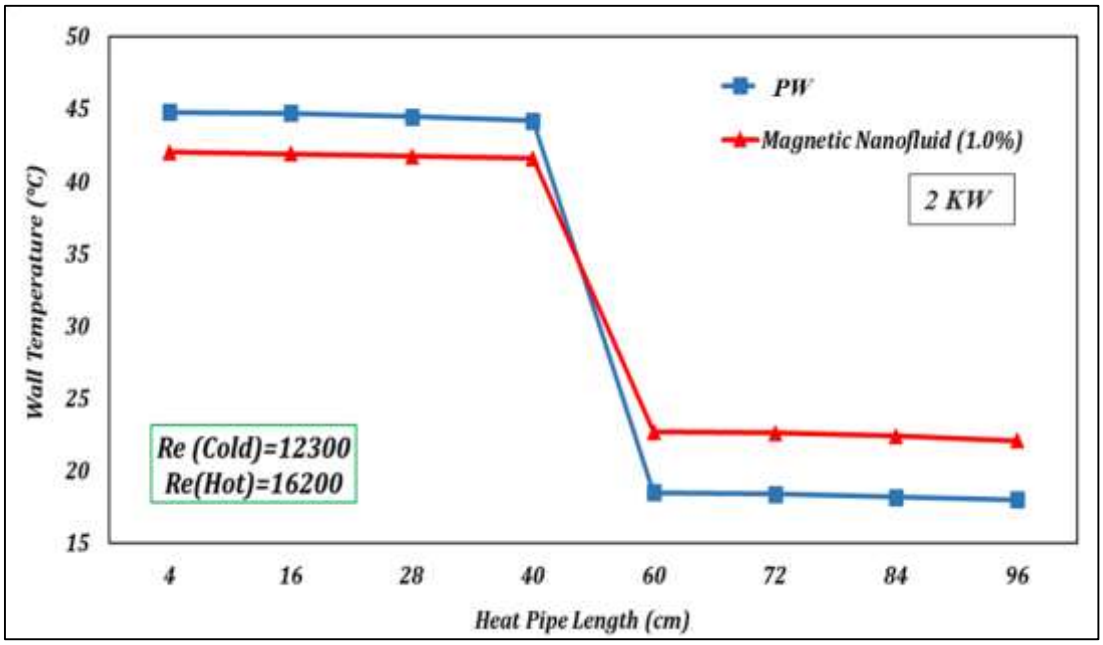


Figure 6.2. Estimated temperature amounts at diverse areas along heat pipe wall under magnetic nanofluid and pure water at (1 wt. %) and 2 KW input heat.

This graphic was created primarily to clarify the effects of magnetic-nanoparticles on changes in temperature at optimum concentration parameters. Similar comparisons for the 0.5 wt. % and 1 wt. % affecting wall temperatures are shown in Figures 6.3 and 6.4.

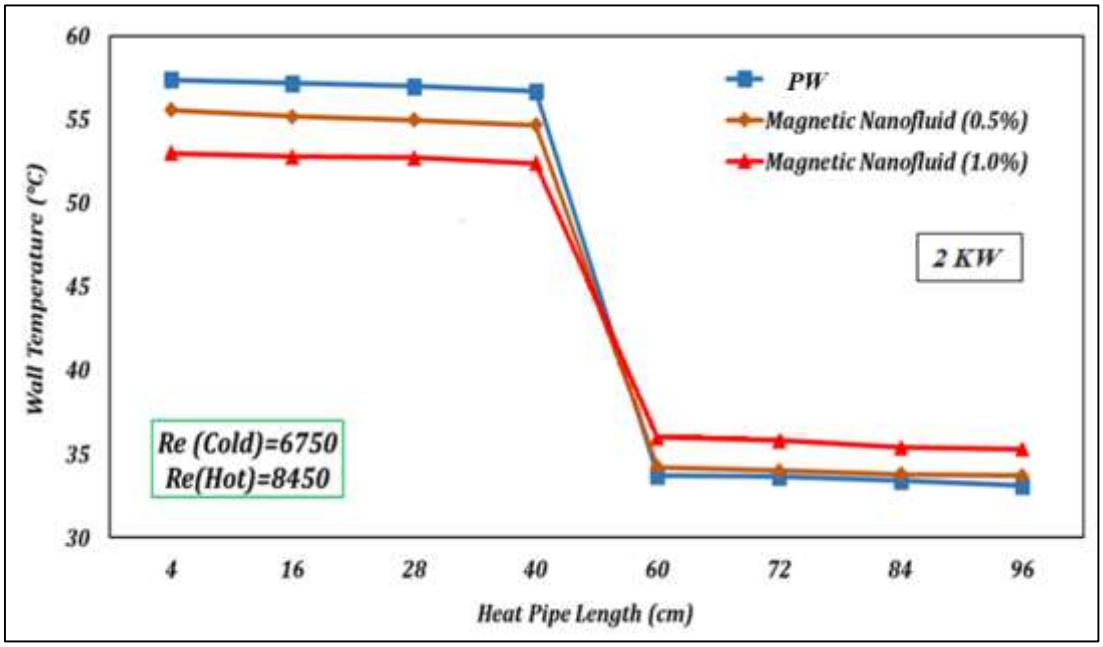


Figure 6.3. Comparison of wall temperature under magnetic nanofluids and pure water at 2KW input heat.

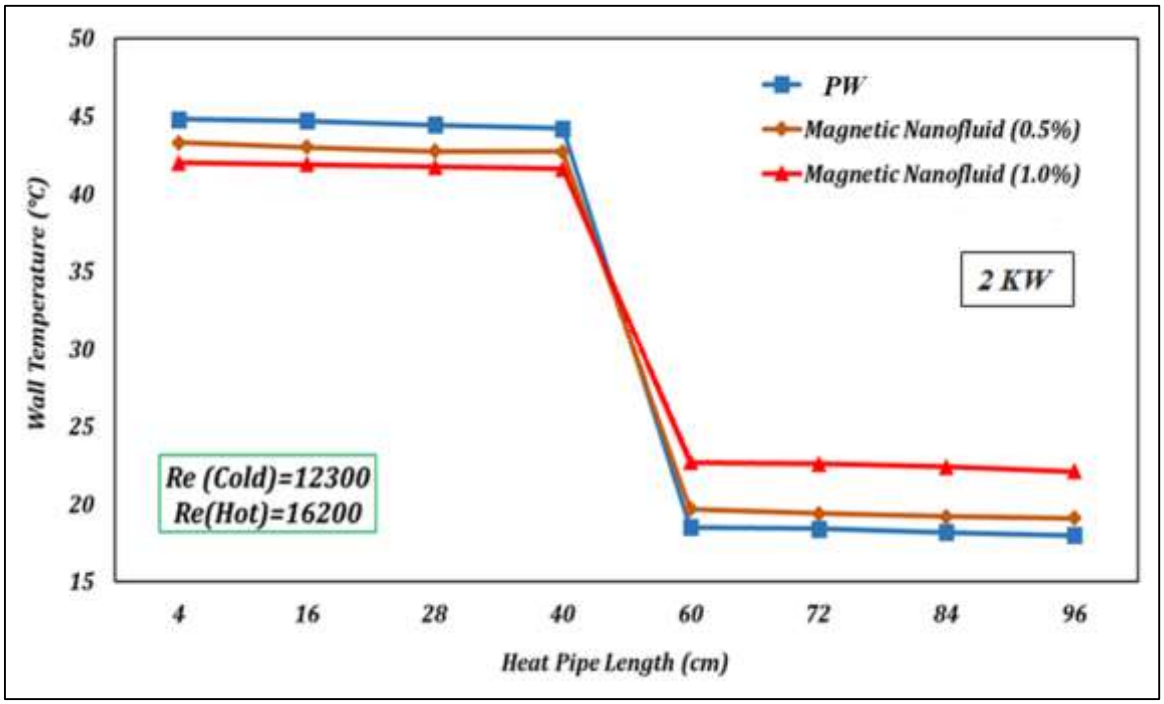


Figure 6.4. Comparison of wall temperature under magnetic nanofluids and pure water at 2KW input heat.

The two experimental setups that produced the fastest boosts to thermal efficiency have been displayed in Figures 6.2 to 6.4. These data were examined, and it was discovered that the temperature disparities across the heat pipes' condenser and evaporator parts were reduced when magnetic nanofluid was used in place of pure water. Consequently, by employing magnetic-nanofluids, the heat pipe's thermal resistance was reduced. Additionally, a rise in nanofluid particle numbers has a beneficial effect upon thermal resistance. The thermal resistances decrease with increasing weight percent. Higher heat transfer results achieved from lower thermal resistant’s.

The usage of nanofluids decreased the evaporator temperatures, which indicates that the evaporation process occurs at fewer degrees when nanofluids are employed rather than pure water, which was a further significant conclusion drawn from these data. As a result, the system's usage of magnetic-nanofluid allows it to recover heat from low-temperature supply.

The thermal efficiency numbers are one of the performance measures for heat pipes, as is common knowledge. Figure 6.5's bar graph displays the heat pipe's thermal efficiency numbers. The graph was created by taking into account the rising cold duct Re numbers. Values for the hot duct Re numbers were also supplied in brackets.

When this diagram is taken into account, it is clear that using magnetic nanofluids instead of pure water resulted in greater efficiency ratings across all of the experiments. The thermal efficiency ratings have likewise risen as nano-particle concentration rises. The relationship among concentrations and efficiency, was non-linear, therefore twice the concentration does not automatically result in a 2-fold boost in efficiency. For instance, raising the concentration from 0.5 wt. % to 1 wt. % increased efficiency from 20.1% to 25.2% while the cold tunnel Re Number equal to 7050.

When the cold channel Re number was up to 12400 and the hot channel Re Number was 16500, the highest efficiency ratings for every operating fluid were obtained. For both hot and cold channels, these Re numbers were the highest. The greatest efficacy was 25.4% and 30.9% at 0.5 wt. % and 1 wt. %. As well as under pure water the efficiency enhancement was calculated to be 22.9%.

The efficiency growth percentage is shown in Figure 6.5. Magnetic-nanofluid at a 1 1 wt. % improves significantly under all circumstances. The cool air channel Re number at which the highest improvement rate of 85.2% had been achieved was 6750.

Particles concentration, improving rates numbers, and thermal efficiency must all be taken into consideration when determining the heat exchanger system's optimal conditions for operation. Enhancement rate numbers and efficiency in the cool air stream were 60.2% and 15.7%, respectively, at 7050 Re Number. Those were the conditions where the partial maximum levels of improvement rate and efficiency could be found. Those conditions were 1 wt. % as well as 8900 Re Number respectively.

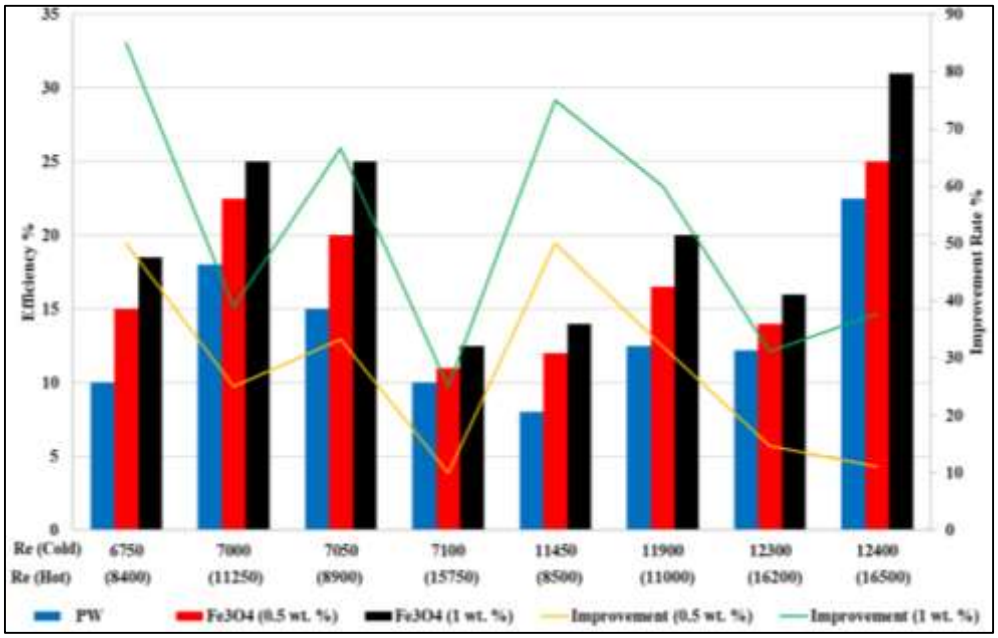


Figure 6.5. Comparison of improvement rates and efficiency amounts for magnetic nanofluids and pure water under rising Re Number.

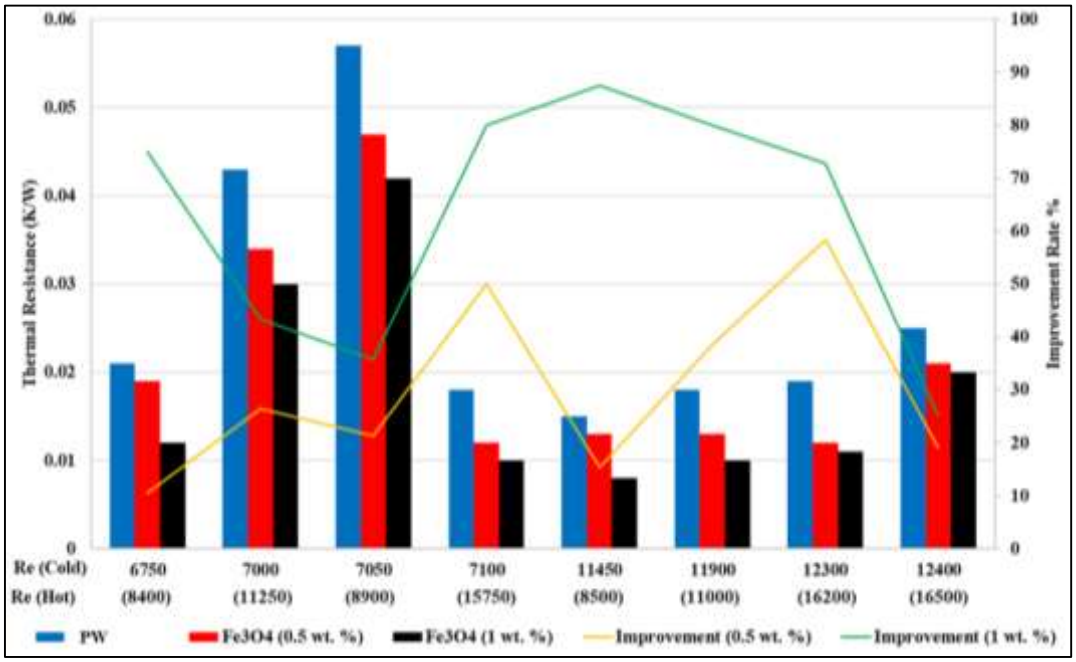


Figure 6.6. Comparison of improvement rates and thermal resistance amounts for magnetic nanofluids and pure water throughout rising Re number.

Thermal resistant was another enactment indicator at heat pipe heat exchangers. It is expected that more inferior thermal resistant's were performed by employing nano-fluids within heat pipes since descending thermal resistant indicates a more elevated heat transfer rate. Figure 6.6 demonstrates the thermal resistant's and also a comparison of all operating

liquids. This figure overly displays that utilizing magnetic-nanofluids in place of pure water delivered an influence on reducing thermal resistant's. Enriching the particles concentration diminished the thermal resistant at all conditions. The highest reduction in thermal resistant's was performed at 1 wt. %. When the cold chimney Re Number was 11450, the lowest thermal resistant amounts were conducted at all operating fluids. In this state, the highest decrement rate was performed up to 87.5% at 1 wt. %.

6.2. Results From Concentric Tube Heat Exchanger System (Parallel And Counter Flow Regimes)

In this analysis, the enactment of a counter and parallel-flow system working under Fe_3O_4@Fe_2O_3/PW hybrid magnetic is experimentally studied compared to pure water, and (Fe_3O_4/PW) & (Fe_2O_3/PW) poly magnetic-nanofluids.

6.2.1. Wall temperature distribution (°C)

Figures 6.7 and 6.8 show the temperature variance of two distinct fluids as well as the wall temperature across the counter and parallel-flow systems. The hybrid magnetic-nanofluid running via the inner at Reynolds number of 27162, while the water passing through the exterior pipe is maintained at a Re Number of 14630. Comparisons have been made between base fluid, hybrid magnetic-nanofluids and two poly magnetic-nanofluids with 0.5 wt. %.

Depending on what appears in these two figures, the hybrid magnetic-nanofluid has a lower wall temperature than conventional working fluids and a higher outlet temperature for cold flow. Heating the water inside the outside pipe was the purpose of using hybrid magnetic-nanofluid, and it can be accomplished due to the improved of hybrid magnetic nanofluid capabilities. The fluid inside the outside tube has a higher exit temperature when employing the same cold fluid with merely a combination of high thermal conductivity nano-particles.

A number of factors have an impact on the hybrid magnetic-nanofluid's output temperature. As was already noted, hybrid magnetic-nanofluid has improved thermal conductivity. This factor directly affects the hybrid magnetic-nanofluid's output temperature. It is possible to conclude that thermal conductivity has a constant influence based on the increase in output temperature. Another problem was that the hybrid magnetic-nanofluids temperature changes

more quickly than that the poly magnetic-nanofluid and pure water. This happens because the thermal conductivity of the hybrid magnetic nanofluid increases by 13.6% and 8.6% in comparison to poly magnetic-nanofluids Fe_2O_3/PW and Fe_3O_4/PW.

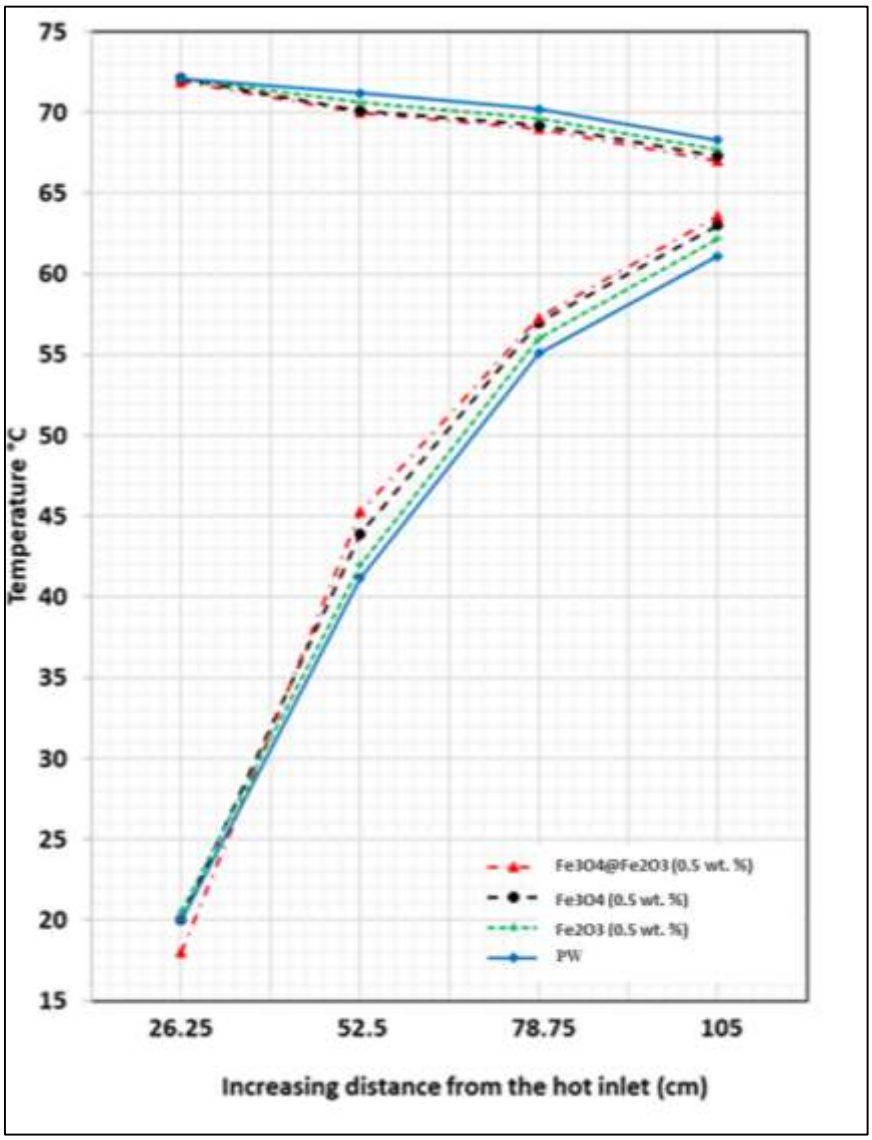


Figure 6.7. Temperature deviation during counter-flow along the system under 14629.6 Re Number of coolant as well as 27161.6 Re Number of hot fluid.

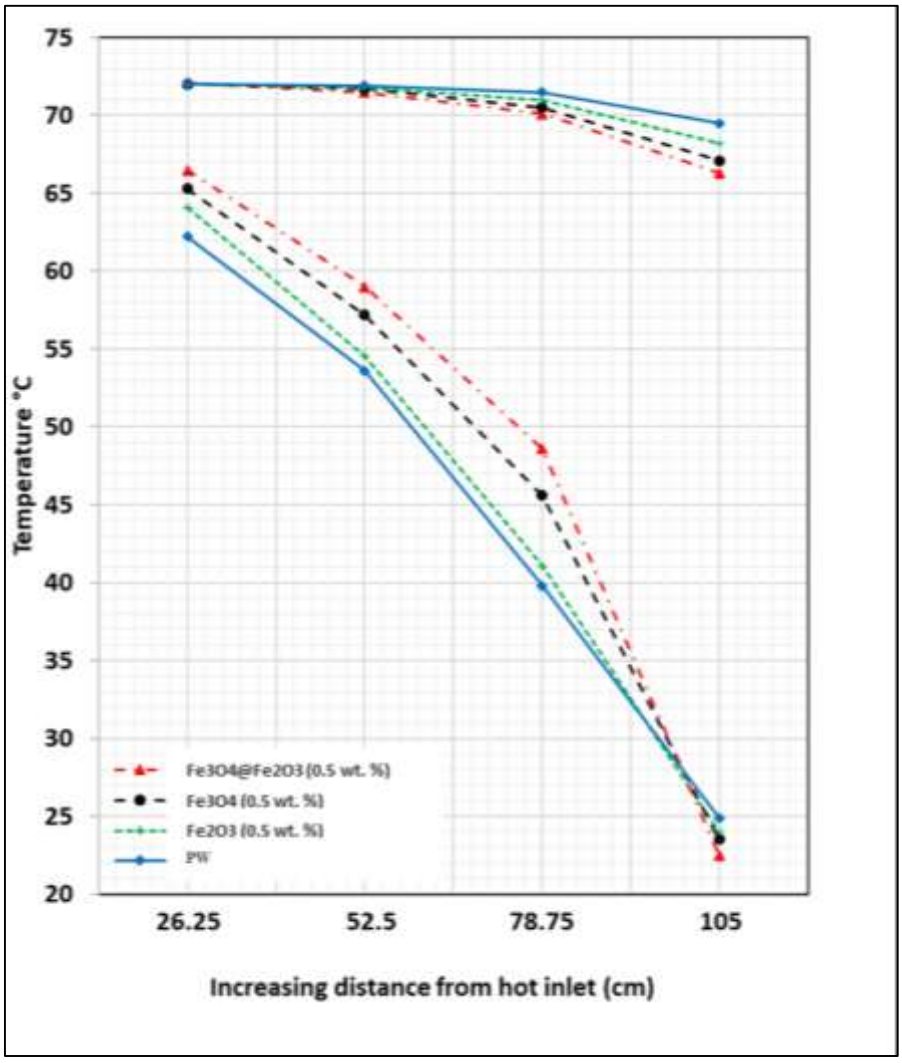


Figure 6.8. Temperature deviation during counter-flow along the system under 14629.6 Re Number of coolant as well as 27161.6 Re Number of hot fluid.

6.2.2. Overall heat transfer coefficient (U)

It is evident from Figures 6.9 and 6.10. As the expansion in Re Number from 13581 to 40742, the overall heat transfer coefficient enhances at both counter and parallel-flow systems, which happened due to the growth at convective heat transfer coefficient of the inner tube. For a given Re Number, the hybrid magnetic-nanofluids overall heat transfer coefficient was higher than the pure water as well as poly magnetic-nanofluid. The most elevated improvements' in overall heat transfer coefficient were conducted along the parallel-flow mode up to 49.8% while operating Fe_3O_4@Fe_2O_3/PW hybrid magnetic-nanofluid related to pure water under 31689 Re Number.

The approach also demonstrated high thermal performances at 31688.5 Re Number, which were 14.1% and 9.7% in comparison with the poly magnetic-nanofluids mentioned earlier. Additionally, 20.5%and 18.46% in contrast to Fe_2O_3/PW and Fe_3O_4/PW magnetic-nanofluids at 36215 Re Number. Nonetheless, this is a variations points as might be observed from the error bars shown in Figure 6.10. However, with the counter-flow system, the highest improvements were 28.57% when using hybrid magnetic-nanofluid compared to pure water and 8.36% and 5.42%, as compared to Fe_2O_3/PW and Fe_3O_4/PW poly magnetic-nanofluid, respectively at during 36215 Re Number.

These results might be made clearer by increasing the working fluid's capacity for heat transmission by mixing in two different kinds of magnetic-nanoparticles that have high thermal conductivity. Additionally, the improvements in hybrid magnetic-nanofluid thermal conductivity within the inner flow and the uneven particle concentrations throughout the tube as a result of the variations in the density of the two types of magnetic-nanoparticles provide important explanations for these improvements.

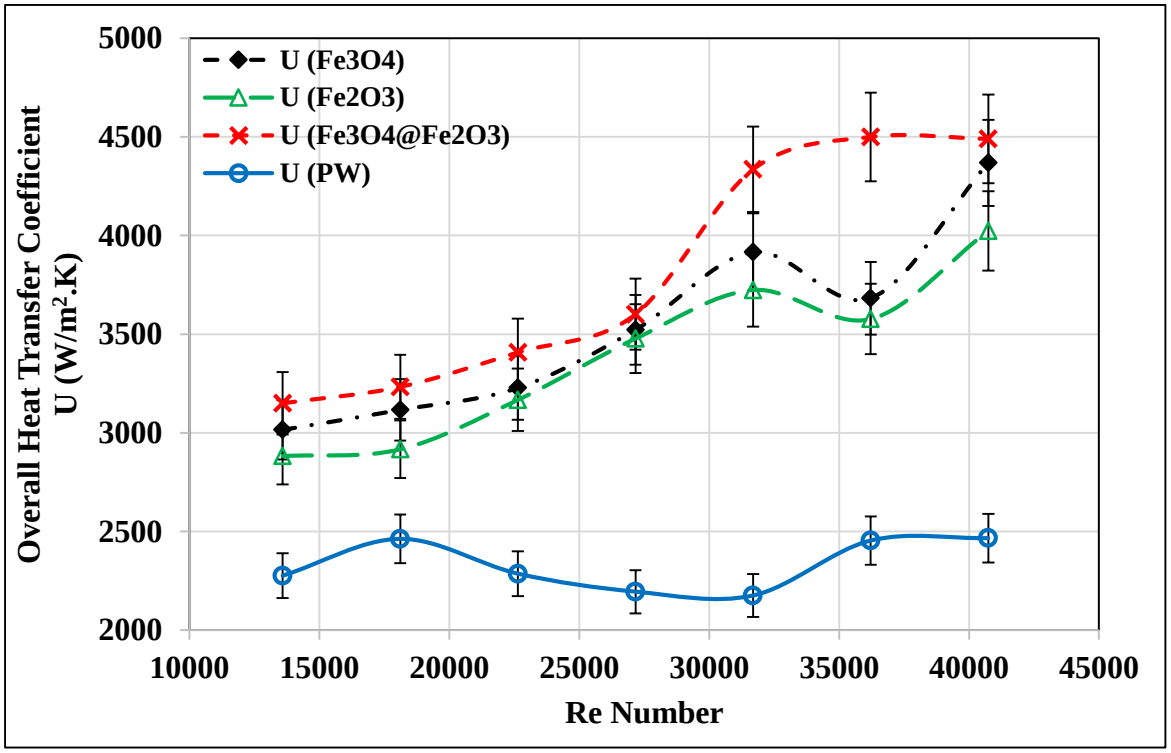


Figure 6.9. Overall heat transfer coefficient as a function of Re Number at parallel-flow regime under 10 g/s coolant mass flow.

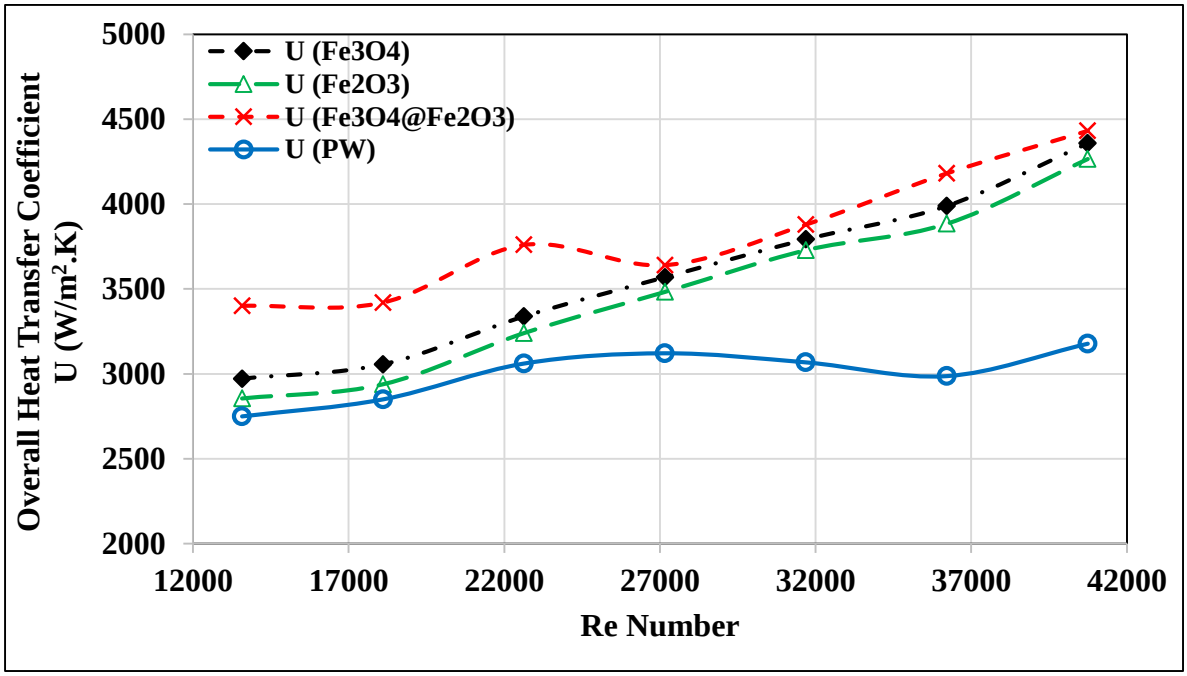


Figure 6.10. Overall heat transfer coefficient as a function of Re Number at counter-flow regime under 10 g/s coolant mass flow.

6.2.3. Heat transfer coefficient in the hot stream (h_{hot})

Figures 6.11 and 6.12, show the hot stream's (h_{hot}) heat transfer coefficient in counter- and parallel-flow modes as a function of Re Number. It is clear from both Figures that all operating fluids responded to the rise in Re Number in the same way. Due to more intense nano-particles motions and a larger speed variance between base fluid and particles a, heat transfer coefficient increases as the Re Number rises.

Heat transfer coefficient of the inner stream, which included Fe_2O_3/PW, Fe_3O_4/PW magnetic-nanofluids, and pure water, significantly increased while using Fe_3O_4@Fe_2O_3/PW hybrid magnetic-nanofluid. During the parallel-flow system, using hybrid magnetic-nanofluid increased the heat transfer coefficient by as much as 47.97% when compared with pure water during 40742 Re Number and by 16.94% and 14.49% when comparing to Fe_2O_3/PW and Fe_3O_4/PW poly magnetic-nanofluids at 36215 Re Number. When used during the counter-flow system, hybrid magnetic-nanofluid boosted the heat transfer coefficient by as much as 28.31% when compared with pure water for 40742 Re Number as well as by 7.1% and 4.59% when poly magnetic-nanofluids Fe_2O_3/PW and Fe_3O_4/PW were used at 36215 Re Number.

The utilization of hybrid magnetic-nanofluids results in a substantial boost in the working fluid's viscosity, which can reach as high as 13.32% when contrasted with pure water as well as 6.9% and 10.11% when comparing with Fe_2O_3/PW and Fe_3O_4/PW magnetic-nanofluids. Furthermore, the hybrid magnetic-nanofluids thermal conductivity was improved by 22.47% in comparison to pure water as well as by 13.58% and 8.6% in comparison with Fe_2O_3/PW and Fe_3O_4/PW, respectively, poly magnetic-nanofluids.

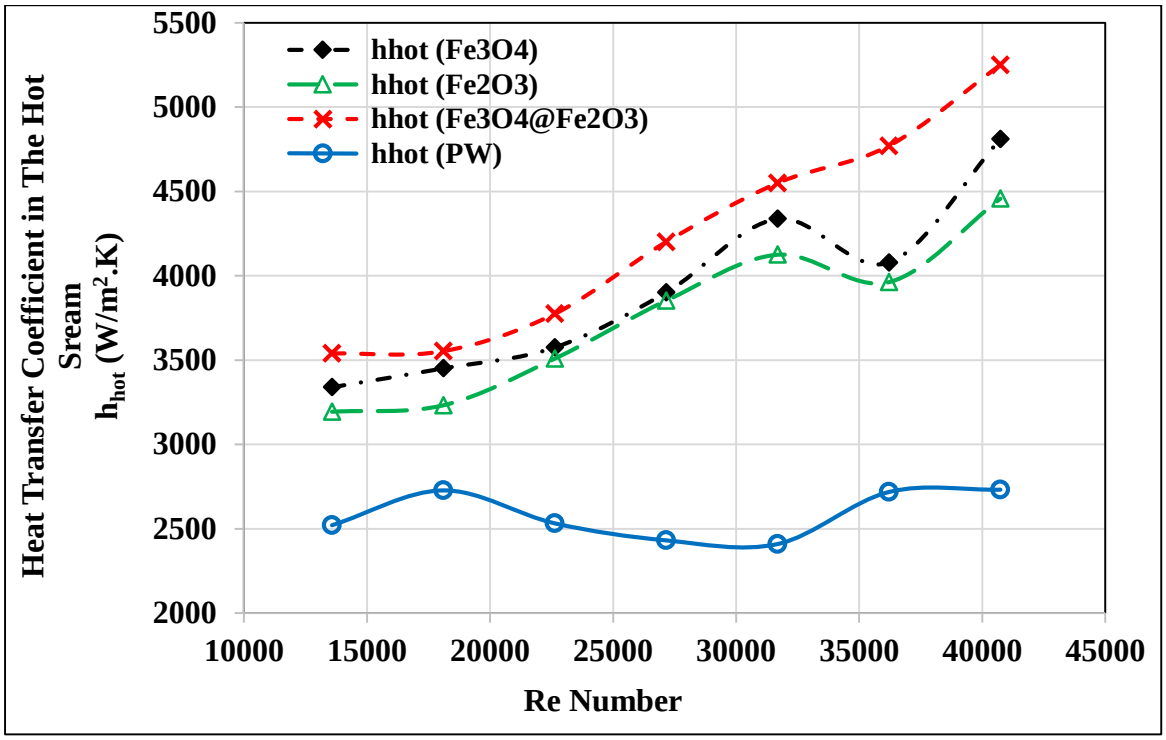


Figure 6.11. Heat transfer coefficient in hot stream as a function of Re Number at parallel-flow concentric tube heat exchanger system under 10 g/s coolant mass flow.

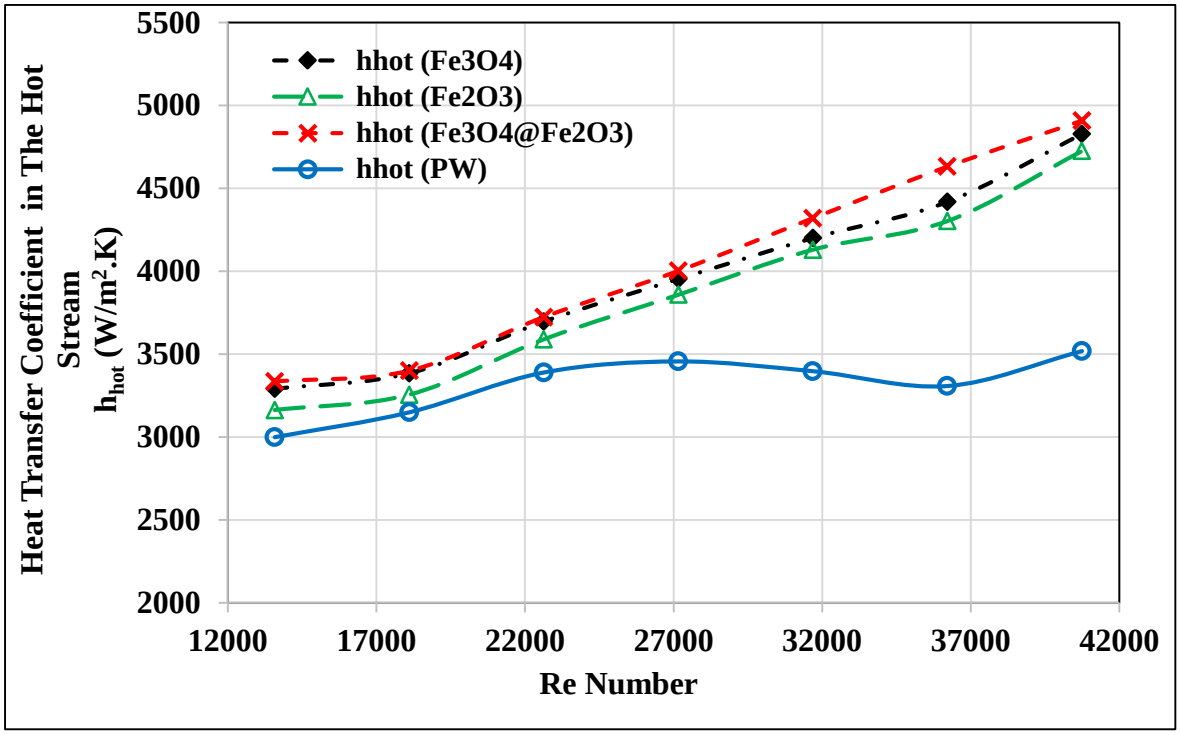


Figure 6.12. Heat transfer coefficient in hot stream as a function of Re Number at counter-flow concentric tube heat exchanger system under 10 g/s coolant mass flow.

6.2.4. Heat transfer coefficient in the cold stream (h_{cold})

Figures 6.13 and 6.14, for counter and parallel-flow centric pipe heat exchangers, respectively, provide a comparison of the heat transfer coefficient at the cold channel using, poly magnetic-nanofluids, hybrid magnetic-nanofluid as well as pure water at different Re Numbers. The hybrid magnetic-nanofluid Fe_3O_4@Fe_2O_3/PW revealed a considerable enhancement in the convective heat transfer coefficient across both counter and parallel systems at a given amount of Re number. In comparison to water at (22635 and 31689) Re number, the enhancement rates were around 11.66% and 25.12%, respectively.

While the improvement rates were 17.07% and 16.9% corresponding to Fe_2O_3/PW and Fe_3O_4/PW, respectively at the parallel system under 36216 Re number. Nonetheless, in the counter system was 3.844% and 4.45% under 27162 Re Number. Similarly, with the increase of nanofluids flow, the impact of nanoparticles collision with wall increases, which conducts to temperature elevation. Thus, rise in temperature, nano-fluids kinematic viscosity drops, conducting to a more elevated Re Number. The findings of this analysis reveal that the heat transfer coefficient of hybrid magnetic-nanofluids grows significantly.

This is mostly due to the addition of 50:50 two various magnetic-nanoparticles enhanced the fluid heat transfer enactment. Heat transfer refinement could be impacted by multiple mechanisms like, nanoparticles colliding with molecules of water as well as the wall, therefore intensification energy transfer and the nanofluid improved friction among fluid and wall, enhancing heat exchange.

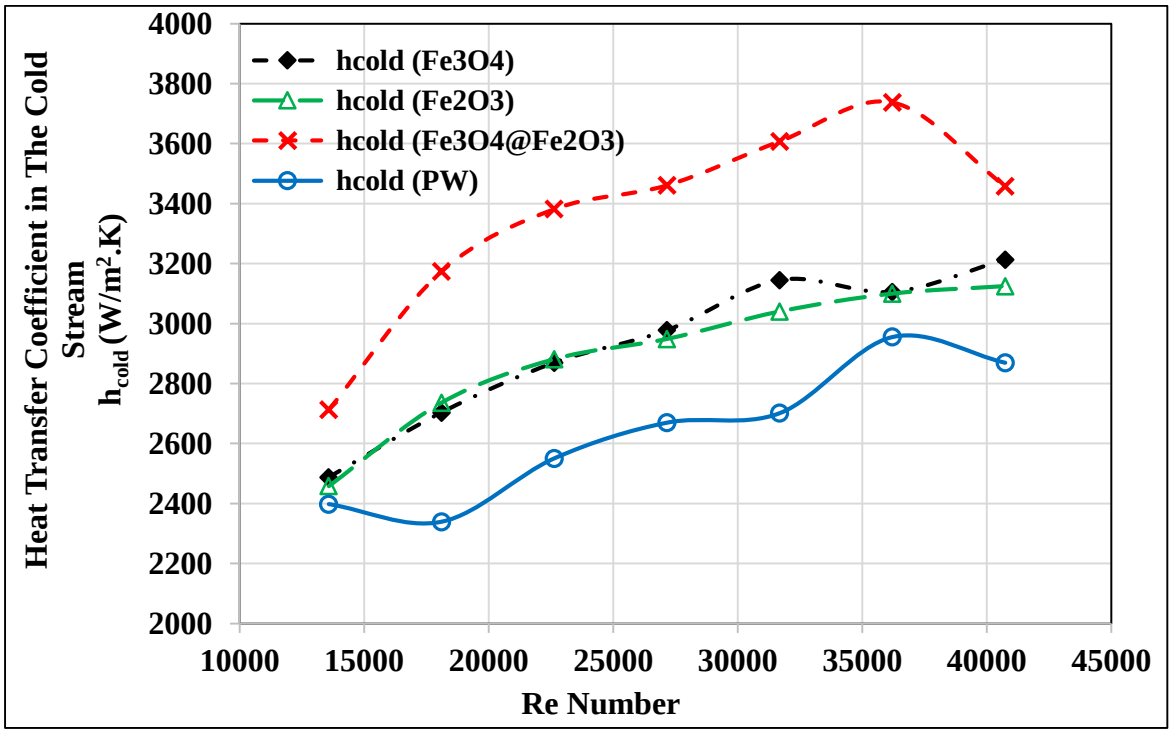


Figure 6.13. Cold stream heat transfer coefficient as a function of Re Number at parallel-flow concentric pipe heat exchanger system under 10 g/s coolant mass flow.

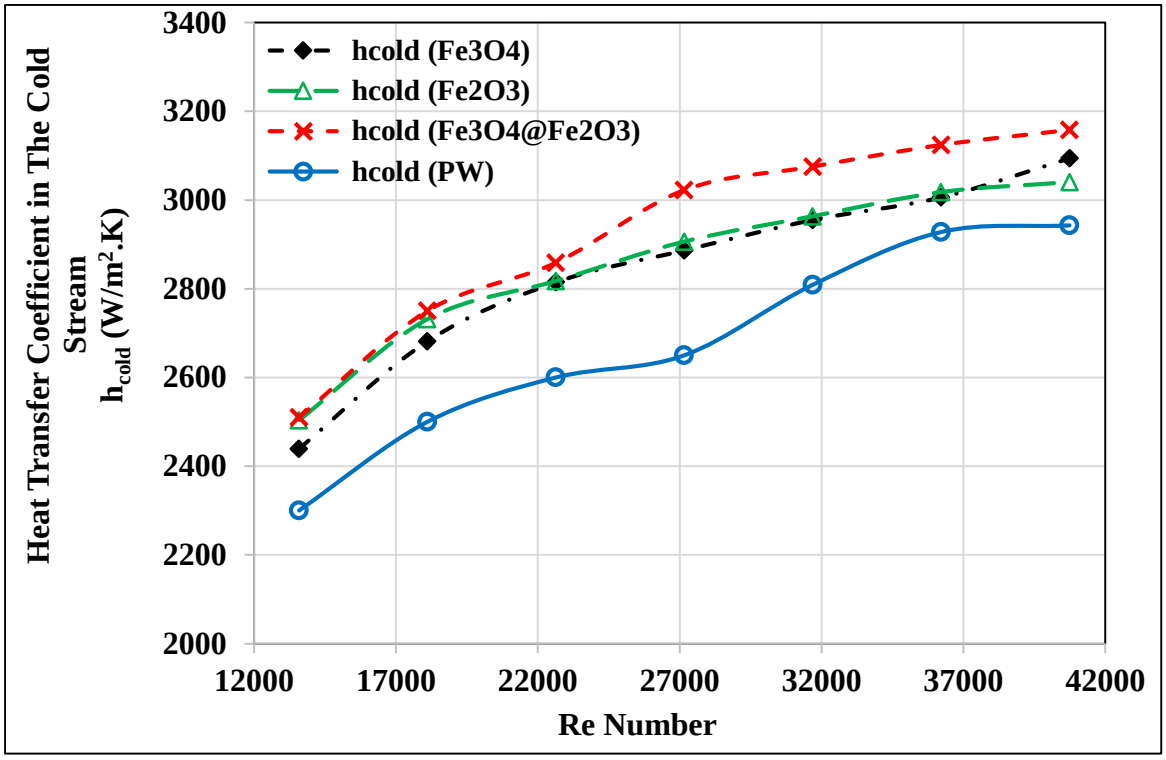


Figure 6.14. Cold stream heat transfer coefficient as a function of Re Number at counter-flow concentric pipe heat exchanger system under 10 g/s coolant mass flow.

6.2.5. Heat transfer coefficient ratio and improvements

Figures 6.15 and 6.16 display the change in the heat transfer coefficient ratio for poly and hybrid magnetic-nanofluids compared to base liquid evaluated at various Re Numbers. When hybrid magnetic-nanofluids were used, the overall heat transfer coefficient proportion to foundation fluid achieved its maximum value, up to 1.4 and 1.99 under 36216 and 31689 Re Numbers for the counter and parallel-flow concentric pipe systems, respectively.

For parallel-flow concentric pipe exchanger structures, the highest values of the heat transfer coefficient at cold and hot channels in relation to the base fluid proportion additionally showed up in the case of using hybrid magnetic-nanofluids, reaching as high as 1.88 and1.35, respectively, at 31689 Re Numbers. In the counter-flow concentric tube heat exchanger system, these proportions were 1.39 and1.13 at 36216 and 22635 Re Numbers, respectively.

This indicates that, as can be seen in Figure 6.17, the Fe_3O_4@Fe_2O_3/PW hybrid magnetic-nanofluids had greater heat transfer coefficients in both systems than the pure water with a range of approximately 28-48% at hot channel and 11.6-25.1% at cold stream. It has been discovered that a combination of two different kinds of poly magnetic-nanoparticles boosts the viscosity, density, as well as thermal conductivity.

Nevertheless, the convective heat transfer coefficient growths related to water because of the gain in thermal conductivity, lowering the thermal boundary layer consistency (motion of particles around the wall, migration of these particles to the middle of the tube, also decrease viscosity effective on the wall) and likely improvement of heat transfer ability due to many slips nanofluid mechanism. The convection heat transfer coefficient of different nano-fluids grew up to maximum in the case of hybrid magnetic-nanofluids and also declined subsequently. That might be connected with the consequence of elevated viscosity that generates in thickening at hydraulic and thermal boundary layer.

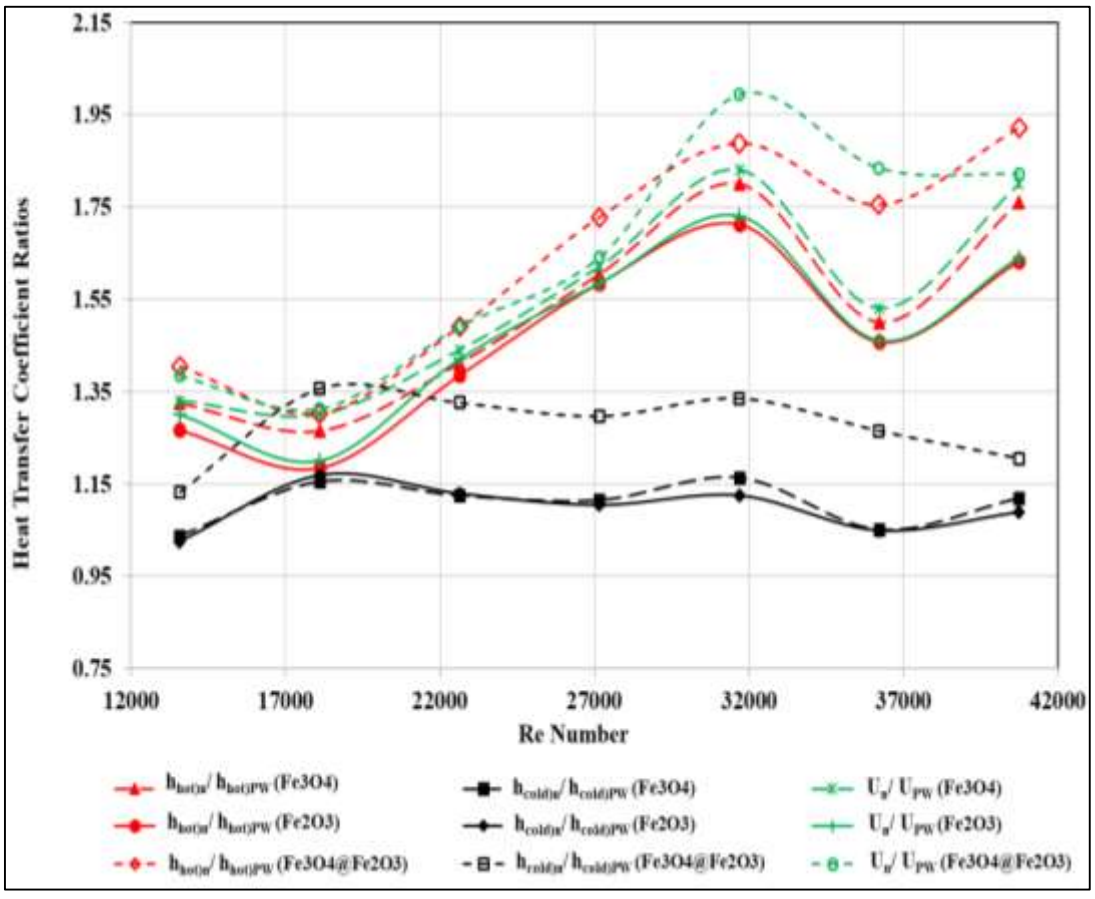


Figure 6.15. Heat transfer coefficient ratio as a function of Re Numbers at parallel-flow concentric pipe system under 10 g/s (coolant mass flow).

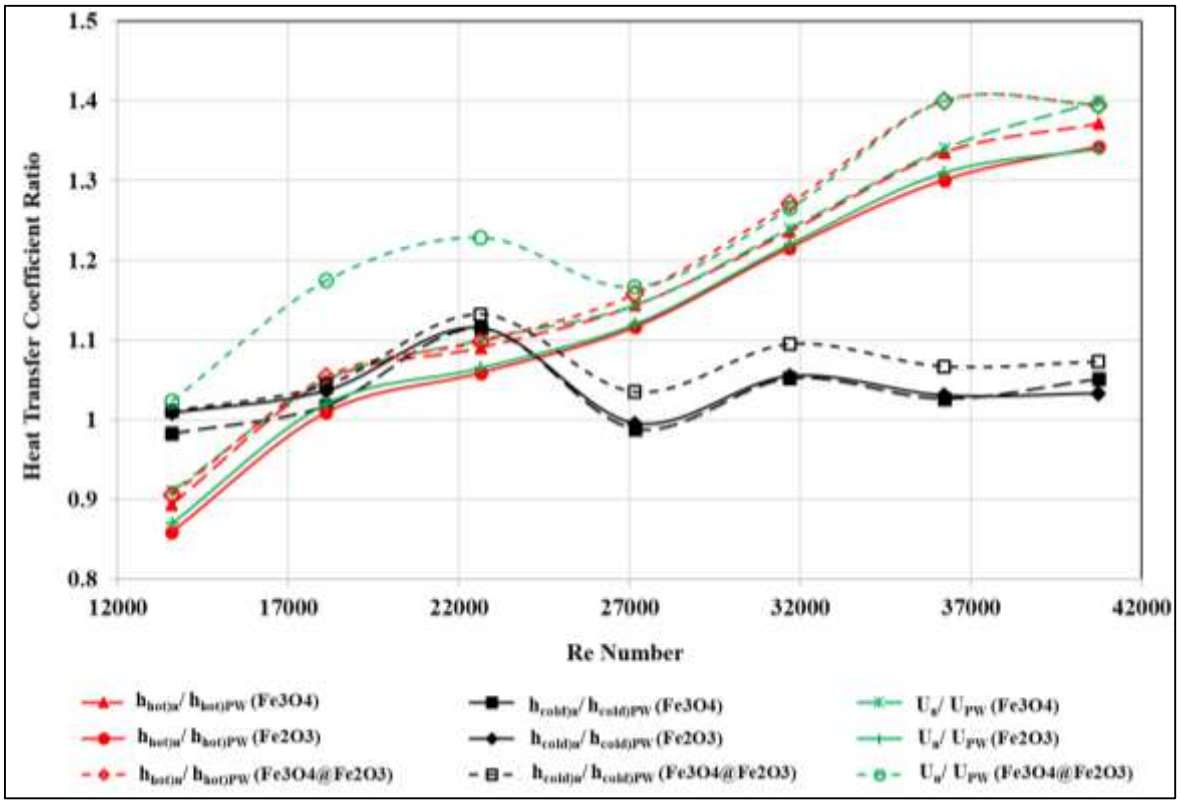


Figure 6.16. Heat transfer coefficient ratio as a function of Re Numbers at counter-flow concentric pipe system under 10 g/s (coolant mass flow).

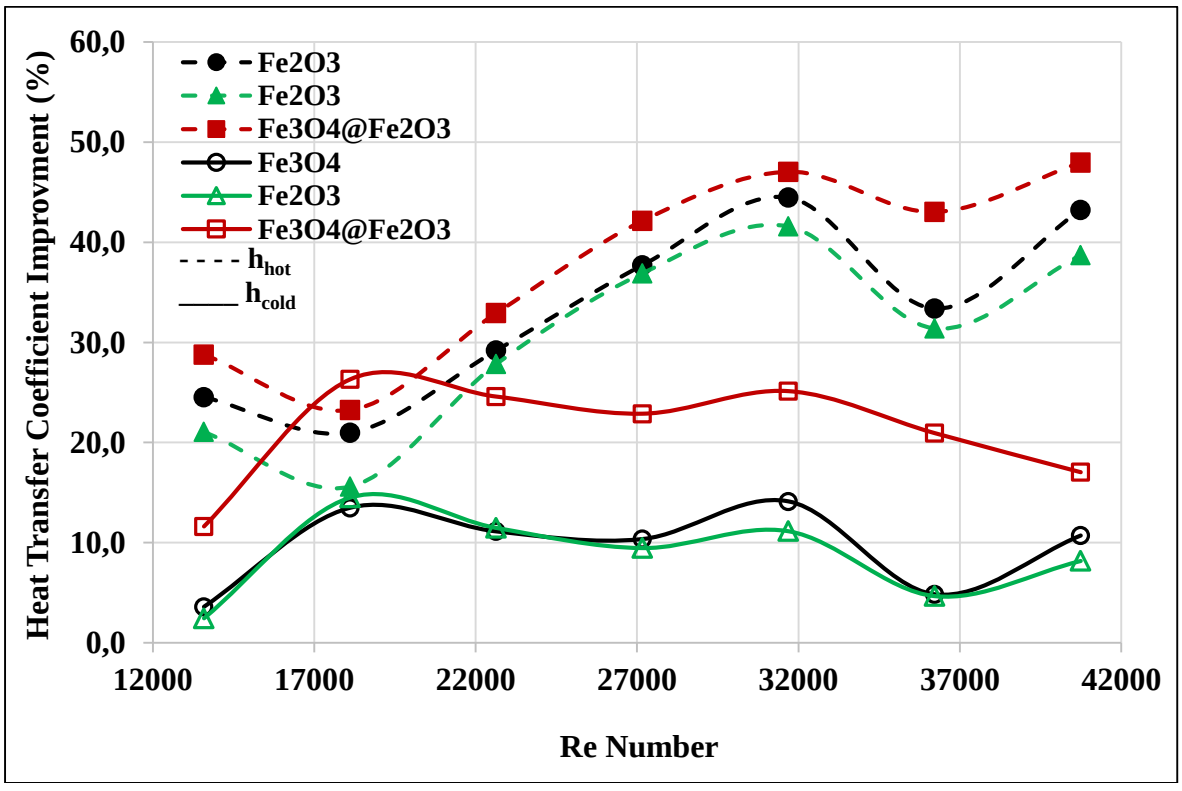


Figure 6.17. Heat transfer coefficient enhancement amount in Cold and Hot Streams within parallel systems for both poly and Hybrid magnetic-nanofluid.

6.2.6. Performance index (Efficiency %)

Figures 6.18 and 6.19 show the Re Number performance index for both counter and parallel-flow centric pipe heat exchanger device for various operating fluid kinds. With a rise in Re Number, the performance index significantly decreased in each of the counter and parallel-flow modes.

The explanation was that the heat exchanger under study was mini and hence, the pressure drop increases largely with the growth in Re Number because of the tube's small diameter. It might be noticed at both figures the hybrid magnetic-nanofluid efficiency is more elevated than the poly magnetic-nanofluids as well as base fluid. The highest average efficiency achieved was 92.7% and 96.2% under Fe_3O_4@Fe_2O_3/PW hybrid magnetic-nanofluid at counter and parallel systems respectively.

The cause was operating hybrid magnetite-nanofluids have more noticeable effect on thermal conductivity corresponding to mixing (Fe_2O_3/PW) and (Fe_3O_4/PW) into the base liquid. Operating hybrid magnetic-nanofluids containing Fe_3O_4@Fe_2O_3 produce an increase in thermal enactment by 11.3%, 7.9%, and 5.3% compared to pure water, Fe_3O_4, and Fe_2O , respectively within parallel systems. Similarly, at Re Number Re=18107.7, employing hybrid magnetic-nanofluids in a counter-flow design an expansion at thermal performance by 10.7%, 6.7%, and 4.7% corresponding to the same poly magnetic-nanofluids as well as pure water respectively.

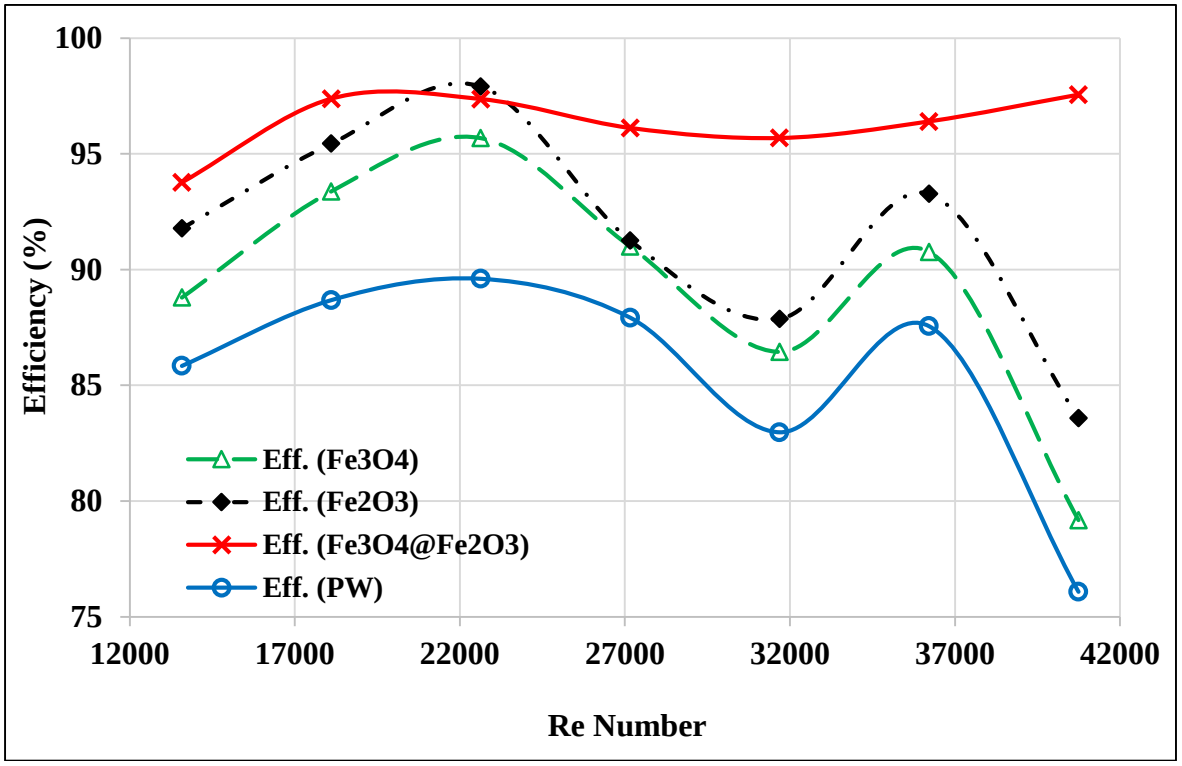


Figure 6.18. Thermal efficiency as a function of Re Number through parallel-flow concentric tube system at 10 g/s coolant mass flow.

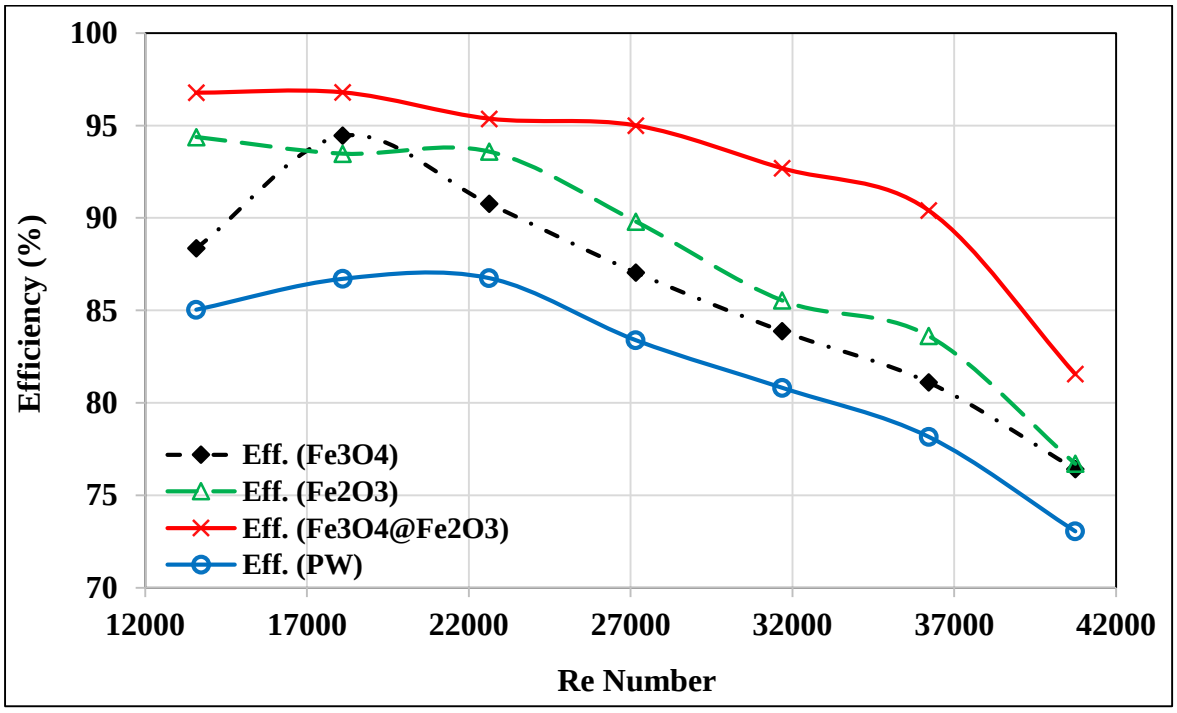


Figure 6.19. Thermal efficiency as a function of Re Numbers through counter-flow concentric tube system at 10 g/s coolant mass flow rate.

6.2.7. Nusselt number

Figure 6.20 shows the comparison of base fluid and nanofluid Nu numbers in a counter and parallel-flow concentric tube exchanger device. As it has been shown, in contrast to poly magnetic-nanofluids and base fluid, heat transfer with Fe_3O_4@Fe_2O_3/PW hybrid magnetic-nanofluid is significantly improved in both regimes. It apparent at Re numbers between (13581 and 27162), this proportion is practically equal to 1.

Nevertheless, by increasing hot fluid velocity the variance between nano-fluid and base fluid extends, getting maximum as 1.4 and 1.62 in case of Fe_3O_4@Fe_2O_3/PW hybrid magnetic-nanofluid within counter and parallel-flow concentric tube system at 36216 and 31689 Re number respectively. these improvements in heat transfer while using hybrid magnetic-nanofluid has been resulted from the subsequent factor, mixing particles with ratio of 50:50 of two various sorts of nano-particles increases the solution's thermal conductivity as a result the hybrid magnetic-nanofluids thermal conductivity were higher than poly and base fluid. The Nu Numbers behavior as a function of Re numbers at various kinds of operating fluids were displayed in Figure 6.21. As illustrated in this figure, at 0.5 wt. % Fe_3O_4@Fe_2O_3/PW hybrid magnetic-nanofluid, the Nu numbers were raised corresponding to poly magnetic-nanofluid as well as base fluid reaching to 38.1% related to pure water under 31689 Re numbers and 14.8% and 13.2% compared to Fe_2O_3/PW and Fe_3O_4/PW poly magnetic-nanofluids respectively under 36216 Re number. Heat transfer enlargement via utilizing hybrid magnetic-nanofluids generated due to thermal conductivity improvements, energy transfer with nano-particles diffusion, Brownian movement of the particle’s combination. A comparison between empirical and experimental Nu amounts has been performed and displayed in Figure 6.22.

The numerical procedure is presented establishing on experimental outcomes of nano-fluids, which was investigated utilizing 0.5 wt. % Fe_3O_4@Fe_2O_3/PW hybrid magnetic-nanofluid. From Figure 6.22, it was conducted that the numerical correlation presented in this study delivers predictions conforming to experimental outcomes. The highest error between numerical and experimental data was 6.23% at 22635 Re Number and 3.06% at 31689 Re Number throughout counter parallel-flow regimes, respectively. The average errors were 4.62% and 3.99%, respectively at entire flow range.

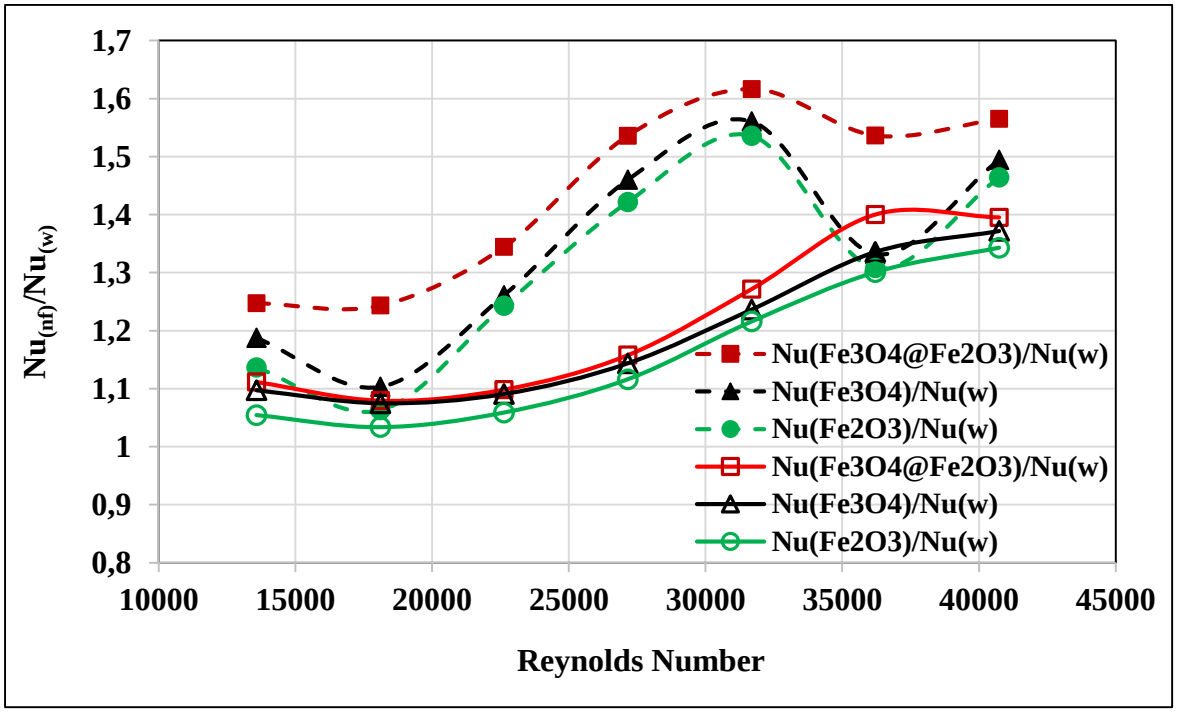


Figure 6.20. The Nu number of poly and poly and hybrid magnetic-nanofluid corresponds to water at counter and parallel-flow concentric tube heat exchanger design.

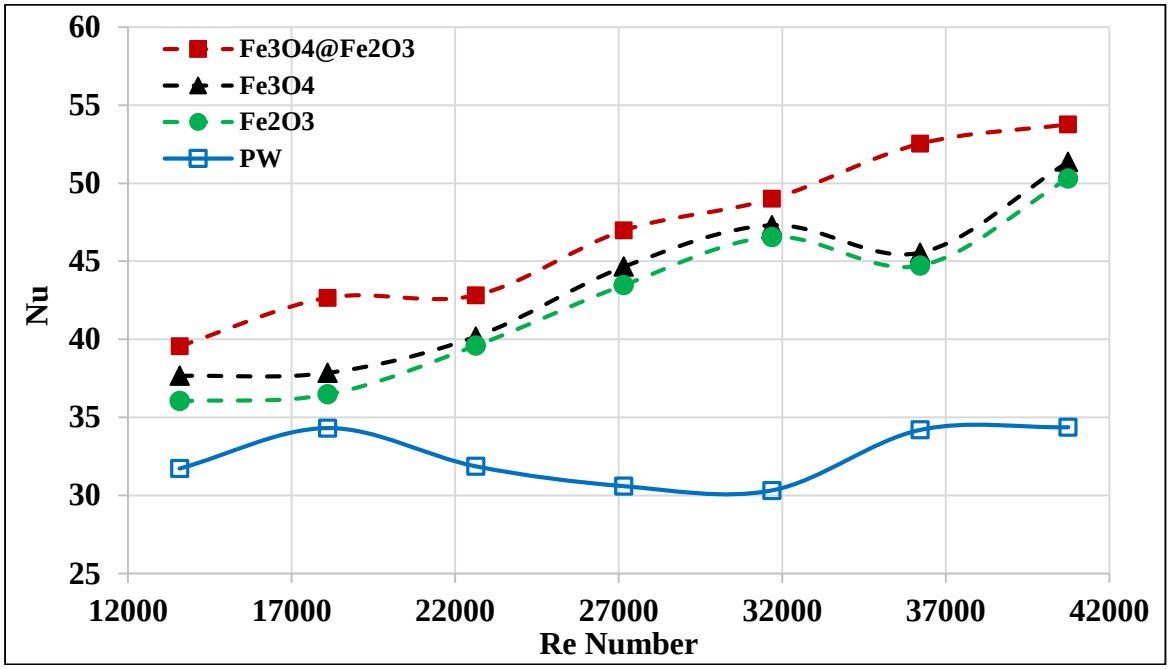


Figure 6.21. Nu number of pure water poly and hybrids magnetic-nanofluid at counter and parallel-flow concentric tube heat exchanger design under various Re numbers.

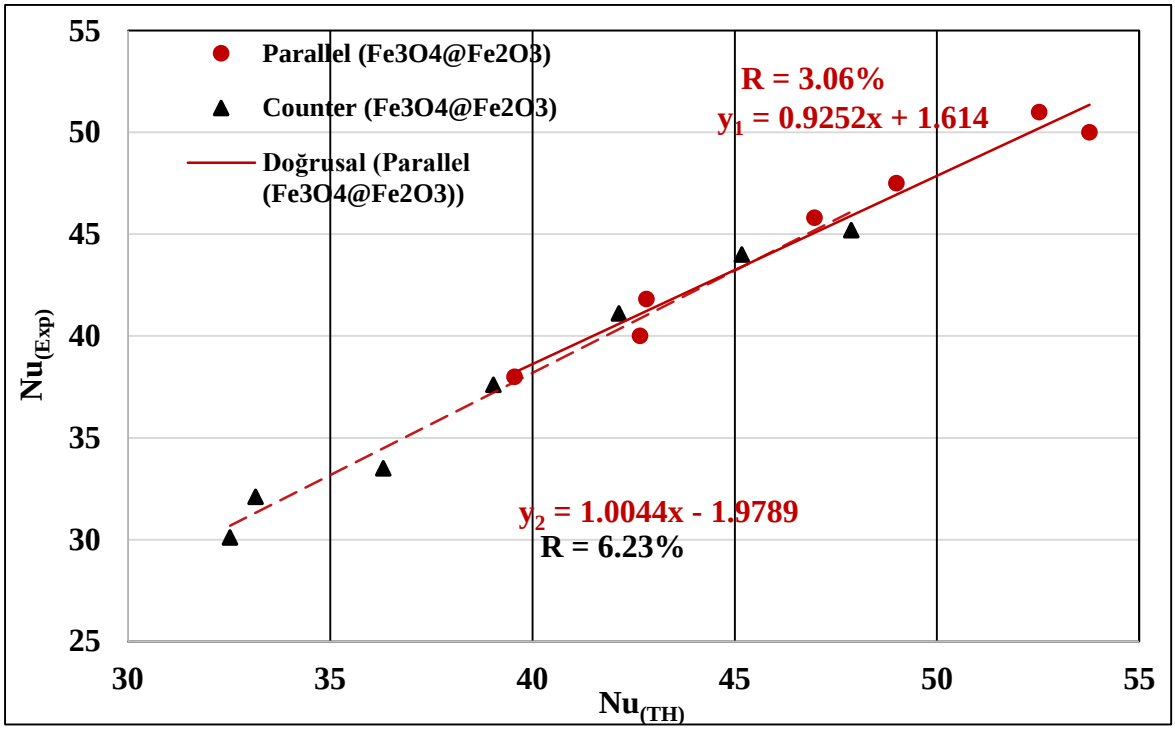


Figure 6.22. Comprising among empirical and experimental Nu numbers for Fe_3O_4@Fe_2O_3/PW hybrid nano-fluid.

6.3. Mono and Hybrid Magnetic Nanofluids in Thermosyphon Natural Convection Heat Pipe

Heat pipe's thermal performance was experimentally analyzed by employing three separate operating fluids, iron oxide-ferric oxide hybrid magnetic nanofluid, nickel ferrite mono-magnetic nanofluid, and pure water under diverse operating conditions such as coolant mass flow rate, input heat, and weight percent of 0.5% and 1%.

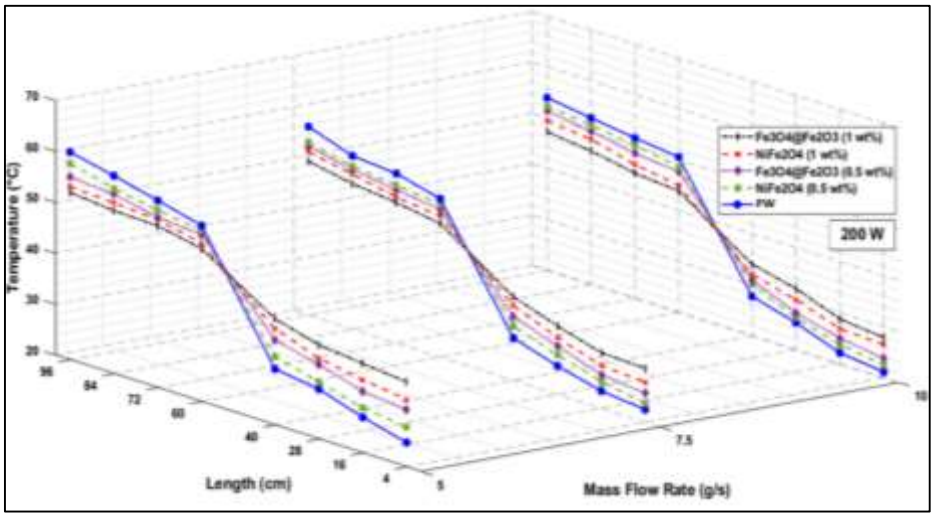
6.3.1. Wall temperature distributions

Figure 6.23, which was obtained from experiment using pure water, Fe_3O_4@Fe_2O_3/PW, and $NiFe_2O_4$/PW hybrid and poly magnetic-nanofluids at two distinct percentages of 0.5 wt. % and 1 wt. %, represents the fluctuation in wall temperatures. Figure 6.23 makes it abundantly clear that under all working conditions, a gradual drop in temperature has been noticed along the heat pipe's wall. Accordingly, it was found that when $NiFe_2O_4$/PW and Fe_3O_4@Fe_2O_3/PW poly and hybrid magnetic-nanofluid were utilized to be a fluid of operation at 400W heat input and 1 wt.%, the mean wall temperature reduced by 7.6°C and 11.09°C , respectively. Regarding pure water, Fe_3O_4@Fe_2O_3/PW

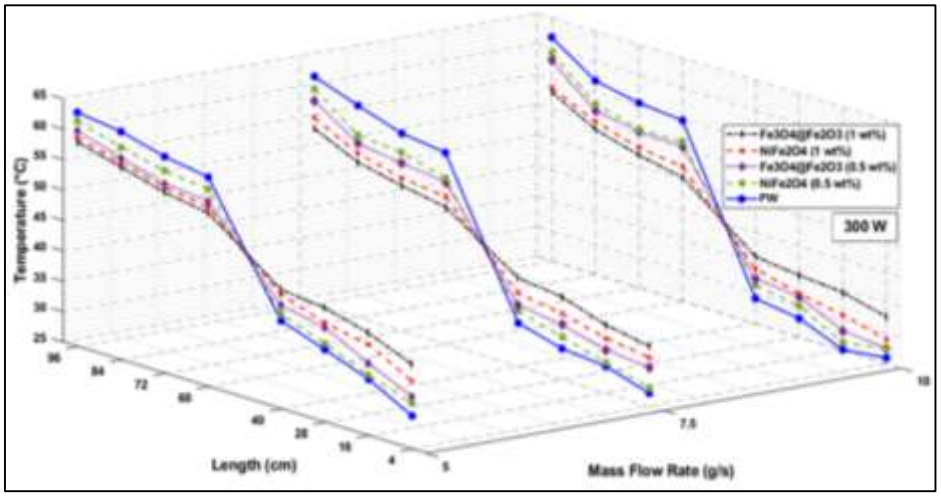
and $NiFe_2O_4$/PW hybrid and poly magnetic-nanofluid, the average ranges of the temperature obtained in the evaporator section were 70.8°C, 59.6°C, and 63.01°C, respectively.

It was certainly the case that at all heating loads, the Fe_3O_4@Fe_2O_3/PW hybrid magnetic-nanofluid boiled at a lower temperature compared to pure water. With an increase of heat supply, the temperature of the condenser and evaporator area continuously rose dramatically. In addition, 400W was used to indicate the highest temperature increment. To clearly summarize the experimental results, $NiFe_2O_4$/PW and Fe_3O_4@Fe_2O_3/PW poly and hybrid magnetic-nanofluid boiled at lower temperatures, which matched the boiling point of pure water.

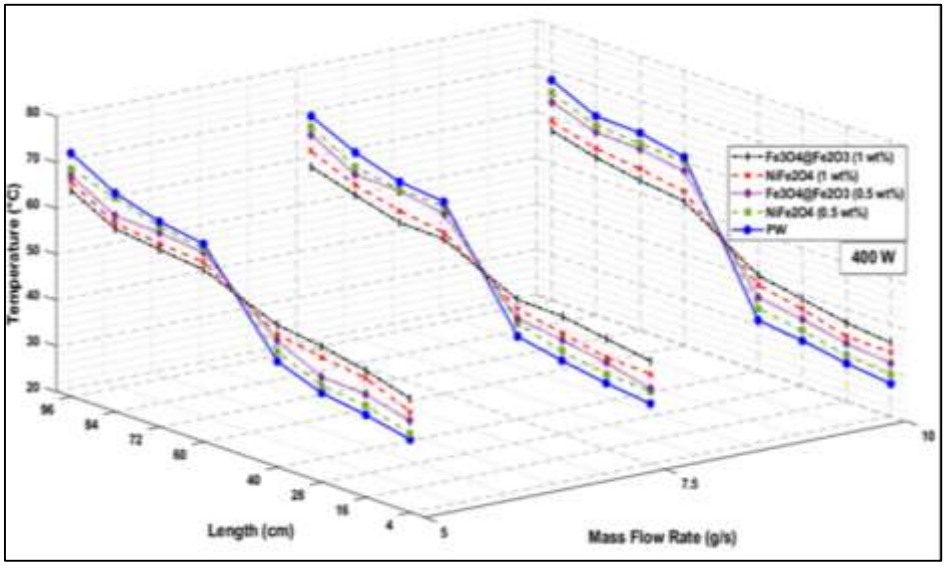
Due to the advantages of magnetic-nanoparticle insertion into the base fluid, significantly increase the region of heat transfer within the base fluid resulting in improved thermal conductivity. That indicates the use of poly and hybrid magnetic-nanofluids increases its storage capacity. Similar to how the temperature of the solution enhances the interaction of the dissolved magnetic-nanoparticles in the poly and hybrid magnetic-nanofluid, increasing the potential of the particles colliding against the wall.



a



b



c

Figure 6.23. Test outcomes of wall temperatures under all operating requirements (a. 200W, b. 300W, and c. 400W) intake heat.

6.3.2. Thermal efficiency

By integrating the experimental results for each operating fluid separately—pure water, $NiFe_2O_4$/PW and Fe_3O_4@Fe_2O_3/PW poly and hybrid magnetic-nanofluid, at two distinct weight percentages of 0.5% and 1%, the heat pipe efficiencies at various operating conditions have been determined and displayed in Figure 6.24.

Particular attention was paid to the driving efficiency values for 400W, 300W, and 200W, heat supplied. Because there is a lower thermal resistant at elevated heating levels, thermal efficiency grows as the amount of heat that is exposed to the evaporator does. At 400W heating load and 10 g/s cooler mass flow rate condition, the highest efficiency was reached as 70.06%, 89.2%, and 95.3% for pure water, $NiFe_2O_4$/PW, and Fe_3O_4@Fe_2O_3/PW magnetic-nanofluid, respectively. This corresponds to a 19.14% and 25.24% increase in heat pipe's efficiency, respectively.

However, at 2 106 Ra number and 200W heat supply and operating circumstances, the greatest efficiency increase values were recorded as 27.3 and 30.9 % and at 1 wt. % and at $NiFe_2O_4$/PW and Fe_3O_4@Fe_2O_3/PW poly and magnetic-nanofluid. Utilizing mono and hybrid magnetic-nanofluids in place of pure water resulted in a noticeable increase in efficiency. Additionally, these enhancements get better as the weight percentage of the nano-particles rises.

These enhancements were made achievable by adding Fe_3O_4 and Fe_2O_3 magnetic-nanoparticles into the base fluid along with a 50/50 mixing ratio. As an outcome, the poly and hybrid magnetic-nanofluid have higher thermal conductivity as well as specific heat over pure water, and because of the chaotic motion of particles, the procedure of transferring energy is intensified, increasing efficiency.

It was immediately realized that using hybrid magnetic-nanofluid to be the working fluid increased heat pipe's efficiency at all test settings. Additionally, the increase in thermal efficiency might be attributed to particles migration, irregular thermal conductivity diffusion, and viscosity of the nano-fluid, which reduces the uniformity of the barrier layer and delays the formation regarding thermal boundary layer.

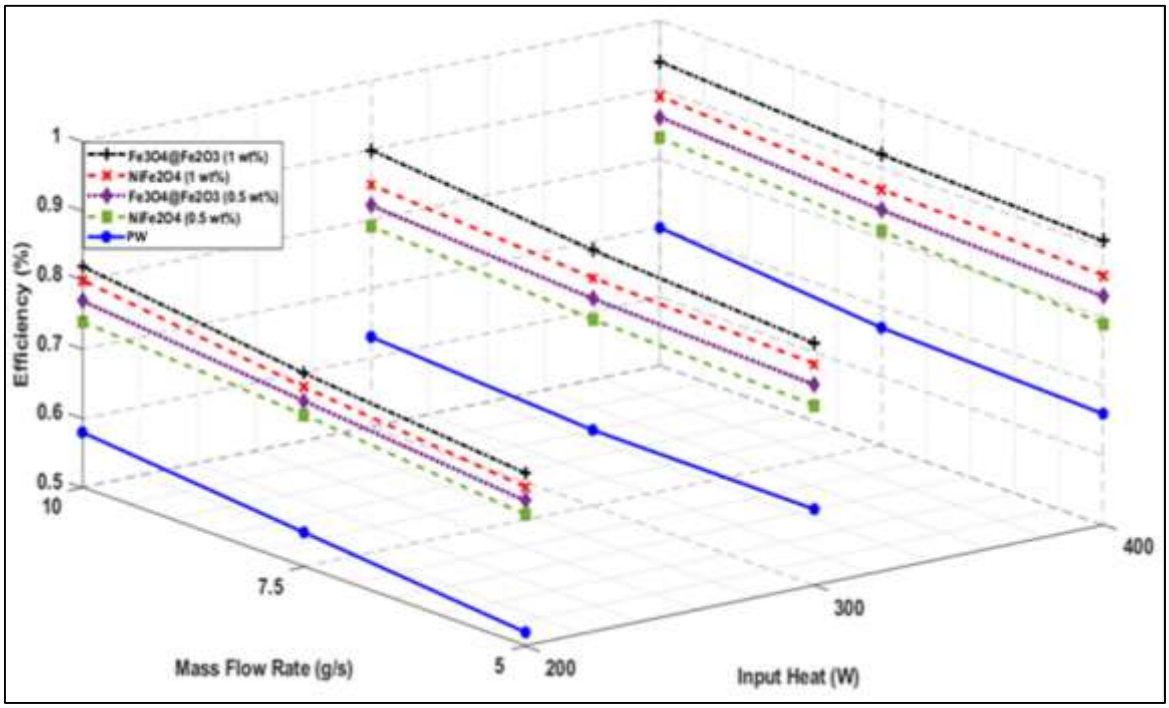


Figure 6.24. System efficiency in relation to supplied heat as well as mass flow.

6.3.3. Thermal resistance

Under all operational circumstances, the heat pipe's thermal resistances were experimentally examined. The results are shown in Figure 6.25. This figure makes it clear that using Fe_3O_4@Fe_2O_3/PW and $NiFe_2O_4$/PW magnetic-nanofluid being the working fluid instead of purified water will greatly reduce the thermal resistance. The highest thermal resistance reduction percentages were 43.97% and 61.83% at $NiFe_2O_4$/PW and Fe_3O_4@Fe_2O_3/PW poly and hybrid magnetic-nanofluid under 1 wt. %, 2×10^6 Ra number respectively, and 400 W intake heat, nevertheless, the highest reduction within thermal resistances were 17.3% and 30.5% under $NiFe_2O_4$/PW and Fe_3O_4@Fe_2O_3/PW poly and hybrid magnetic-nanofluid at 1.4×108 and 2×106 Ra number, 0.5 wt. %, and 300W and 200W intake heat, respectively, corresponded to pure water, it indicated that the thermal resistant reduced along with raising the weight percentages regarding to both mono and hybrid magnetic-nanofluids.

Furthermore, for a particular weight percentage and Ra number, using hybrid magnetic-nanofluid resulted in a considerable reduction in the thermal resistant contrasted with $NiFe_2O_4$/PW poly magnetic-nanofluid. The reductions reached 18.7% and 32.65%, respectively, at and 0.5 wt. % and 1 wt. %, $2x10^6$ and $8x10^7$ Ra numbers, and 200 and 400 watts heat supplied. Due to a boost in the liquid layer film's thickness while less

heat supplied, which results in slightly heightened thermal resistant, whenever the system is running with pure water as the working fluid, the thermal resistances became greater at smaller input heat amounts. Nevertheless, less increase in thermal resistant is observed in the heat pipe using $NiFe_2O_4$/PW and Fe_3O_4@Fe_2O_3 poly and hybrid magnetic-nanofluid when additional heat is applied downward.

Additionally, the increase in thermal resistant of the heat pipe when using pure water at low heat input is significantly less than that of poly and hybrid magnetic-nanofluids. The employment of poly and hybrid magnetic-nanofluids, resulting in more dependent uniformity of the liquid film layer within the evaporator and consequently decreases thermal resistant in the heat pipe, may have increased the heat pipe's capacity for heat transfer.

The evaporator's wick texture was formed with a thin coating layer using magnetic-nanofluid to simulate operational fluid in heat pipe, increasing its capillary action and heat transmission area. The composition of the wick surfaces in the presence of magnetic-nanoparticles heavily depends on the weight percentage and characteristics of the magnetic-nanofluid. Following an increase in the weight percentage of magnetic nanoparticles in both poly and hybrid magnetic-nanofluid, the heat pipe's thermal resistant falls.

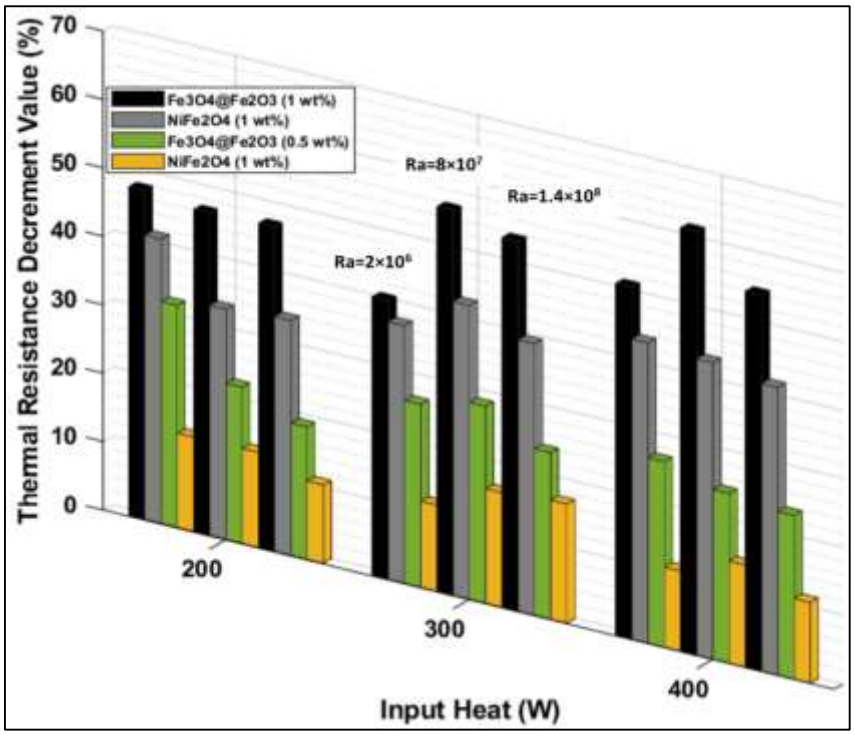


Figure 6.25. Heat pipe thermal resistance reduction percent in both operating fluids within changing operating conditions.

6.3.4. Nusselt number

Figure 6.26 in three dimensions illustrates how the Nusselt number varies in relation to changes in the Ra number and heat input. Therefore, it can be shown that increasing the Ra number emphasizes the buoyancy effect over the viscosity effects, producing higher Nu numbers. The flow is diverted to the cold-predisposed wall and falls downward to form a single-core vortex. Furthermore, increasing the amount of input could generate an upward motion that is enclosed by invisible barriers.

Additionally, it has been found that the Nu number grows with weight percent mainly a result of the expansion of the magnetic-nanoparticles' uncontrolled motion within the base fluid, which boosts the operating fluid's capacity for heat transfer. Additionally, the degree of accumulation, thermophoresis, as well as the significance of the particle-liquid interaction may all intensify at high concentrations and significantly affect the properties of natural convection heat transmission. It must be noted that the data Nu versus Ra changed into the left through increasing the weight percentage of nano-particles due to a significant variation in Prandtl number, which is reliant on the thermophysical characteristics of nano-fluids.

By using $NiFe_2O_4$/PW poly magnetic-nanofluid and Fe_3O_4@Fe_2O_3/PW hybrid magnetic-nanofluid instead of pure water, at 1 wt. %, 200W supply heat, and 8 107 Ra number, the greatest enhancement in Nu number has been demonstrated to increase up to 10.22% and 26.97%, respectively. Furthermore, using Fe_3O_4@Fe_2O_3/PW magnetic-nanofluid $NiFe_2O_4$/PW hybrid and poly magnetic-nanofluid at 1 wt. %, 400W supply heat, and 1.4×10^8 Ra number yielded the greatest Nu numbers of 97 and 120, respectively.

This takes place as a result of the hybrids magnetic-nanofluids high thermal conductivity in relation with the thermal conductivity for pure water and poly magnetic-nanofluid. The increase in thermal conductivity reached up to 26.97% and 20.5% when compared with pure water, as well as 8.14 % when comparing to $NiFe_2O_4$/PW mono magnetic-nanofluid at 0.5 wt. %. It also reached up with 22.47% and 19.5% when comparing to pure water.

The results are illustrated in Figure 6.27, and the experimental Nu number has been verified compared to the theoretical Nu number computed using the Kumar & Kalam and Ilyas et al. theories and reported in Eqs. 5.22, and 5.23. It has been determined that there is an analogous

tendency between the theoretical and experimental Nu number quantities and Ra number expansion. Given a mean error of 2.15% and 1.22% over $NiFe_2O_4$/PW and Fe_3O_4@Fe_2O_3/PW hybrid and mono magnetic-nanofluid, respectively, at 1 wt. % [89] and [90], it is demonstrated that the obtained data were reasonably comparable with the predicted values derived from empirical correlation.

Figure 6.28 illustrates the Nu number comparison between pure water and nanofluids in relation to Ra number and supplied heat. As is seen, for a given weight percent, transfer of heat is substantially better for Fe_3O_4@Fe_2O_3/PW hybrids magnetic-nanofluid than $NiFe_2O_4$/PW mono magnetic-nanofluid as well as pure water. As may have observed, for 200W heat supply, the proportion is essentially comparable to 1.03. However, the variance between a nano-fluid and pure water grows with increasing heat supply and weight percentage, reaching a maximum of 1.4 in the case of Fe_3O_4@Fe_2O_3/PW hybrid magnetic-nanofluid and 1.21 in the instance of $NiFe_2O_4$/PW magnetic-nanofluid at 1 wt. %. This increase at heat transfer while using hybrid magnetic-nanofluid could be developed due to the suspension of two different types of nano-particles in a proportion of 50:50, increases the thermal conductivity within the mixture, leading to a higher thermal conductivity for the hybrid magnetic-nanofluid than that of poly magnetic-nanofluid as well as pure water.

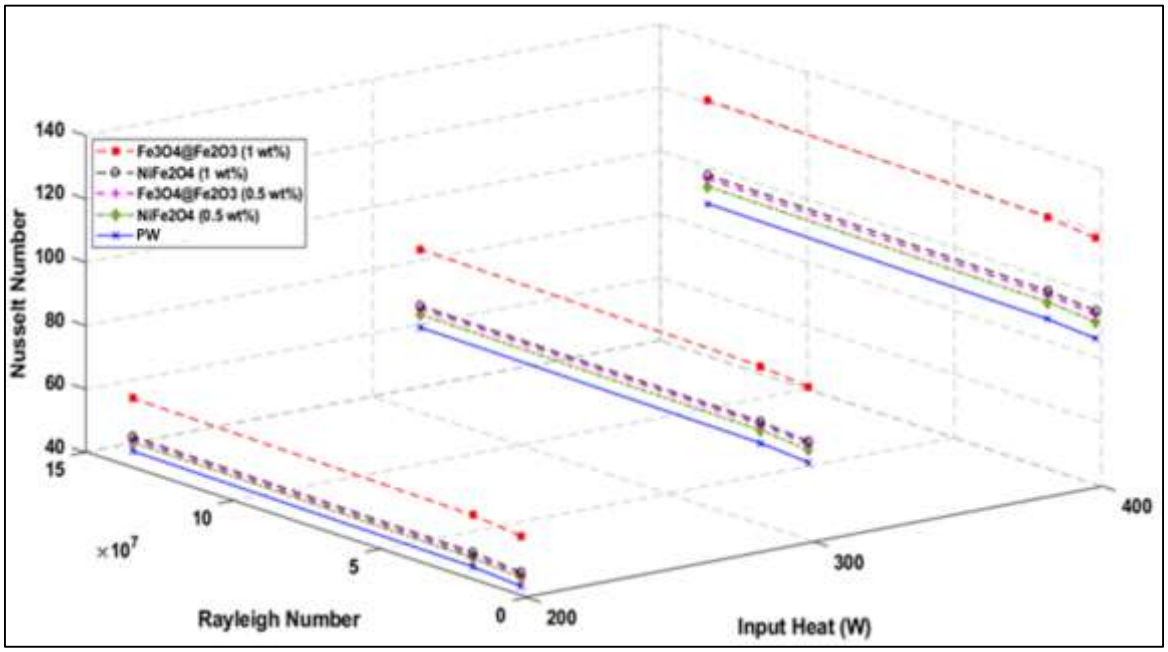


Figure 6.26. Average Nu number varies depending on the weight percentage.

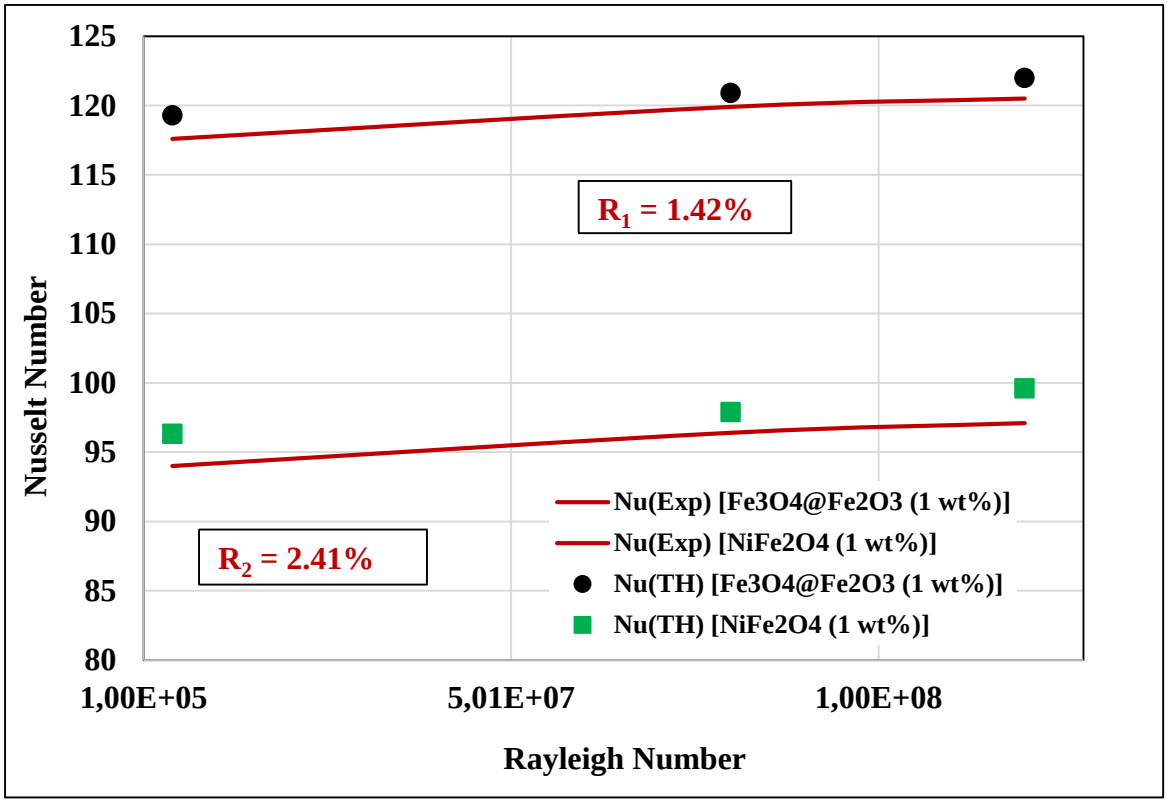


Figure 6.27. Comparison among theoretical and experimental findings for the Nu number.

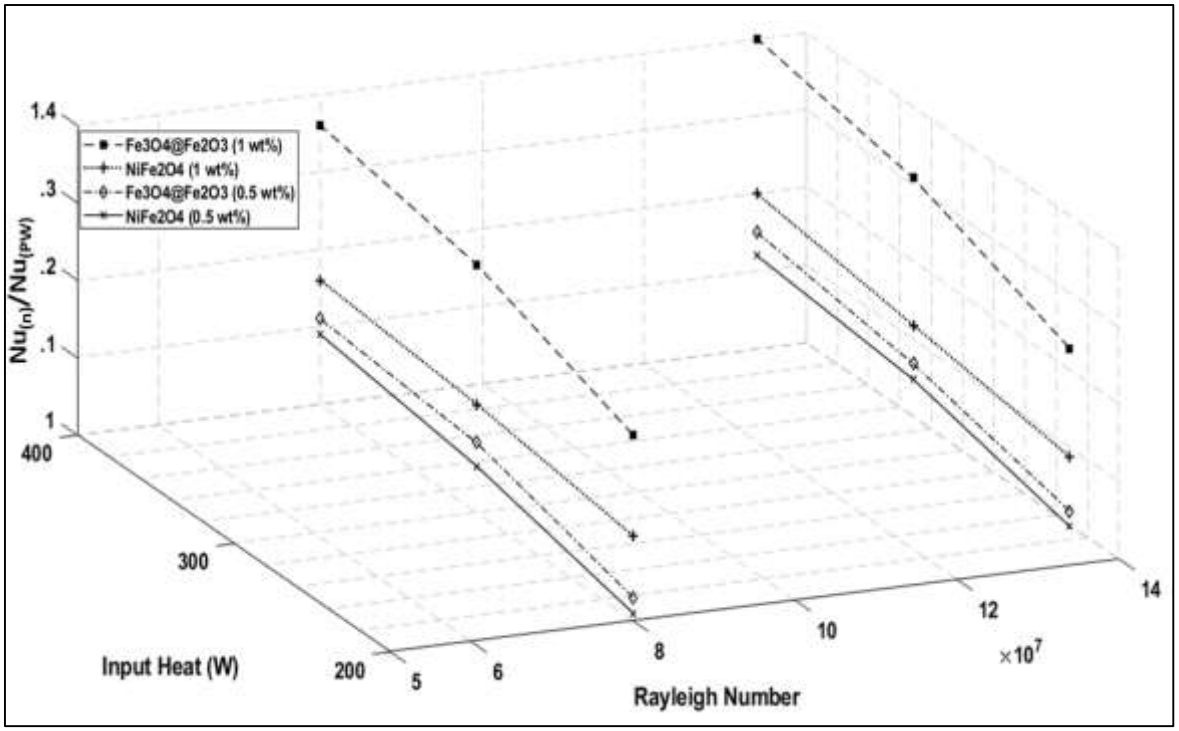


Figure 6.28. Nanofluid Nu number varies in relation to Rayleigh number and heat supply.

6.4. Modeling Thermosyphon Natural Convection Heat Pipe System Utilizing MATLAB/Simulink® Software

As shown in Figure 6.29, the typical equation used by Ilyas et al. was compared to the adequate thermal conductivity of magnetic-nanofluids ($K_{(n)}/K_{(PW)}$ ratio of nano-fluid thermal conductivity to base fluid thermal conductivity). Due to unexpected Brownian movement, a greater proportion of magnetic-nanoparticles distributed in the foundational fluid clearly results in greater thermal conductivity. Additionally, the proportion of the fluid's mass to volume was employed to calculate the densities of magnetic nanofluids made of NiFe2O4/PW, Fe2O3/PW, and Fe3O4/PW. Figure 6.30 shows the difference among the experimental and calculated densities. This chart shows that the estimated and measured densities are reasonably in agreement with one another. a maximum inaccuracy of 0.156% and a mean error of deviation of the experimental data up to 1.98% [89].

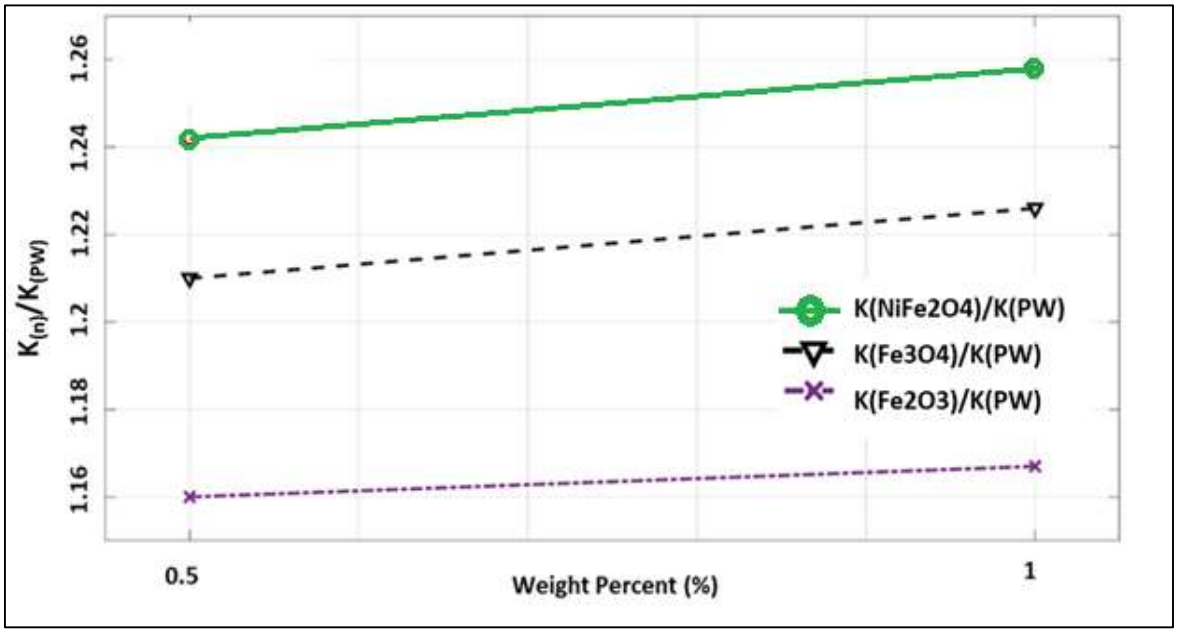


Figure 6.29. Base fluid with magnetic-nanofluid proportion versus weight percentage.

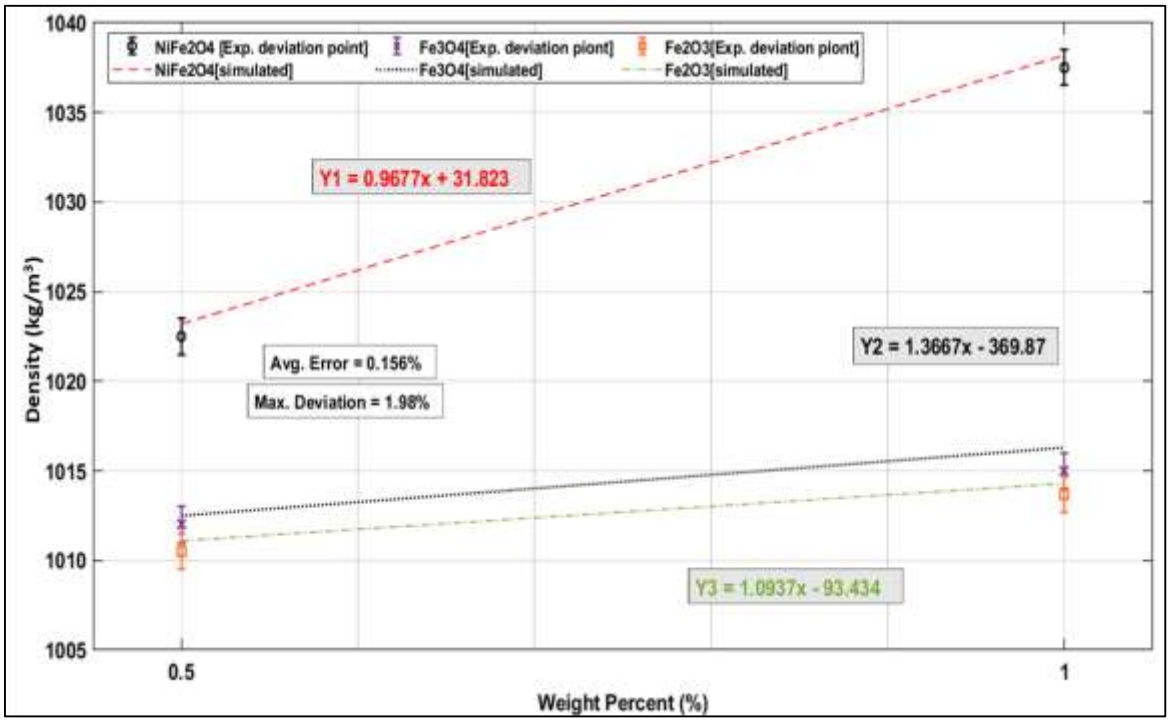


Figure 6.30. Difference between the predicted and observed magnetic-nanofluid density.

6.4.1. Evaporator and condenser surface temperature

The deviation in the evaporator's wall temperatures calculated via the theoretical model at a specific period equal to 40 minutes was examined under three dissimilar coolant mass flows (5g/s, 7.5g/s, and 10g/s) and three distinguishable exposed powers (200W, 300W, and 400W). Which are displayed in Figure 6.31 (a, b, and c). It could be seen from this figure the evaporator's wall temperatures rise with time until reaching constant value.

It is evident that when magnetic-nanofluids are applied to be the medium of operation in place of water, the wall temperatures reduce in both theoretical and experimental. This is because magnetic-nanofluid has high heat capacity, allowing for greater heat transfer among walls and the working medium than water does. When operating a magnetic-nanofluid comprising , Fe_2O_3/PW, Fe_3O_4/PW, $NiFe_2O_4$/PW at 400 W power input, 10 g/s cooling mass flow, and 1 weight percent associated to purified water, however, the largest temperature decrease across the evaporator was 5.5, 7, and 9, °C, respectively. Striate line was also used for representing the theoretical values, which were slightly greater than the experimental findings. As expected, the weight proportions of magnetic-nanoparticles in the base-fluid had a significant impact on the temperature of the evaporator's wall. By enlarging

the weight proportion of the magnetic-nanoparticles by 0.5 wt. % to 1 wt. %, it’s dropped by around 66.6%.

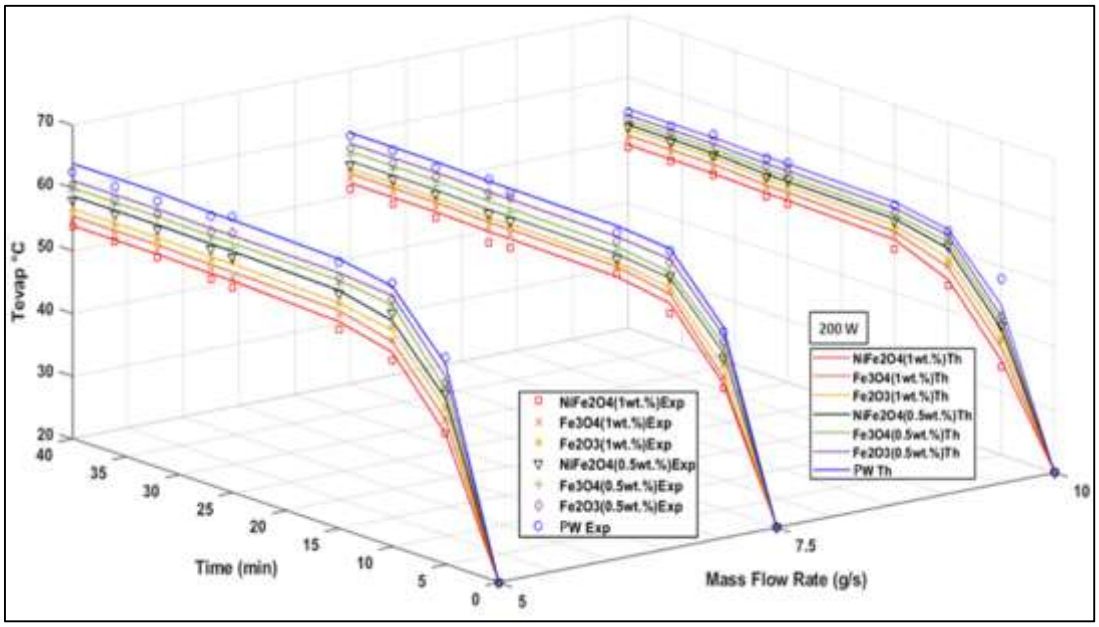
For the reason why which was established that: adding nano-particles enables some of them to be coated on the surface that is heated throughout the nucleate boiling process and create a porosity layer. This layer greatly enhances the surface's witting capacity. In order to reduce the temperature gradients, the operational fluid's thermal conductivity is typically high.

The 3D Figure 6.32 (a and b), that was created by tests under pure water, Fe_3O_4/PW, Fe_2O_3/PW, and $NiFe_2O_4$/PW magnetic-nanofluid at two different weight percent of 0.5 wt. % and 1 wt. %, shows a fluctuation of the wall temperature throughout the heat pipe. It was obvious from Fig. 10 that in all working conditions, the wall temperature on the entire heat pipe lowers equally. Consequently, it was shown that using magnetic-nanofluids of Fe_2O_3/PW, Fe_3O_4/PW, and $NiFe_2O_4$/PW, at 1% and 400W inputs of heat caused the average wall temperature to drop approximately 8.8%, 11.47%, 15.25%, respectively.

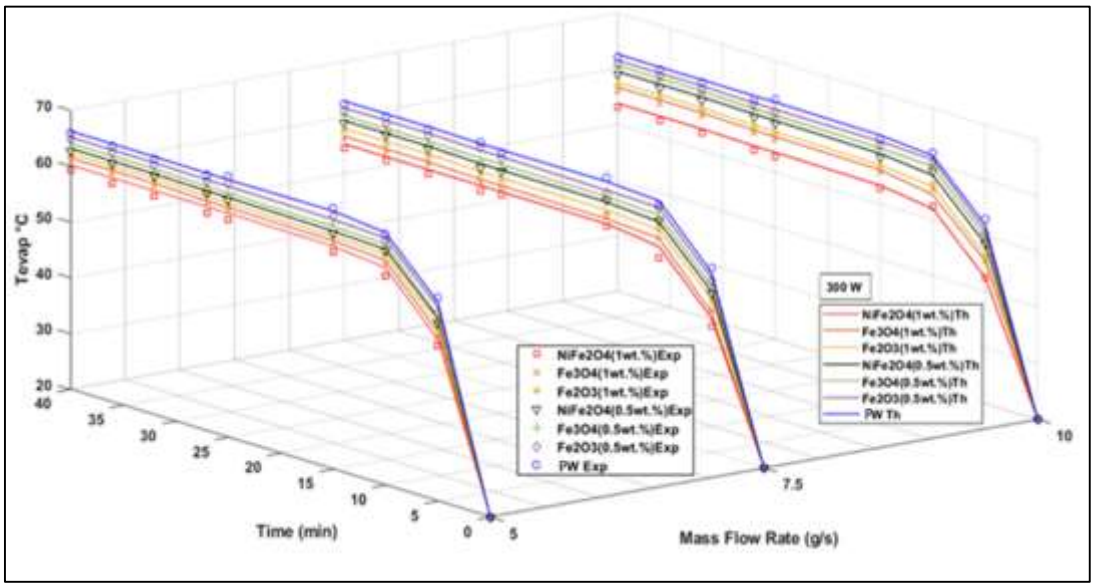
For pure water, $NiFe_2O_4$/PW, Fe_2O_3/PW, and Fe_3O_4/PW magnetic-nanofluid, the mean temperature obtained in the evaporator segment was 59.01, 62.5, 68.1 °C, respectively. It was agreed that during all working conditions, the $NiFe_2O_4$/PW magnetic-nanofluid boils at a temperature less than purified water as well as the other two magnetic-nanofluids under all inputs power. By increasing inputs power, the temperature in the evaporator and condenser sections rose dramatically. Additionally, 400 W was used to indicate the greatest increase in temperature. The working fluids $NiFe_2O_4$/PW, Fe_2O_3/PW, and Fe_3O_4/PW boiled at temperatures lower than pure water to optimize the results from the test rig. As a result the advantageous effects of including magnetic-nanoparticles within the base fluid, magnetic-nanoparticles significantly increase the heat transfer areas of the base fluid and subsequently thermal conductivity. In other words, the use of magnetic-nanofluids increases the storage capacity. The fluid temperature rises in parallel with the interaction of the dispersed magnetic-nanoparticles in it, increasing the probability of the particles colliding against the wall. Additionally, Figure 6.33's results for the evaporator exterior temperatures from the MATLAB/Simulink® model demonstrated excellent agreement compared to the experimental findings having an error of approximately 3.52%.

It may be concluded from the simulated model results that, if magnetic-nanofluids were used as shown in Figure 6.34, greater condenser wall temperature might be reached with low evaporator wall temperature. The operating fluid's improved thermal conductivity, brought on by the presence of magnetic-nanoparticles with large thermal conductivity, raises the rate of heat transmitted through the evaporator into the condenser. Due to the magnetic-nanofluids ability to evaporate and condensate as the fluid of operation, the heat pipe condenser part receives additional heat from evaporator part. According to the theoretical model's predictions, utilizing Fe_2O_3/PW, Fe_3O_4/PW, and $NiFe_2O_4$/PW magnetic-nanofluids will raise the condenser temperature by 15, 20, 26.66%, respectively, compared to pure water at 1wt. %, 5 g/s mass flow-rate, as well as 200 W power input, the condenser temperature rises to 13.43% as the weight percent of magnetic-nanoparticles within the base fluid rises. The temperature at which the ferrous liquid boiling and evaporated is given highest temperature.

Figure 6.35 illustrates the mean difference in temperature between the evaporator and condenser in order to heat supplied and coolant mass flow. The mean temperature gradients rises with heat supply and coolant mass flow rise. Yet, the mean temperature variance is greatly reduced by using magnetic-nanofluids. For Fe_2O_3/PW, Fe_3O_4/PW, and $NiFe_2O_4$/PW, the amount of decrease in the mean temperature variation among the condenser and evaporator areas was as great as 27.58% 34.48%, and 42.69%, compared to pure water at 1 wt. %, 5 g/s, 200W. Additionally, the variation in temperatures decreased by 44% when the weight percent of magnetic-nanoparticles increased. At a steady temperature variation, the heat pipe was capable of carry greater heat flux due to the enhanced heat transfer ability of the magnetic-nanofluids, emphasizing the capacity of magnetic-nanofluids as a working substance.

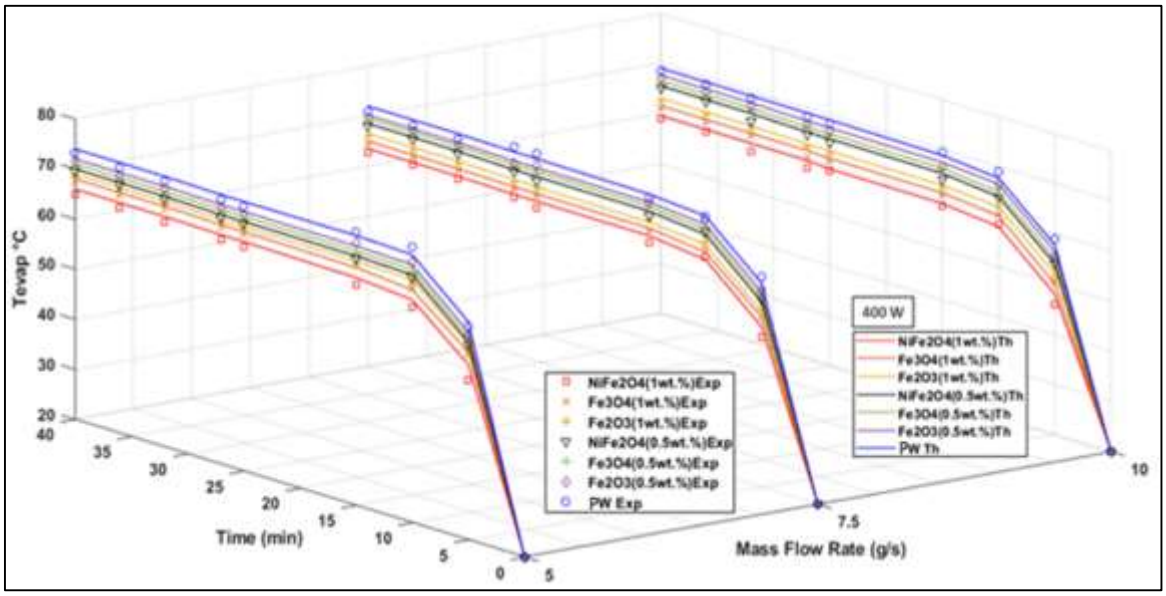


a



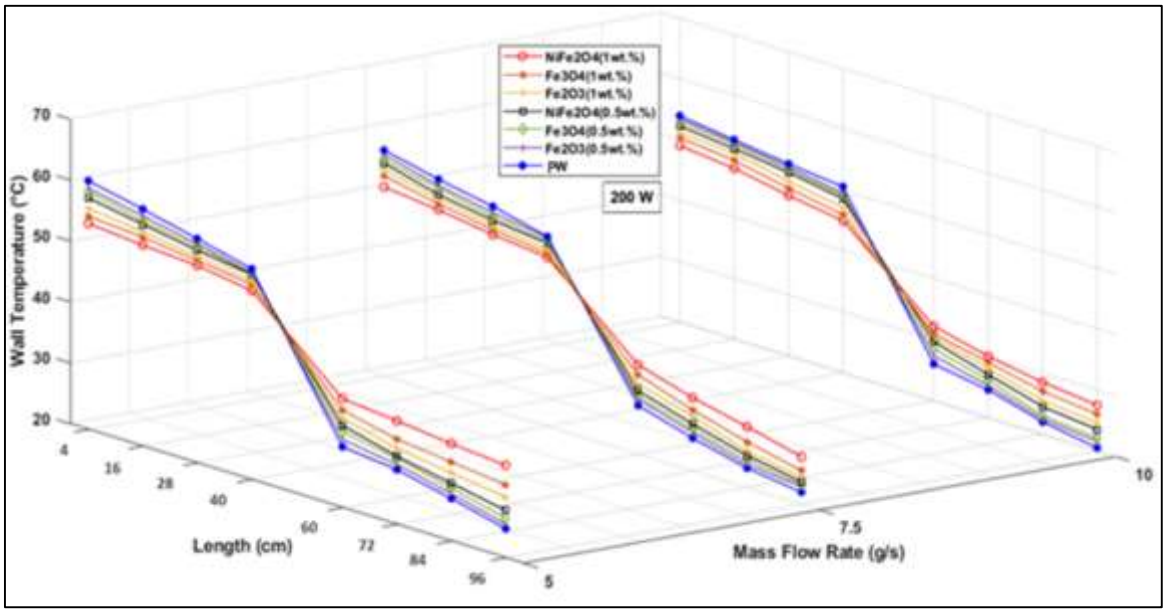
b

Figure 6.31. The Evaporator's temperature as a function of mass flow rate and time and at variance exposed power (a) 200W (b) 300W, & (c) 400W.

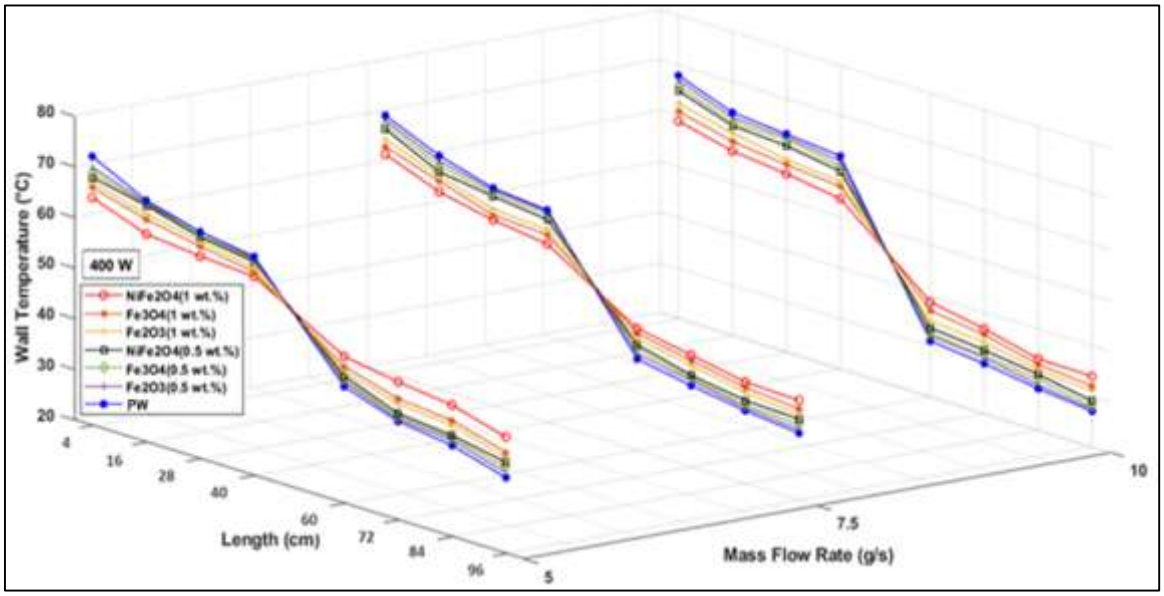


c

Figure 6.31. (continue) The Evaporator's temperature as a function of mass flow rate and time and at variance exposed power (a) 200W (b) 300W, & (c) 400W.



a



b

Figure 6.32. Temperature fluctuation and mass flow rate across the heat pipe wall at various input powers (a) 200W & (b) 400W.

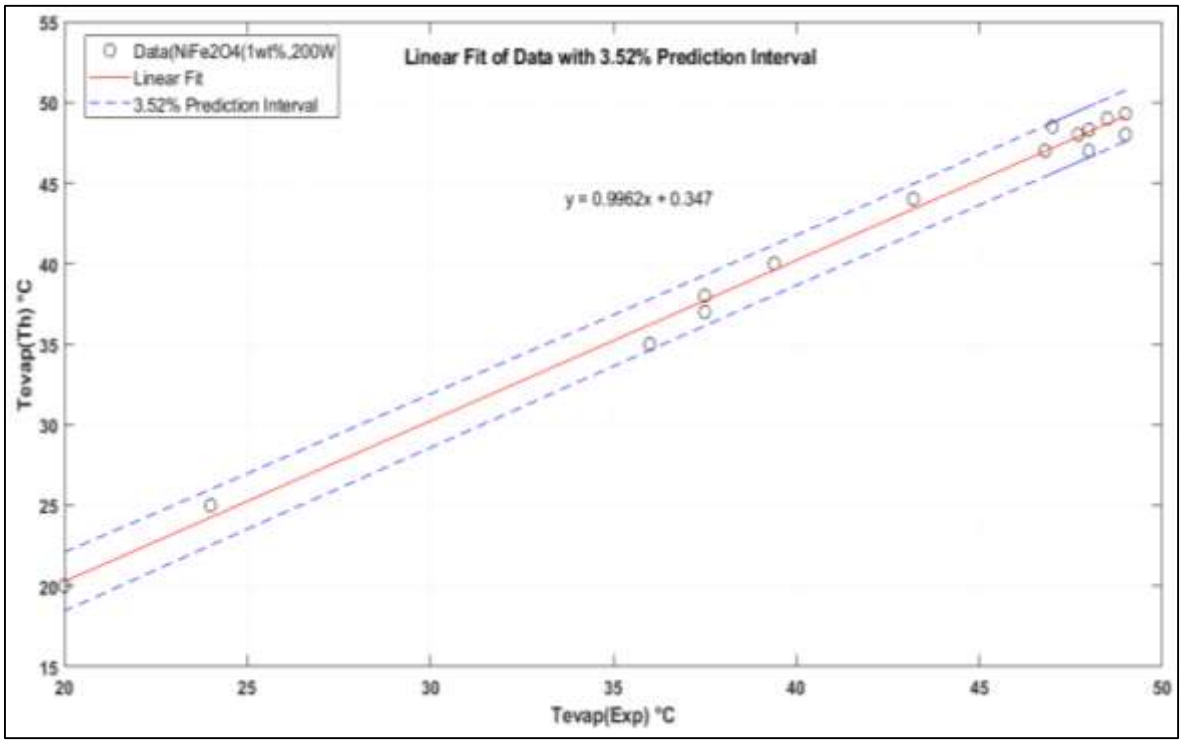


Figure 6.33. Comparison between the MATLAB/Simulink model outcomes against experimental findings of evaporator temperature.

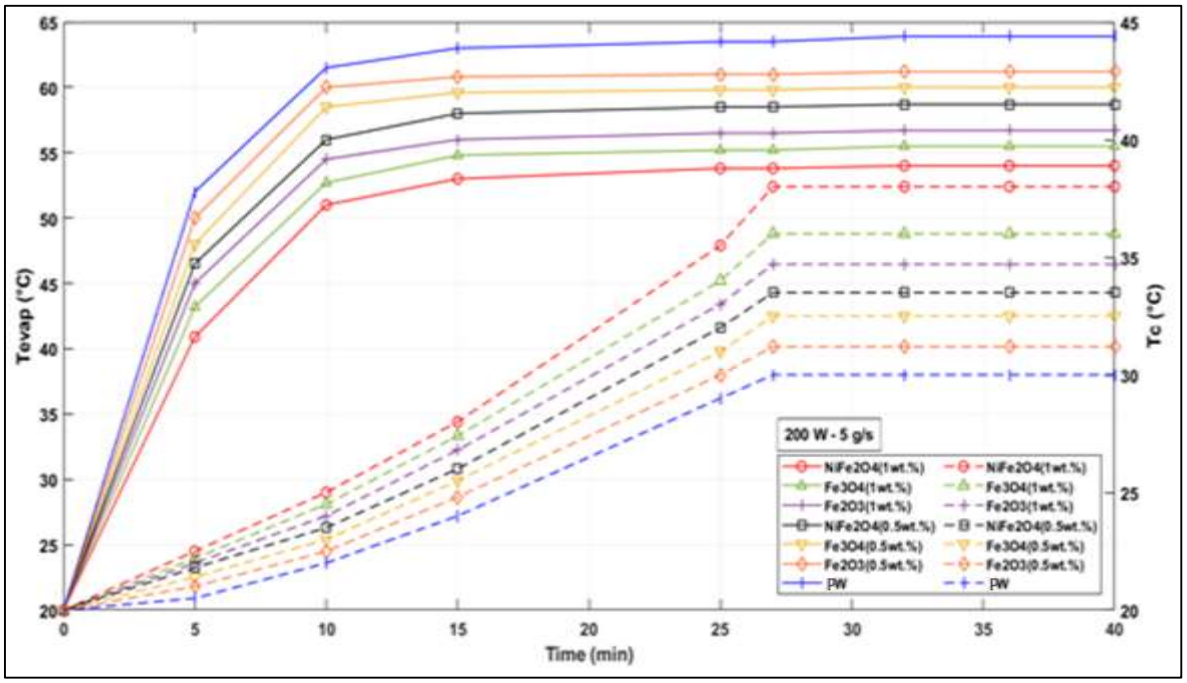


Figure 6.34. Deviation in the condenser and evaporator's wall temperatures acquired by MATLAB/Simulink model as a function of time.

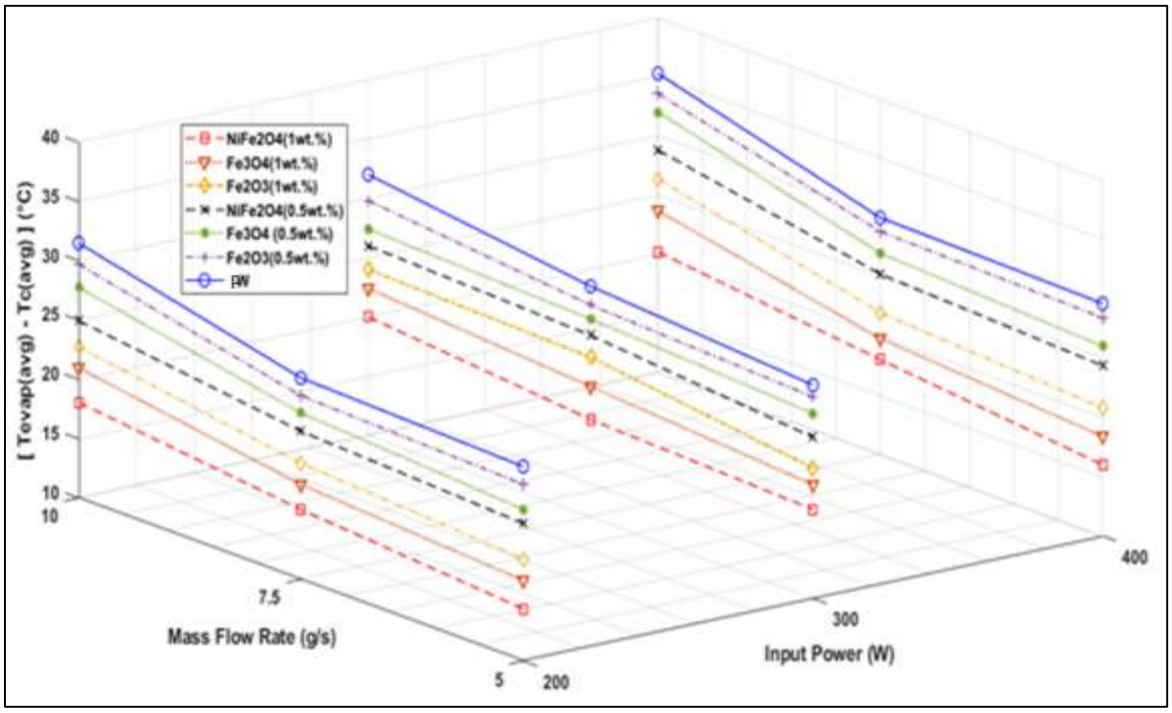


Figure 6.35. Condenser and Evaporator mean wall temperature variance at all operating states.

6.4.2. Thermal resistance

The three-dimensional Figure 6.36 shows a comparison of the experimental and simulated thermal resistance as a function of the evaporator's input power (200, 300, and 400 W) at various coolant mass flow rates (5, 7.5, and 10 g/s). It was evident that the qualitative tendency of decreasing thermal resistance with increased input power was seen in all circumstances. Several authors have noted this pattern [97, 98, 99, and 100]. The maximum reduction at thermal resistance was achieved via the use of $NiFe_2O_4$/PW, Fe_3O_4/PW, and Fe_2O_3/PW, respectively, in comparison to pure water at 400 W input power and 1 wt. %. In particular, the thermal resistance heavily depends on the imposed power to the evaporator and the type of working fluid. While using $NiFe_2O_4$/PW instead of Fe_3O_4/PW, and Fe_2O_3/PW at the same operating circumstances which previously mentioned, the highest reduction in thermal resistance was reached around 24.4% and 13.95%, respectively. By raising the weight percentages of the $NiFe_2O_4$/PW from 0.5 wt. % to 1 wt. %, the thermal resistance was reduced about 36 %. Thermal resistances measured experimentally and numerically show excellent agreement. The largest average difference between the actual thermal resistance and the simulation was calculated to be 4.51%. In comparison to the heat pipe at pure water with same heat power, the rise in thermal resistance employing magnetic-

nanofluids is noticeably less. This may be because employing magnetic nanofluids increases the heat pipe's ability to transfer heat, which results in a thinner liquid film layer in the evaporator and lowers the heat pipe's thermal resistance. An insignificant coating is formed on the evaporator's structure when magnetic nanofluid is used as the operating fluid, which increases capillary activity and heat transfer area. The weight percentage and characteristics of the magnetic nanofluid have a significant role in determining the evaporator surface's composition when magnetic nanoparticles are present. As the weight percentage of magnetic nanoparticles increases, the heat pipe's thermal resistance falls.

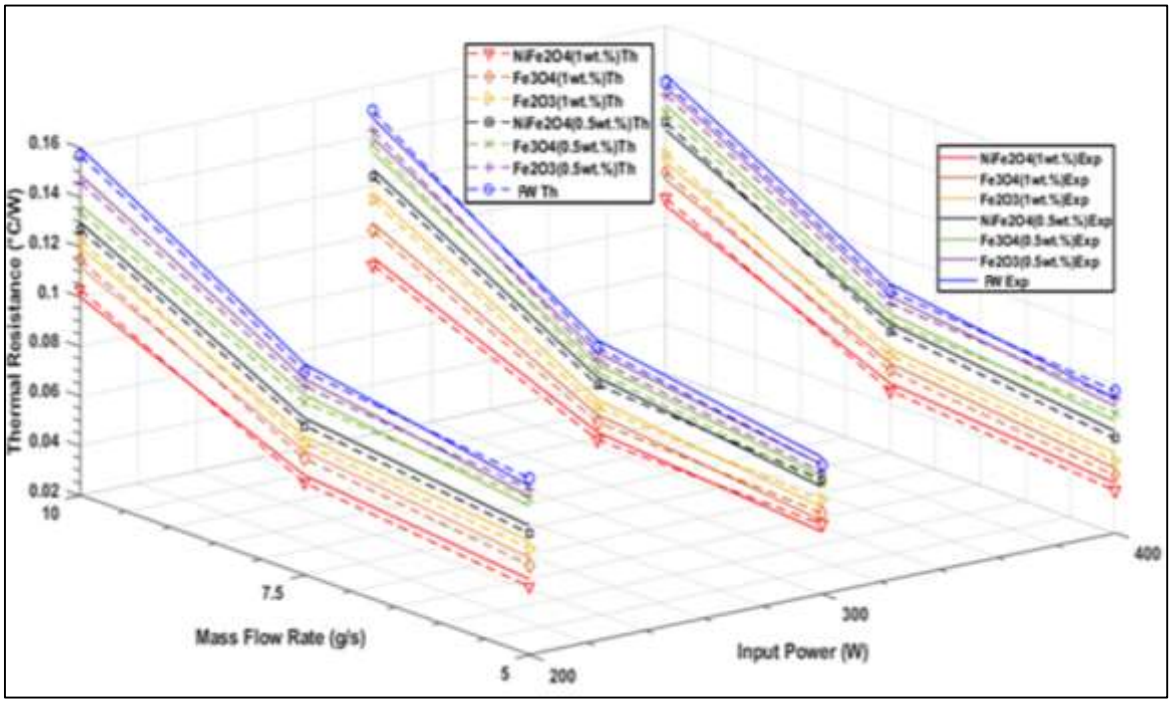


Figure 6.36. Experimentally and empirically estimated thermal resistant as a function of mass flow rates and input powers.

6.4.3. Nusselt number

The comparison between magnetic-nanofluids Nu number and pure water was displayed in Figure 6.37 as a function of Ra number and input power. May have noticed, the heat transfer of $NiFe_2O_4$/PW nano-fluid was particularly improved compared to Fe_3O_4/PW and Fe_2O_3/PW for a specific weight percentage. It may be recognizable, that ratio is almost equivalent to 1.16 during 200W power input, $8*10^7$ Rayleigh number, and 0.5 wt. %. Nevertheless, the distinction between nano-fluid and pure water expands with rising input power and weight percentages, achieving a max value of 1.34 in the case of the $NiFe_2O_4$/PW nano-fluid and

1.24 and 1.26 in the case of Fe_2O_3/PW and Fe_3O_4/PW nano-fluids, respectively, at 1 wt. %. These expansions in heat transfer were because using $NiFe_2O_4$/PW conduct to suspension of elevated thermal conductivity of the $NiFe_2O_4$ nano-particles corresponded to Fe_3O_4 and Fe_2O_3 nano-particles. The $NiFe_2O_4$/PW thermal conductivity nano-fluid was improved by about 2.53% and 7.21% compared to Fe2O3/PW and Fe_3O_4/PW nano-fluids, respectively. The experimental Nu numbers were demonstrated in comparison with the simulated Nu numbers evaluated by applying the model delivered in Eq. 5.39 [89], the outcomes were indicated in Figure 6.38. which demonstrates that the achieved data were valid with the simulated results at an average error equal to 3.5% and 2.3% on $NiFe_2O_4$/PW and Fe_3O_4/PW magnetic nano-fluid respectively at 1 wt. %.

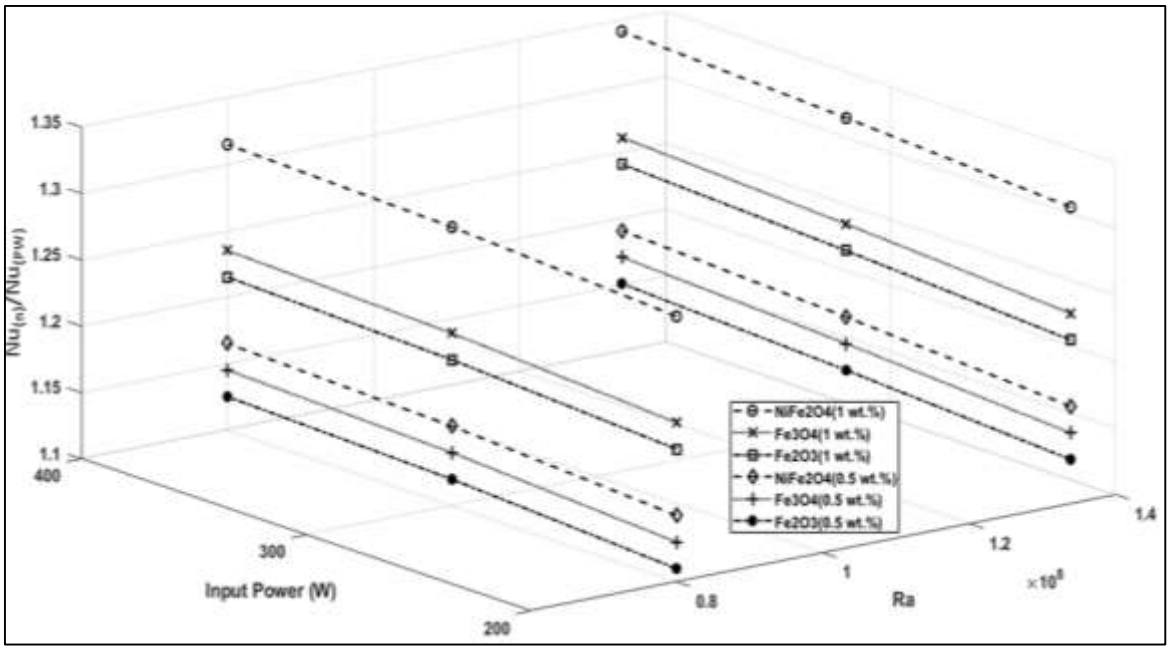


Figure 6.37. Ratio of Nu number of magnetic-nanofluids to pure water related to delivered heat and Ra Number.

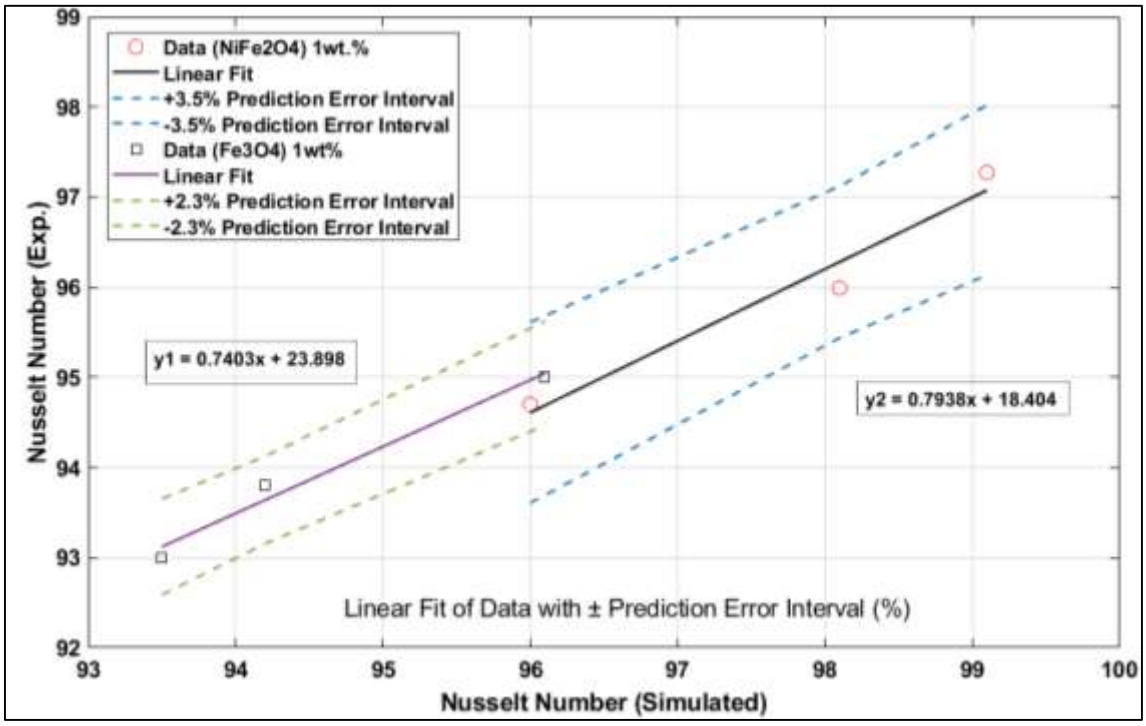


Figure 6.38. Verification of simulated & experimental Nu number.

6.4.4. Efficiency

The heat pipe tested under various working states was calculated by applying the experimental data from the operational medium separately, which was $NiFe_2O_4$/PW, Fe_3O_4/PW, Fe_2O_3/PW nano-fluid, also pure water at two distinct weight percentages (0.5% & 1%) which clarified in Figure 6.39. The quantity of the driven efficiency was discussed precisely at 200 W, 300W, and 400W delivered power.

Increasing the input heat to the evaporator section led to increments in the thermal efficiency because at high input heats the thermal resistance is less. 89.97% was the maximum efficiency obtained $NiFe_2O_4$/PW nano-fluid and 85% and 86.3% under Fe_2O_3/PW and Fe_3O_4/PW nano-fluid respectively on 14×10^7 Ra number and 400W input heat. Nevertheless, the considerably increased efficiency enhancement rate was accomplished as 22.24% at 400 W input heat, 1 wt. % and at $NiFe_2O_4$/PW magnetic-nanofluid and 14×10^7 Ra working requirements. Prominent efficiency enhancements were performed by utilizing magnetic-nanofluids instead of pure water.

Additionally, these enhancements boost by extending the nano-particles weight percentage. Improvement was performed due to $NiFe_2O_4$, Fe_3O_4, and Fe_2O_3 nano-particles that were

blended with base fluid. Suitably, the magnetic-nanofluid specific heat also thermal conductivity was higher than pure water [101], [102] at the same time particles' random movement boosts the methodology of the transferred energy likewise efficiencies were enhanced [42], [71], and [33].

It was unexpectedly witnessed that the heat pipe's efficiency was higher at all testing circumstances when $NiFe_2O_4$/PW was the operating fluid. Besides, the growth at thermal efficiency could be given to the particle's thermal conductivity varying, transmigration, and magnetic-nanofluid's viscosity which reduces the boundary layer thickness, generating a delay at the expansion in the thermal boundary layer [103], [104].

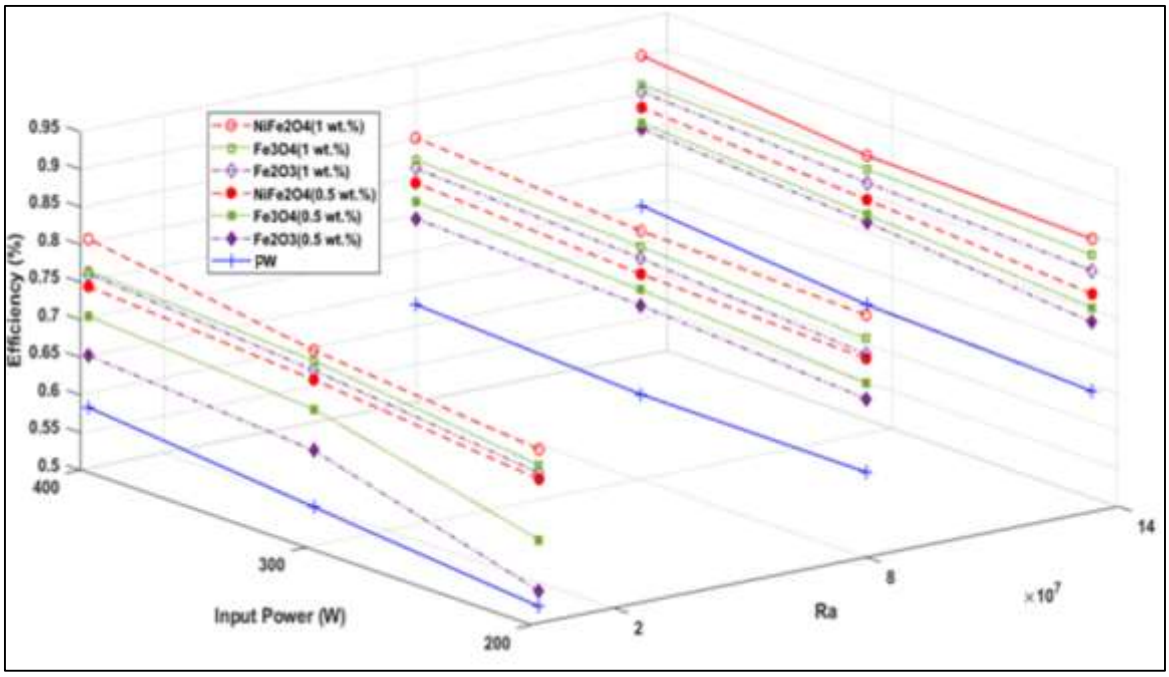


Figure 6.39. System’s efficiency as a function of mass flow rate as well as intake heat.

7. CONCLUSIONS

(Fe_3O_4@Fe_2O_3/PW) hybrid magnetic nanofluid and ($NiFe_2O_4$/PW), (Fe_3O_4/PW), and (Fe_2O_3/PW) mono-magnetic nanofluid used as operating fluid instead of the commercial one (i.e. Pure water) in three different thermal systems (air-to-air heat pipe heat exchanger system, concentric tube heat exchanger system, as well as thermosyphon natural convection heat pipe) for the purpose of heat transfer improvement were experimentally and numerically analyzed in this work. Nanoparticles were produced by crushing the raw iron oxide, ferric oxide, and nickel ferrite metals and blended with pure water and Triton X-100 at a concentration of 0.2 wt. %. Temperature alterations throughout the heat pipe wall, thermal resistance, and Nusselt number, and thermal efficiency, convective heat transfer coefficient were investigated for each working fluid in each system. The essential results of this analysis can be summed up as follows:

- Rising nanoparticles concentration enhanced the thermal efficiencies of all systems.

- The thermal resistance was lowered by employing magnetic nanofluids. An expansion in nanoparticles concentrations provided a reduction in thermal resistance in the three thermal system.

- Mixing magnetic nanoparticles with pure water declined its boiling pinpoint particularly, that could be apparently witnessed from experimental and numerical outcomes, and similarly enhances heat transfer of the condenser region.

- Employing hybrid magnetic nanofluids at higher Reynolds numbers carry further influence on convection heat transfer coefficient and Nusselt number improvement.

- The overall heat transfer coefficient ratios were more than one, which demonstrates that the system's thermal performance was enhanced by utilizing magnetic nanofluid rather than ionized water even in extremely inferior concentrations. Due to their heightened thermal conductivity as well as heat capability which is conducted to raise the thermal conductivity of the fluid itself. The thermal conductivity of the Fe_3O_4, Fe_2O_3, $NiFe_2O_4$ mono-magnetic nanofluids and Fe_3O_4@Fe_2O_3 hybrid magnetic nanofluid 18.44%,14.32%, 20.5% and 26.16% respectively higher than the base fluid.

- Iron oxide-ferric oxide hybrid magnetic nanofluid was the working medium which leads higher performance inside the thermosyphon natural convection heat pipe system in the simulated and experimental results mainly at high heat input, and a high concentration ratio resembled NiFe3O4 mono-magnetic nanofluid as well as pure water.

- By utilizing Fe_3O_4/PW magnetic nanofluid an enhancement rate of By utilizing Fe_3O_4/PW of 13.9%, (6.02%, 9.4%), and 23.2% has been notice in air-to-air heat pipe exchanger system, concentric tube heat exchanger system (parallel and counter regime respectively) and natural convection heat pipe system respectively at 1 wt. %.

- Using Fe_2O_3/PW magnetic nanofluid produced an enhancement rate in the thermal efficiency equal to (4.8%, 8.5%), and 21.2% at concentric tube heat exchanger system (parallel and counter regime respectively) and natural convection heat pipe system respectively under 1 wt. %.

- System's thermal efficiency was increased to 27.3% by employing $NiFe_2O_4$/PW magnetic nanofluid rather of ionized water in the natural convection heat pipe system respectively.

- By utilizing Fe_3O_4@Fe_2O_3/PW hybrid magnetic nanofluid an enhancement rate of the thermal efficiency of (15.66%, 12%), and 36.02% has been notice in concentric tube heat exchanger system (parallel and counter regime respectively) and natural convection heat pipe system respectively.

REFERENCES

1. Yılmaz, M. (2012). Türkiye'nin enerji potansiyeli ve yenilenebilir enerji kaynaklarının elektrik enerjisi açısından önemi. *Ankara Üniversitesi Çevrebilimleri Dergisi*, 4(2), 33-54.

2. Manay, E., Şahin, B., Akyürek, E. F. ve Çomaklı, Ö. (2012). Mikrokanallarda nanoakışkanların kullanımı. *TMMOB MMO Mühendis ve Makina Dergisi*, 53(627), 38-2.

3. Murugesan, C. and Tamilkolundu, S. (2012). *Mechanism of forced convective heat transfer in Al2O3/water nanofluid under laminar and turbulent flow*. 2nd International Conference on Chemical, Ecology and Environmental Sciences, Singapore, 28-29.

4. Xuan, Y. and Li, Q. (2000). Heat transfer enhancement of nanofluids. *International Journal of Heat and Fluid Flow*, 21(1), 58-64.

5. D'agostino, D., Marino, C. and Minichiello, F. (2020). Earth to-air versus air-to-air heat exchangers: a numerical study on the energetic, economic, and environmental performances for Italian office buildings. *Heat Transfer Engineering*, 41, 1040-1051.

6. Sözen, A., Filiz, Ç., Aytaç, İ., Martin, K., Ali, H.M., Boran, K. and Yetişken, Y. (2021). Upgrading of the performance of an air-to-air heat exchanger using graphene/water nanofluid. *International Journal Thermophys*, 5(1), 42-35.

7. Parametthanuwat, T., Rittidech, S. and Pattiya A. (2010). A correlation to predict heat-transfer rates of a two-phase closed thermosyphon (TPCT) using silver nanofluid at normal operating conditions. *International Journal Heat Mass Transfer*, 53(2), 4960-4965.

8. Allouhi, A. and Benzakour, M. (2021). Heat pipe flat plate solar collectors operating with nanofluids. *Solar Energy Mater Solar Cells*, 219(2), 110-122.

9. Martin, K., Sözen, A., Çiftçi, E. and Ali, H. M. (2020). An experimental investigation on aqueous Fe-CuO hybrid nanofluid usage in a plain heat pipe. *International Journal Thermophys*, 41(3), 135-155.

10. Huminic, G. and Huminic, A. (2011). Heat transfer characteristics of a two-phase closed thermosyphons using nanofluids. *Experimental Thermal Fluid Science*, 35(3), 550-557.

11. Sadeghinezhad, E., Mehrali, M., Rosen, MA., Akhiani, AR., Latibari, ST., Mehrali, M. and Metselaar, HSC. (2016). Experimental investigation of the effect of graphene nanofluids on heat pipe thermal performance. *Applied Thermal Eng*ineering, 100, 775-787.

12. Nabil, M. F., Azmi, W. H., Hamid, K. A. and Mamat, R. (2018). Experimental investigation of heat transfer and friction factor of TiO2-SiO2 nanofluids in water: ethylene glycol mixture. *International Journal Heat Mass Transfer*, 143(4), 129-145.

13. Gupta, N. K., Verma, S. K., Rathore, P. K. S. and Sharma, A. (2020). Effects of CuO/water nanofluid application on thermal performance of mesh wick heat pipe. *Heat Transfer Research*, 51, 837-850.

14. Putra, N., Saleh, R., Septiadi, W. N., Okta, A. and Hamid, Z. (2014). Thermal performance of biomaterial wick loop heat pipes with water-base Al2O3 nanofluids. *International Journal. Thermal. Science,* 76, 128-136.

15. Bumataria, R. K., Chavda, N. K. and Panchal, H. (2019). Current research aspects in mono and hybrid nanofluid based heat pipe Technologies. *Heliyon*, 5, 16-27.

16. Tanshen, M. R., Lee, S., Kim, J., Kang, D., Noh, J., Chung, H., Jeong, H. and Huh, D. (2014). Pressure distribution inside oscillating heat pipe charged with aqueous Al2O3 nanoparticles MWCNTs and their hybrid. *Journal Center South University,* 21, 2341-2348.

17. Saleh, R., Putra, N., Prakoso, S. P. and Septiadi, W. N. (2013), Experimental investigation of thermal conductivity and heat pipe thermal performance of ZnO nanofluids. *International. Journal Thermal Science*, 63, 125-132.

18. Zufar, M., Gunnasegaran, P., Kumar, H. M. and Neg, K. C. (2020). Numerical and experimental investigations of hybrid nanofluids on pulsating heat pipe performance. *International Journal Heat Mass Transfer*, 146, 119-187.

19. Sözen, A., Öztürk, A., Özalp, M. and Çiftçi, E. (2019). Influences of alumina and fly ash nanofluid usage on the performance of recuperator including heat pipe bundle. *International Journal Enviroment Science Technology*, 16, 5095-5100.

20. Aytaç, İ., Sözen, A., Martin, K., Filiz, Ç. and Ali, H. M. (2020). Improvement of thermal performance using spineloxides/water nanofluids in the heat recovery unit with air-to-air thermosiphone mechanism. *International Journal Thermophys*, 41, 158-166.

21. Akkaya, M., Menlik, T., Sözen, A. and Gürü, M. (2021). The effects of triton X-100 and Tween 80 surfactants on the thermal performance of a nano-lubricant: an experimental study. *International Journal Precise Engineering Manuaturing*, 8, 955-967.

22. Khanlari, A. (2020). The effect of utilizing Al2O3-SiO2/deionized water hybrid nanofluid in a tube-type heat exchanger. *Heat Transfer Research*, 51, 991-1005.

23. Gürbüz, E. Y., Sözen, A., Variyenli, H. İ., Khanlari, A. and Tunce, A. D. (2020). A comparative study on utilizing hybrid-type nanofluid in plate heat exchangers with different number of plates. *Journal Brazilian Society Mechanical Science and Engineering*, 42, 524-532.

24. Selimefendigil, F. and Öztop, H. F. (2020). Identification of pulsating flow effects with CNT nanoparticles on the performance enhancements of thermoelectric generator (TEG) module in renewable energy applications. *Renewable Energy*, 162, 1076-1086.

25. Akkaya, M., Menlik, T., Sözen, A. and Gürü, M. (2020). Experimental investigation of nanolubricant usage in a cooling system at different nanoparticle concentrations. *Heat Transfer Research*, 51, 949-965.

26. Mashayekhi, R., Khodabandeh, E., Bahiraei, M., Bahrami, L., Toghraie, D. and Akbari, OA. (2017). Application of a novel conical strip insert to improve the efficacy of water–Ag nanofluid for utilization in thermal systems: A two-phase simulation. *Energy Conversion Management*, 151, 573-586.

27. Yu, W., Xie, H., Chen, L. and Li, Y. 2010. Enhancement of thermal conductivity of kerosene-based Fe3O4 nanofluids prepared via phase-transfer method. *Colloids Surface A Physicochem. Engineering*, 355, 109-126.

28. Nkurikiyimfura, Y. I., Wang, Z. and Hu, P. (2011), *Enhancement of thermal conductivity of magnetic nanofluids in magnetic field*. IEEE Proceedings of the International Conference on Materials for Renewable Energy & Environment (ICMREE), 1333.

29. Kirithiga, R. and Hemalatha, J. (2020). Investigation of thermophysical properties of aqueous magnesium ferrite nanofluids. *Journal Molecule Liquid*, 317, 113-144.

30. Kharat, P. B., Kounsalye, J. S., Shisode, M. V. and Jadhav K. M. (2019). Preparation and thermophysical investigations of CoFe2O4-based nanofluid: *a potential heat transfer agentent Journal November Management*, 32, 341-351.

31. Bahiraei, M. and Hangi, M. (2016). An empirical study to develop temperature-dependent models for thermal conductivity and viscosity of water-Fe3O4 magnetic nanofluid. *Mater Chemical Physics*, 181, 333-355.

32. Sundar, L., Singh, M. K. and Sousa, A. C. M. (2014). Enhanced heat transfer and friction factor of MWCNT–Fe3O4/water hybrid nanofluids. *International Communications Heat and Mass Transfer*, 52, 73-86.

33. Tetuko, A. P., Nurdiyansah, L. F., Addin, M., Setiadi, E. A., Ginting, M. and Sebayang, P. (2019). Magnetic nanofluids as heat transfer media in heat pipes. *Advance National Science Nanoscience*, 11, 440-453.

34. Afshari, F., Sözen, A., Khanlari, A. and Tuncer, A. D., (2021), Heat transfer enhancement of finned shell and tube heat exchanger using Fe2O3/water nanofluid, *Journal Center South University*, 28, 3297-3309.

35. Alam, T., and Kim, M. H., (2018). A comprehensive review on single phase heat transfer enhancement techniques in heat exchanger applications, *Renewable Sustainable Energy*, 81, 813-839.

36. Kavitha, R., Methkal, Y., Kulkarni, K. and Gupta, M. (2022). Heat transfer enhancement in a double pipe heat exchanger with copper oxide nanofluid: An experimental study, *Material Today Process*, 88, 12-25.

37. Sundar, L. S., Punnaiah, V., Sharma, K. V., Chamkha, A. J., and Sousa, A. C. M., (2021).Thermal entropy and exergy efficiency analyses of nanodiamond/water nanofluid flow in a plate heat exchanger, *Dimensional Related Material* 60(1),33-46.

38. Somasekhar, K., Malleswara Rao, K. N. D., Sankararao, V., Mohammed, R., Veerendra, M. and Venkateswararao, T. (2018). A CFD Investigation of Heat Transfer

Enhancement of Shell and Tube Heat Exchanger Using Al2 O3/Water Nanofluid, Material *Today Process*, 5, 1057-1062.

39. Huang, D., Wu, Z. and Sunden, B. (2016). Effects of hybrid nanofluid mixture in plate heat exchangers, *Experimental Thermal Fluid Science,* 72, 190-196.

40. Alklaibi, A. M., Sundar, L. S. and Chandra Mouli, K. V. V. (2022). Experimental investigation on the performance of hybrid Fe3O4 coated MWCNT/Water nanofluidas a coolant of a Plate heat exchanger, *International Journal Thermal Sci*ence, 10(13), 22-30.

41. Sarafraz, M. M., Hormozi, F. and Nikkhah, V. (2016). Thermal performance of a counter-current double pipe heat exchanger working with COOH-CNT/water nanofluids, *Experimental Thermal Fluid Science*, 20(3), 39-50.

42. Babat, R. A. A., Martin, K., Çiftçi, E. and Sözen, A. (2022). Experimental study on the utilization of magnetic nanofluids in an air-to-air heat pipe heat exchanger, *Chemical Engineering Communication*, 19(4), 33-66.

43. Vermahmoudi, Y., Peyghambarzadeh, S. M., Hashemabadi, S. H. and Naraki, M. (2014). Experimental investigation on heat transfer performance of Fe2O3/water nanofluid in an air-finned heat exchanger, *Europe Journal Mechanical Fluids*, 44(4), 32-41,

44. Aghabozorg, M. H., Rashidi, A. and Mohammadi, S. (2016). Experimental investigation of heat transfer enhancement of Fe2O3-CNT/water magnetic nanofluids under laminar, transient and turbulent flow inside a horizontal shell and tube heat exchanger. *Experimental Thermal Fluid Science,* 72(2), 182-189,

45. Kumar, N. T. R., Sundar, L. S. and Bhramara, P. (2016). Effectiveness and Overall Heat Transfer Coefficient of Fe3O4 /Water Nanofluid Flow in a Double Pipe Heat Exchanger with Return Bend. *International Journal Dynamics Fluids*, 12(1), 19-36.

46. Ravi Kumar, N. T., Bhramara, P., Addis, B. M., Sundar, L. S., Singh, M. K. and Sousa, A. C. M. (2017). Heat transfer, friction factor and effectiveness analysis of Fe3O4/water nanofluid flow in a double pipe heat exchanger with return bend, *International Communications Heat Mass Transfer*, 81(3), 155–163.

47. Baba, M. S., Raju, A. V. S. R. and Rao, M. B. (2018). Heat transfer enhancement and pressure drop of Fe3O4 -water nanofluid in a double tube counter flow heat exchanger with internal longitudinal fins, *Case Study Thermal Engineering*, 12, 600-607.

48. Abdulwahab, M. R., Che Sidik, N. A., Yusof, S. N. A. and Jamil, M. M. (2020). Magnetic Nanofluids for Heat Transfer Enhancement inside Straight Channels, *Journal Advanced Research Material Science*, 68(1), 8-19.

49. Zheng, D., Wang, J., Chen, Z., Baleta, J. and Sundén, B. (2020). Performance analysis of a plate heat exchanger using various nanofluids, *International Journal Heat Mass Transfer*, 158(2), 55-60.

50. Noorbakhsh, M., Ajarostaghi, S. S. M., Zaboli, M. and Kiani, B., (2022). Thermal analysis of nanofluids flow in a double pipe heat exchanger with twisted tapes insert in both sides. *Journal of Thermal Analysis and Calorimetry*, 147(5), 3965-3976.

51. Mansoury, D., Ilami Doshmanziari, F., Rezaie, S. and Rashidi, M. M. (2019). Effect of Al2O3/water nanofluid on performance of parallel flow heat exchangers. *Journal of Thermal Analysis and Calorimetry*, 135(1), 625-643.

52. Choi, S. U. S. (1995). Developments and Application of Non-Newtonian Flows. *American Society of Mechanical Engineers*, 66(2), 99-105.

53. Goodarzi, M., Kherbeet, A. S., Afrand, M., Sadeghinezhad, E., Mehrali, M., Zahedi, P., Wongwises, S. and Dahari, M. (2016). Investigation of heat transfer performance and friction factor of a counter-flow double-pipe heat exchanger using nitrogen-doped, graphene-based nanofluids. *International Communications in Heat and Mass Transfer*, 76, 16-23.

54. Sözen, A., Variyenli, H. İ., Özdemir, M. B., Gürü, M. and Aytac, I., (2016). Heat transfer enhancement using alumina and fly ash nanofluids in parallel and cross-flow concentric tube heat exchangers. *Journal of the Energy Institute*, 89(3), 414-424.

55. Bahmani, M. H., Sheikhzadeh, G., Zarringhalam, M., Akbari, O. A., Alrashed, A. A., Shabani, G. A. S. and Goodarzi, M. (2018). Investigation of turbulent heat transfer and nanofluid flow in a double pipe heat exchanger. *Advanced Powder Technology*, 29(2), 273-282.

56. Shahsavar, A., Godini, A., Sardari, P. T., Toghraie, D. and Salehipour, H. (2019). Impact of variable fluid properties on forced convection of Fe3O4/CNT/water hybrid nanofluid in a double-pipe mini-channel heat exchanger. *Journal of Thermal Analysis and Calorimetry*, 137(3), 1031-1043.

57. Maddah, H., Aghayari, R., Mirzaee, M., Ahmadi, M. H., Sadeghzadeh, M. and Chamkha, A. J. (2018). Factorial experimental design for the thermal performance of a double pipe heat exchanger using Al2O3-TiO2 hybrid nanofluid. *International Communications in Heat and Mass Transfer*, 97, 92-102.

58. Hashemi Karouei, S. H., Ajarostaghi, S. S. M., Gorji-Bandpy, M. and Hosseini Fard, S. R. (2021). Laminar heat transfer and fluid flow of two various hybrid nanofluids in a helical double-pipe heat exchanger equipped with an innovative curved conical turbulator. *Journal of Thermal Analysis and Calorimetry*, 143(2), 1455-1466.

59. Gürü, M., Sözen, A., Karakaya, U. and Çiftçi E. (2019). Influences of bentonite-deionized water nanofluid utilization at different concentrations on heat pipe performance: an experimental study. *Applied Thermal Engineering*, 148, 632-640,

60. Gupta, N. K., Tiwari, A. K. and Ghosh, S. K. (2015). Experimental study of thermal performance of nanofluid-filled and nanoparticles-coated mesh wick heat pipes. *Journal Heat Transfer*, 140(10), 102403-102403.

61. Kavusi, H. and Toghraie, D. A. (2017). Comprehensive study of the performance of a heat pipe by using of various nanofluids. *Advanced Powder Technology*, 28, 3074-3084,

62. Ağbulut, Ü. and Saridemir S. (2018). A general view to converting fossil fuels to cleaner energy source by adding nanoparticles. *International Journal Ambient Energy*, 42(13), 1569-1574.

63. Venkatachalapathy, S., Kumaresan, G. and Suresh, S. (2015). Performance analysis of cylindrical heat pipe using nanofluids – an experimental study. *International Journal Multiphasic Flow*, 72, 188-197.

64. Tharayil, T., Asirvatham, L. G., Ravindran, V. and Wongwises S. (2015). Thermal performance of miniature loop heat pipe with graphene–water nano fluid. *International Journal Heat Mass Transfer*, 93, 657-968.

65. Menlik, T., Sözen, A., Gürü, M. and Öztaş, S. (2015). Heat transfer enhancement using MgO/ water nanofluid in heat pipe. *Journal Energy Institute*, 88(3), 247-257.

66. Sözen, A., Menlik, T., Aktaş, M. and Gürü, M., (2017). Utilization of blast furnace slag nano-fluids in two-phase closed thermos-syphon heat pipes for enhancing heat transfer. *Experimantal Heat Transfer*, 30(2), 112-125,

67. Sözen, A., Gürü, M., Menlik, T., Karakaya, U. and Çiftçi, E. (2018). Experimental comparison of triton x–100 and sodium dodecyl benzene sulfonate (SDBS) surfactants on thermal performance of TiO2-deionized water nanofluid in a thermosiphon. *Experimental Heat Transfer*, 31, 450-469.

68. Kiseev, V. and Sazhin, O. (2019). Heat transfer enhancement in a loop thermosyphon using nanoparticles/water nanofluid. *International Journal Heat Mass Transfer*, 132, 557–564.

69. Aneesh, V., Antony, R., Paramasivan, G. and Selvaraju, N. (2016). Distillation technology and need of simultaneous design and control: A review. *Chem. Eng. Process. Process Intensif.*, 104, 219–242,

70. Kiss, A. A., Landaeta, S. J. F. and Ferreira, C. A. I. (2012). Towards energy efficient distillation technologies - making the right choice. *Energy*, 47, 531-542.

71. Kang, S. W., Wei, W. C., Tsai, S. H. and Yang, S. Y. (2006). Experimental investigation of silver nanofluid on heat pipe thermal performance. *Applied Thermal Engineering*, 26, 2377-2382.

72. Yang, X. F., Liu, Z. H. and Zhao, J. (2008). Heat transfer performance of a horizontal micro-grooved heat pipe using CuO nanofluid. *Journal of Micromechanics and Microengineering*, 18(3), 99-108.

73. Naphon, P., Thongkum, D. and Assadamongkol P. (2009). Heat pipe efficiency enhancement with refrigerant–nanoparticles mixtures. *Energy Conversion Management*, 50, 772-776.

74. Huminic, G. and Huminic, A. (2013). Numerical study on heat transfer characteristics of thermosyphon heat pipes using nanofluids, *Energy Conversion and Management*, 76, 393-399.

75. Su, U., Sözen, A. and Menlik, T. (2019). Heat Pipe Evacuated Tubular Solar Collector Performance Improvement By Applications of Nanofluid. *Journal of Polytechnic-Politeknik Dergisi.* 22(1), 12-30.

76. Kanti, P., Sharma, K. V., Ceg, R. and Azmi, W. H. (2021). Experimental determination of thermophysical properties of Indonesian fly-ash nanofluid for heat transfer applications. *Particulate Science and Technology*, 39(5), 597-606.

77. Kanti, P. K., Sharma, K. V., Minea, A. A. and Kesti, V. (2021). Experimental and computational determination of heat transfer, entropy generation and pressure drop under turbulent flow in a tube with fly ash-Cu hybrid nanofluid. *International Journal of Thermal Sciences*, 167, 10-16.

78. Marulasiddeshi, H. B., Kanti, P. K., Jamei, M., Prakash, S. B., Sridhara, S. N. and Said, Z. (2022). Experimental study on the thermal properties of Al2O3-CuO/water hybrid nanofluids: Development of an artificial intelligence model. *International Journal of Energy Research*, 99(1), 108-118.

79. Roodbari, M., Alimoradi, H., Shams, M. and Aghanajafi, C. (2022). An experimental investigation of microstructure surface roughness on pool boiling characteristics of TiO 2 nanofluid. *Journal of Thermal Analysis and Calorimetry*, 147(4), 3283-3298.

80. Roodbari, M., Abbasi, M., Arabha, S., Gharedaghi, A. and Rajabpour, A. (2022). Interfacial thermal conductance between TiO2 nanoparticle and water: A molecular dynamics study. *Journal of Molecular Liquids*, 348, 118-133.

81. Maxwell, J. C. (1881). *A Treatise on Electricity and Magnetism*. (2. Edition). UK: Clarendon Press, Oxford University.

82. Pantzali, M. N., Mouza, A. A. and Paras, S. V. (2009). Investigating the efficacy of nanofluids as coolants in plate heat exchangers (PHE). *Chemical Engineering Science*, 64, 3290-3300.

83. Arani, A. A. and Amani, J. (2013). Experimental investigation of diameter effect on heat transfer performance and pressure drop of TiO2– water nanofluid. *Experimental Thermal Fluid Science*, 44, 520-33.

84. Pak, B. C. and Cho, Y. I. (1998). Hydrodynamic and heat transfer study of dispersed fluids with submicron metallic oxide particles. *Experimental Heat Transfer*, 11(2), 151-170.

85. Ghachem, K., Aich, W. and Kolsi, L. (2021). Computational analysis of hybrid nanofluid enhanced heat transfer in cross flow micro heat exchanger with rectangular wavy channels. *Case Study Engineering*, 24, 1-14.

86. Chamkha, A. J. and Abu-Nada, E. (2012). Mixed convection flow in single-and double-lid driven square cavities filled with water–Al2O3 nanofluid: Effect of viscosity models. *European Journal of Mechanics Fluids*, 36, 82-96.

87. Li, Q. and Xuan, Y. (2002). Convective heat transfer and flow characteristics of Cu–water nanofluid. *Science China Search. Technology Science*, 45(4), 408-416.

88. Sonawane, S. S., Khedkar, R. S. and Wasewar, K. L. (2013). Study on concentric tube heat exchanger heat transfer performance using Al2O3–water based nanofluids. *International communications in heat and mass transfer*, 49, 60-68.

89. Ilyas, S. U., Pendyala, R. and Narahari, M. (2017). An experimental study on the natural convection heat transfer in rectangular enclosure using functionalized alumina-thermal oil-based nanofluids. *Applied Thermal Engineering*, 127, 765-775.

90. Kumar, R. and Kalam, M. A., (1991). Laminar thermal convection between vertical coaxial isothermal cylinders. *International journal of heat and mass transfer*, 34(2), 513-524.

91. Chamkha, A. J., and Abu-Nada, E. (2012). Mixed convection flow in single-and double-lid driven square cavities filled with water–Al2O3 nanofluid: Effect of viscosity models. *European Journal of Mechanics Fluids*, 36, 82-96.

92. Rashad, A. M., Chamkha, A. J., Ismael, M. A. and Salah T. (2018). Magnetohydrodynamics natural convection in a triangular cavity filled with a Cu-Al2O3/water hybrid nanofluid with localized heating from below and internal heat generation. *Journal of Heat Transfer*, 140(7), 122-133.

93. Rehan, Z. (2020). Application of First-Order Differential Equation to Heat Convection in Fluid. *Journal of Applied Mathematics and Physics*, 8(8), 14-56.

94. Park, Y. J., Kang, H. K. and Kim, C. J. (2002). Heat transfer characteristics of a two-phase closed thermosyphon to the fill charge ratio. *International Journal Heat Mass Transfer*, 45, 4655-4661.

95. Reay, D., McGlen, R. and Kew, P. (2013). Heat pipes: theory, design and applications. *Butterworth-Heinemann*, 55, 60-99.

96. Wang, L. (2020). *PID control system design and automatic tuning using MATLAB/Simulink*. (2. Edition). John Wiley & Sons.

97. Alammar, A. A., Al-Dadah, R. K. and Mahmoud, S. M. (2016). Numerical investigation of effect of fill ratio and inclination angle on a thermosiphon heat pipe thermal performance. *Applied Thermal Engineering*, 108, 1055-1065.

98. Cataldo, F. and Thome, J. R. (2017). Experimental evaluation of the thermal performances of a thermosyphon cooling system rejecting heat by natural and forced convection. *Applied Thermal Engineering*, 127, 1404-1415.

99. Jafari, D., Filippeschi, S., Franco, A. and Di Marco, P. (2017). Unsteady experimental and numerical analysis of a two-phase closed thermosyphon at different filling ratios. *Experimental Thermal Fluid Science*, 81, 164–174.

100. Jouhara, H. and Robinson, A. J. (2010). Experimental investigation of small diameter two-phase closed thermosyphons charged with water, FC-84, FC-77 and FC-3283. *Applied Thermal Engineering*, 30, 201–211.

101. Aydın, D. Y., Aydin, E. and Gürü, M. (2023). The effects of particle mass fraction and static magnetic field on the thermal performance of NiFe2O4 nanofluid in a heat pipe. *International Journal of Thermal Sciences*, 183, 107-175.

102. Dehaj, M. S., Rezaeian, M., Mousavi, D., Shamsi, S. and Salarmofrad, M. (2021). Efficiency of the parabolic through solar collector using NiFe2O4/Water nanofluid and U-tube. *Journal of the Taiwan Institute of Chemical Engineers*, 120, 136-149.

103. Garud, K. S. and Lee, M. Y. (2021). Numerical Investigations on Heat Transfer Characteristics of Single Particle and Hybrid Nanofluids in Uniformly Heated Tube. *Symmetry*, 13(5), 876-891.



Gazili olmak ayrıcalıktır